Copyright Warning & Restrictions

The copyright law of the United States (Title 17, United States Code) governs the making of photocopies or other reproductions of copyrighted material.

Under certain conditions specified in the law, libraries and archives are authorized to furnish a photocopy or other reproduction. One of these specified conditions is that the photocopy or reproduction is not to be "used for any purpose other than private study, scholarship, or research." If a, user makes a request for, or later uses, a photocopy or reproduction for purposes in excess of "fair use" that user may be liable for copyright infringement,

This institution reserves the right to refuse to accept a copying order if, in its judgment, fulfillment of the order would involve violation of copyright law.

Please Note: The author retains the copyright while the New Jersey Institute of Technology reserves the right to distribute this thesis or dissertation

Printing note: If you do not wish to print this page, then select "Pages from: first page # to: last page #" on the print dialog screen

ABSTRACT

CHARACTERIZATION OF MICROPOROUS ECTFE MEMBRANES EXPOSED TO DIFFERENT LIQUID MEDIA AND γ-RADIATION AND NANOPARTICLE MICROFILTRATION THROUGH SUCH MEMBRANES

by
Na Yao

Microporous polymeric membranes are used in a variety of applications for separations, purification as well as barrier function. A major application is for microfiltration (MF). Changes in the properties of MF membranes exposed to acids, bases and organic solvents are of interest in semiconductor processing as well as in membrane contactor applications. Microfiltration membranes used for sterilization in beverage, biotechnology and pharmaceutical industries are sterilized by gamma radiation among others. Irradiation-induced degradation in membrane properties should be known. A variety of fluoropolymer-based microporous membranes are available with varying properties. Ethylene chlorotrifluoroethylene (ECTFE) membranes are a new addition and are of potential interest. Microporous membranes of ECTFE membranes subjected to caustic soaking, organic solvent soaking and γ-irradiation were characterized extensively and compared with widely-used polyvinylidene fluoride (PVDF) membranes for selected properties.

ECTFE membrane swellings by seven solvents including tri-n-octylamine (TOA) were much larger than those of nonporous ECTFE films. Scanning electron microscopy (SEM), atomic force microscopy (AFM), differential scanning calorimetry (DSC) and X-ray diffraction (XRD) indicated significant defects in TOA-soaked membranes. Bubble-point-pressure (BPP) based maximum pore diameters of selected solvent-soaked ECTFE membranes are in good agreement with the pore size distribution estimated from AFM. Fourier transform infrared and Raman spectroscopies were used to study the solvent-

membrane interactions: TOA introduced C-H stretching and deformation. Thermogravimetric analysis (TGA) and DSC confirmed TOA presence in membrane pores. Solvents tetrahydrofuran, toluene, acetonitrile and TOA decreased Young's modulus by 6 to 30%. ECTFE membranes resisted plasticization by these solvents: glass transition temperature variations were limited. In TOA-treated membranes, XRD indicated more significant defects in PVDF membranes. Treatment with NaOH solutions showed no effect on contact angle and BPP. Only 3M caustic solution reduced liquid entry pressure by 13.8 kPag. ECTFE membranes showed greater hydrophobicity, stronger wetting resistance and better ability to maintain hydrophobicity vis-à-vis PVDF membranes. ECTFE membranes subjected to γ-radiation (up to 45 kGy) showed almost no effect on morphology, porosity and Young's modulus. Slight variations were observed in BPP, melting enthalpy obtained via DSC and energy loss measured in dielectric relaxation spectroscopy.

The solvent resistance of ECTFE membranes, especially to TOA, is important especially in membrane solvent extraction in the presence of diluents e.g., xylene. Many characterization techniques were employed to study solvent-treatment effects on ECTFE membranes exposed to ethanol, xylene, xylene80/TOA20 and pure TOA. Membrane-surface roughness of virgin, ethanol-soaked and TOA-soaked membranes indicated: TOA-soaked membranes were the roughest, followed by ethanol-soaked and virgin ones. Bubble-point-pressure based maximum pore diameters (d_{max}) of solvent-treated membranes were: $d_{max,\ TOA} > d_{max,\ Xylene/TOA} > d_{max,\ Xylene} > d_{max,\ Ethanol} > d_{max,\ Virgin.}$ In FTIR and Raman spectra, TOA introduced extra peaks contributing to C-H stretching and deformation. Raman spectra of xylene80/TOA20-soaked membrane were a combination

of those of xylene and TOA. The presence of a large amount of diluent reduces the impact of TOA on ECTFE membranes.

In dead-end MF, fouling mechanisms behaved differently for virgin and TOA-soaked membranes; filtrate particle size distributions agreed well with estimated pore sizes. The values of permeance (kg/m^2-s-kPa) determined from the slope of the linear plot of filtration flux vs. the applied pressure difference across the membrane, were 0.39, 0.23 and 0.03 for methanol, ethanol and 2-propanol, respectively. In cross-flow MF using silica nanoparticles suspended in 25% ethanol solution, Particle agglomerates having less than 100 nm size can pass through the membrane; some fouling was observed. The governing fouling mechanisms for tests operated using 3.8 ppm at 6.9 kPag (1 psig) and 13.8 kPag (2 psig) were pore blocking; for tests conducted using 3.8 ppm at 27.6 kPag (4 psig) and 1.9 ppm at 6.9, 13.8 and 27.6 kPag (1, 2 and 4 psig), the mechanism was membrane resistance controlled. Less particles got embedded in membrane pores in experiments operated using suspensions with lower concentrations or higher concentrations with a higher transmembrane pressure. This is in good agreement with the values of the shear rate in the pore flow and SEM images of the membrane after MF.

CHARACTERIZATION OF MICROPOROUS ECTFE MEMBRANES EXPOSED TO DIFFERENT LIQUID MEDIA AND γ-RADIATION AND NANOPARTICLE MICROFILTRATION THROUGH SUCH MEMBRANES

by
Na Yao

A Dissertation
Submitted to the Faculty of
New Jersey Institute of Technology
in Partial Fulfillment of the Requirements for the Degree of
Doctor of Philosophy in Chemical Engineering

Otto H. York Department of
Chemical, Biological and Pharmaceutical Engineering

December 2017

.

APPROVAL PAGE

CHARACTERIZATION OF MICROPOROUS ECTFE MEMBRANES EXPOSED TO DIFFERENT LIQUID MEDIA AND γ-RADIATION AND NANOPARTICLE MICROFILTRATION THROUGH SUCH MEMBRANES

Na Yao

Dr. Kamalesh K. Sirkar, Dissertation Advisor Date
Distinguished Professor of Chemical, Biological and Pharmaceutical Engineering, NJIT

Dr. Boris Khusid, Dissertation Co-Advisor Date
Professor of Chemical, Biological and Pharmaceutical Engineering, NJIT

Dr. Costas G. Gogos, Committee Member Date
Distinguished Research Professor of Chemical, Biological and Pharmaceutical Engineering, NJIT

Dr. Michael Jaffe, Committee Member Date
Research Professor of Biomedical Engineering, NJIT

Dr. Wen Zhang, Committee Member Date
Assistant Professor of Civil and Environmental Engineering, NJIT

BIOGRAPHICAL SKETCH

Author: Na Yao

Degree: Doctor of Philosophy

Date: December 2017

Undergraduate and Graduate Education:

- Doctor of Philosophy in Chemical Engineering,
  New Jersey Institute of Technology, Newark, NJ, 2017
- Master of Science in Chemical Engineering,
  New Jersey Institute of Technology, Newark, NJ, 2013
- Bachelor of Science in Chemical Engineering,
  Shenyang University of Chemical Technology, Shenyang, P. R. China, 2011

Major: Chemical Engineering

Presentations and Publications:

N. Yao, J. Chau, E. Elele, B. Khusid, K.K. Sirkar, D.J. Dehn, Characterization of microporous ECTFE membrane after exposure to different liquid media and radiation, J. Membr. Sci., 532 (2017) 89-104.

N. Yao, B. Khusid, K.K. Sirkar, D.J. Dehn, Effects of tri-n-octylamine with or without diluents on microporous ethylene chlorotrifluoroethylene membranes, Ind. Eng. Chem. Res., 56 (2017) 9698-9709.

N. Yao, B. Khusid, K.K. Sirkar, D.J. Dehn, Nanoparticle filtration through microporous ECTFE membrane in aqueous/organic media, Submitted for publication, (2017).

N. Yao, J. Chau, E. Elele, B. Khusid, K.K. Sirkar, Characterization of microporous ECTFE membrane after exposure to different liquid mediums and radiation. In Engineering Conferences International: Membrane Technology VII, Cork, Ireland, 2016.

To my dear parents Shufan Yong and Hengxiao Yao

献给我的父母 雍淑范和姚恒孝

To Shuo and our coming baby

ACKNOWLEDGMENTS

I would like to express my deepest gratitude to my advisor Prof. Kamalesh K. Sirkar who opened the door for me to start the PhD program, guided me into the field of membrane separations and have my research supported financially via the MAST (Membrane Science, Engineering and Technology) center. I appreciate the opportunity to be one of the MAST center supported students and get a chance to work with the excellent engineers and scientists in the center. My greatest gratitude also goes to my co-advisor Prof. Boris Khusid. His purist attitude inspires me. I benefit a lot from his supervision and feedbacks. It has been a great honor to work closely with both of them. Their valuable advice, encouragements and resources not just inspire this research but my entire professional development.

Additionally, I would like to thank Prof. Costas G. Gogos, Prof. Michael Jaffe and Prof. Wen Zhang for providing me invaluable suggestion and time for this research and serving as committee members. Special thanks to Prof. Jaffe and Prof. Zhang for kindly sharing their instruments for my PhD study. Last but not the least, I appreciate the assistance and encouragement Prof. Gogos has provided throughout my research.

I am grateful to the financial support and research funding provided by the NSF Industry/University Cooperative Research Center (MAST) and the Otto H. York Department of Chemical, Biological and Pharmaceutical Engineering at NJIT. Special thanks to Mr. Derek J. Dehn of 3M for constructive discussions and providing membrane samples, as well as Dr. Christina Carbrello of MilliporeSigma for providing PVDF membranes, and the membrane cells. I would also express my gratitude to all members in

MAST Center, Polymer Processing Institute (PPI) and Materials Characterization Laboratory in York Center, especially thank Dr. Herman Suwardie (PPI) for assisting with thermal analysis. I also acknowledge Park Systems Inc. (Santa Clara, CA) for assistance with AFM measurement.

Finally, I would also like to thank all my family and friends especially my dear parents for their love, support and encouragement, as well as my husband for his companion and love during this period. I could not have done this without them.

TABLE OF CONTENTS

TABLE OF CONTENTS
(Continued)

TABLE OF CONTENTS
(Continued)

TABLE OF CONTENTS
(Continued)

LIST OF TABLES

LIST OF FIGURES

LIST OF FIGURES
(Continued)

LIST OF FIGURES
(Continued)

LIST OF FIGURES
(Continued)

CHAPTER 1

INTRODUCTION

1.1 Fluoropolymers

A variety of porous, microporous and nonporous polymeric membranes are used for separation, purification, concentration, sampling, as well as barrier applications. The application requirements dictate the membrane properties vis-a-vis pore size, porosity, wetting behavior, sorption characteristics, chemical resistance, thermal stability, mechanical strength, ductility, extractability, processability etc. An ideal microporous membrane should have high chemical and thermal resistance and necessary mechanical properties along with the required pore size and wetting behavior.

Fluoropolymers exhibit excellent chemical resistance, lower surface energy, lower dielectric constant and lower coefficient of friction compared with other polymers [1]. They are widely used in chemical processing, electrical applications and communications, automotive and office equipment, houseware, medical, architectural fabric, semiconductor fabrication etc. [1]. The demand for fluoropolymers, shown in Table 1.1, is growing year by year. Table 1.2 provides the general chemical structure, melting temperature (T_m) of common fluoropolymers including partially and fully fluorinated polymers [2]. Even though partially fluorinated polymers have lower T_m and narrower range of chemical resistance than those of fully fluorinated ones, they are quite stiffer than polytetrafluoroethylene (PTFE) copolymers [2, 3] due to their higher cohesive energy density [3]. PTFE, a perfluoropolymer, formed of C-C bonds and C-F bonds, which introduces high melting temperature, excellent chemical and thermal resistance to almost

any chemical/oxidative environment, should be of great interest. However, PTFE is quite expensive, notoriously difficult to process and vulnerable when exposed to radiation [4]. A search has gone on for alternate fluoropolymer candidates having desirable properties and possessing easy processability.

Table 1.1 World Fluoropolymer Demand by Type (thousands of metric tons)

Year	1996	2001	2006	2011	2016
PTFE	70	85	98	125	160
FEP	10	15	21	29	40
PVDF	14	17	20	26	33
Fluoroelastomers	13	16	20	27	35
Other types	8	12	21	28	37
Total	115	145	198	235	305

Source: [5].

Table 1.2 Engineering Thermoplastic Fluoropolymers Generally Used to Construct Fluid and Device Handling Products

Fluoropolymer	Abbreviation	Structure	T_m (^oC)
Polytetrafluoroethylene	PTFE	$-[CF_2CF_2]-$	327
Perfluoroalkoxy	PFA	$-[CF_2CF_2]_{1-x}-[CF_2CF(OR)]_x-$	285-310
Fluorinated ethylene-propylene	FEP	$-[CF_2CF_2]_{1-y}-[CF_2CF(CF_3)]_y-$	250-280
Ethylene-tetrafluoroethylene	ETFE	$-[CH_2CH_2]-[CF_2CF_2]-$	225-270
Ethylene-chlorotrifluoroethylene	ECTFE	$-[CH_2CH_2]-[CF_2CF(Cl)]-$	240
Polyvinylidene fluoride	PVDF	$-[CH_2CF_2]-$	160-170

Note: R for PFA is a perfluoroalkoxy (OC_nF_{2n+1}); x is typically 0.03-0.10; y is 0.10-0.15.
Source: [2].

It has to be mentioned that polyvinylidene fluoride (PVDF) based membranes are being used extensively. Alternate candidate materials include PFA (perfluoroalkoxy), fully fluorinated copolymer; FEP (fluorinated ethylene propylene), a fully fluorinated copolymer; ETFE (ehylene tetrafluoroethylene), a partially fluorinated polymer containing

hydrogen; PDD-TFE [6, 7] (perfluoro-2,2-dimethyl-1,1,3-dioxole copolymerized with tetrafluoroethylene) an amorphous perfluorocopolymer; ECTFE (ethylene chlorotrifluoroethylene), a copolymer of ethylene and chlorotrifluoroethylene, etc. Unfortunately, PVDF has limited pH resistance and is vulnerable to attack by amines as well as many hydrophobic solvents of interest. Although ETFE membranes are very hydrophobic, they are produced by a stretching process which makes it difficult to achieve a defined pore size [8]. Membranes of the PDD-TFE type (generally of the AF type and the polymer manufactured by DuPont) are very costly. Membranes of ECTFE are of interest because these are expected to be highly solvent resistant and possess high thermal resistance.

Although difficult to process, thermally induced phase separation (TIPS) processes have led to the development of a microporous ECTFE membrane structure that provides very hydrophobic membranes having pore size ranges between open-pore microfiltration (MF) membranes to ultrafiltration (UF) membranes [8-13]. Perfluoropolymers such as PTFE, FEP and PFA offer better thermal (higher use temperature) and chemical resistance properties than partially fluorinated polymers like ECTFE. However depending on processing conditions, partially fluorinated resins, such as ECTFE, can provide better mechanical properties (tensile strength, toughness, abrasion and cut-through resistance at ambient temperatures, etc.) and be used for fabrication of filtration cartridges [11-13]. They are also known for extremely high resistance to ozone, strong oxidizing agents [2, 14] and gamma radiation [15] that bring the potential benefit of sterilization for biological applications.

1.2 Fabrication of Microporous ECTFE Membrane, its Properties and Potential Applications

The chemical resistance of the relatively new polymer ECTFE for a variety of applications is supposed to be excellent so that the traditional room-temperature process of immersion precipitation or evaporative casting is unfavorable for ECTFE membrane fabrication [9]. However, ECTFE is soluble in selected solvents, which makes it possible to fabricate ECTFE membrane using TIPS [9, 10, 16]. The basic steps of TIPS were summarized by Ramaswamy et al. [9] and Roh et al. [10] as following: (1) make a homogeneous system of latent solvent (high boiling point, low molecular weight) and polymer at an elevated temperature which is close to the T_m of the polymer; (2) polymer solution is cast into the desired shape; (3) phase separation is introduced via cooling the polymeric solution; (4) latent solvent is extracted with a more volatile solvent; (5) membrane is dried to constant weight. In their studies [9, 10], dibutyl phthalate (DBP) which has a higher boiling point than the T_m of ECTFE was chosen as latent solvent; DBP dissolved ECTFE more quickly and readily than dioctyl phthalate (DOP), another possible latent solvent. 2-propanol was used to get the latent solvent extracted after polymer solidification and phase separation [9, 10].

Interestingly, Pan et al. [16] successfully controlled the membrane morphology using a mixture of bis(2-ethylhexyl) adipate/diethyl phthalate (DEHA/DEP) via TIPS by varying the ratio of DEHA/DEP mixture. The resulting membranes showed different mechanical properties and hydrophobicity depending on how they were prepared, i.e. solid-liquid phase separation or liquid-liquid phase separation. Additionally, Kim et al. [17] provided a detailed table about the chemicals used in ECTFE membrane fabrication via

TIPS as well as the resulting membrane properties, such as structure, mechanical properties, porosity and pore diameter.

Such knowledge and information are essential to developing useful applications of this membrane. Very few studies have been reported on microporous ECTFE membrane characterization, especially for membrane properties subsequent to exposure to organic solvents, caustic solutions, irradiations or other severe environments. Excellent chemical resistance of ECTFE (Halar® 901) to aggressive organic solvents, dimethyl formamide (DMF), dimethyl acetamide (DMAc), N-methyl pyrrolidone (NMP), tetrahydrofuran (THF), toluene, chloroform and acetone, was observed by Simone et al. [18]. The changes of mechanical properties for ECTFE (Halar®) after exposure to organic solvent were characterized by Lee et al. [19]. Singh et al. [20] reported structural and thermal properties of ECTFE films treated by heavy ions such as lithium, carbon, nickel and silver. The structural variations with respect to temperature and dynamic-mechanical relaxations of ECTFE material (Ausimont USA, Thorofare, NJ) were studied by Guerra et al. [21]. ECTFE (Halar® 6014, Ausimont, Italy) used as coating material was immersed in caustic solutions to characterize its corrosion resistance [22]. ECTFE can also be used in data cables so that the dielectric constant and dissipation factor were measured as a function of temperature [23]. ECTFE was also reported to be used as chromatographic support material due to its excellent hydrophobicity as well as good resistance to solvents and pH variations [24]. Drioli et al. [25] conducted research on water recovery and chemical resistance of ECTFE membrane. The properties including contact angle, mechanical properties, pore size and porosity of ECTFE flat membrane prepared by TIPS were compared with those

for PVDF hollow fibers [25]. Table 1.3 provides a comparison between ECTFE and other fluoropolymers, mostly PVDF, in several aspects.

Table 1.3 Property Comparison between ECTFE and Other Fluoropolymers

Properties	Comparing polymer	Performance	Authors
Chemical resistance	PVDF	ECTFE: better	Extrand [2]
Chemical resistance	PVDF	ECTFE: better	Drioli et al. [25]
Water recovery	PVDF	Similar	Drioli et al. [25]
Yield stress, tensile strength	FEP, PFA	ECTFE: better	Lee et al. [19]
HCl, HBr resistance	PVDF	ECTFE: unaffected; PVDF: less ductile	Hedenqvist et al. [26]

In semiconductor manufacturing, MF membranes are extensively used for purification of process fluids e.g., acids, bases, organic solvents and photoresists; the primary application is to remove particulates from the solvents to be used for processing [27]. Any change in the properties of the membrane during/after exposure to such solvents is of significant interest. Another important application of MF membranes is sterilization of various solutions [27]. Complete bacterial retention by 0.22 μm rated MF membrane filter is routinely achieved in applications such as, sterilization of parenterals, water for injection (WFI), ophthalmic solutions, plasma processing, aseptic processing. There are numerous other applications of MF for absolute microbial removal such as, beer stabilization (cold-filtered beer), wine stabilization etc. For such applications, microfilters have to be pre-sterilized.

There are a number of methods widely used for sterilization of MF membrane-containing devices including ethylene oxide (EtO) gas-based sterilization, γ-radiation, steam sterilization. Although EtO gas-based sterilization is widely practiced, there is a

concern with residual EtO in the filters, membranes etc. No such concern exists with γ-radiation. However, one has to ensure that the membrane in the MF device has not been degraded by radiation. Thus the behavior of any new MF membrane when exposed to a variety of solvents and radiation treatment is of significant interest. A fluoropolymer, such as polytetrafluoroethylene (PTFE), which is almost completely inert to almost any chemical/oxidative environment, should be of great interest. However, PTFE is quite expensive, notoriously difficult to process, and vulnerable when exposed to irradiation [4]. A search has gone on for alternate fluoropolymer candidates having desirable properties and possessing easy processability.

Another important membrane-based separation application is pervaporation. In such an application, tri-n-octylamine (TOA) was used by Thongsukmak and Sirkar as a liquid membrane (LM) immobilized in the pores of polypropylene hydrophobic hollow fibers [28, 29] without a direct contact with the aqueous feed solution; they reported that the TOA-based LM showed extraordinarily high selectivity of butanol, acetone and ethanol over water [28] in pervaporation, as well as excellent extended-term stability [29]. One wonders about the effect of TOA on the polymer substrate on a long-term basis. Systematic adoption of ECTFE membranes for a wide range of applications requires knowledge of a variety of its properties. These include: (1) resistance to common organic solvents over a range of temperatures in filtration applications of pharmaceutical manufacturing of active pharmaceutical ingredients (APIs), chemical industry and semiconductor processing; solvents of interest include methanol, ethanol, 2-propanol, 1-butanol, ethyl acetate, isopropyl acetate, acetone, heptane, toluene, THF, acetonitrile, p-xylene, chlorobenzene and TOA. Among these, the effects of the following solvents, methanol, ethanol, 2-

propanol, 1-butanol, THF, toluene, acetonitrile, and TOA, were studied here more extensively; (2) resistance to pH variations especially due to NaOH and amines; (3) stability to oxidation environments including exposure to radiation; (4) effect of mechanical and other processing conditions on the microporous membrane structure and strength; (5) its hydrophobicity influenced by a variety of foulants in filtration applications as well as application to membrane distillation.

Membrane solvent extraction (MSX) [30-32] has been commercially used for the extraction of highly pure precious metals such as platinum [33]. In such applications, TOA is added to the organic phase diluent as a cation exchanger or carrier with the formation of ion-pair with a proton [30, 34, 35]. Thus, it is crucial to know how the ECTFE membrane performs in the environment of organic solvents/diluents containing TOA. It has to be mentioned that in MSX, TOA used was in a TOA-solvent mixture instead of pure TOA. Considering the possibility of defects in ECTFE membranes caused by pure TOA observed in this study (see Chapter 3), less effect is expected when ECTFE membranes are utilized in TOA-containing solvent systems. Sato et al. have successfully carried out extraction of divalent metals, manganese (Mn), cobalt (Co), copper (Cu) and zinc (Zn) from hydrochloric acid solutions [36] as well as uranium (U) from aqueous UO_2Cl_2 solution [37] with TOA in benzene. Desai and Shinde [38] have developed a method for the extraction of thorium (Th) and cerium (Ce) using 5% of TOA solution from a 0.1 M succinic acid solution. Wardell et al. [39] reported the values of the distribution factor for acetic acid in chloroform with different ratios of TOA. Xylene [31], benzene [36, 37] and kerosene [33, 34] are widely used organic solvents along with TOA in solvent extraction. It is also mentioned by Kubišová et al. [32] that with TOA addition, the mass transfer rate of

heterocyclic carboxylic acid in MSX (called pertraction by them) varies in different media; this can be used to adjust the distribution coefficient in a certain system based on the target. Therefore, it is necessary to evaluate how ECTFE membranes act in TOA-solvent mixtures for such applications. Such results will also be useful potentially for evaluating the use of ECTFE membranes for membrane contactor application in gas-liquid containing for CO_2 removal

Another aspect of importance in applications involving membrane solvent extraction or supported liquid membranes involves the effect of radiation on the polymer when extractions of dilute radioactive compounds are to be undertaken; TOA is often employed with diluents in such applications. The radiation resistance of the polymer becomes important in such applications. Ohno et al. have successfully extracted iodine (I), bromine (Br) [40] and thorium (Th) [41] in biological materials with TOA-xylene mixture, and determined by means of neutron-activation analysis. Patkar et al. [42] reported using the mixture of N-n-octylaniline and TOA in xylene to extract thorium (Th) from aqueous sulfuric acid medium. With its inherently strong hydrophobicity, ECTFE-based microporous membranes are then likely to be useful for MSX applications involving radioactive species.

1.3 Microfiltration

Membrane is a selective separation barrier, which allows some component(s) to pass through but ideally prevents the rest [43] when some driving force is applied. The driving force is usually a difference in hydraulic pressure, partial pressure, composition or an electrical potential gradient or temperature across the membrane. Applications of

membranes for liquid separations have been widely developed resulting in a variety of membranes for reverse osmosis (RO), nanofiltration (NF), ultrafiltration (UF), microfiltration (MF), etc. based on the nominal pore size of the membrane. The pore size of MF membranes is about 0.02 – 10 μm. A relatively low feed operating pressure of approximately 103 – 414 kPa (15 – 60 psig) can be applied to the feed for separation by a MF membrane. An extensive earlier review of various aspects of MF are available in Chapters 31-34 of Ho and Sirkar [44].

For dead-end microfiltration of microbial suspensions, Foley [45] has done a review of various factors, including cell size and shape, cell surface properties, ionic environment, fermentation medium components and aging effects, affecting filter cake properties. In cross-flow microfiltration study by Field et al. [46], the concept of critical flux was introduced. It is the flux below which membrane fouling does not occur; however, above it a decline of flux is observed with time [46]. Theory, experiments and applications of critical and sustainable fluxes have been reviewed by Bacchin et al. [47]. Suspensions of silica, yeast, clay, latex, organic matter, etc. have been studied. However, the medium of most suspensions in the studies reported in open literature is water. Results of MF investigation in organic solvents have been rarely reported. Solvent filtration is an important industrial process. It is widely used in pharmaceutical manufacturing, chemical processing industry, semiconductor industry, auto assembly etc.

A most important application of MF membranes involves microfiltration of aqueous and organic solutions. There are numerous applications of MF in aqueous systems using micron-size, submicron and nanoparticles in chemical processing, dairy products, protein products, electronics and semiconductor industries; correspondingly, there are a

large number of publications [48-51]. On the other hand, MF studies in non-aqueous systems are quite limited in open literature. In an MF-based study using Nuclepore polycarbonate membranes [52], Gan et al. reported that with the addition of methanol or ethanol, the flux of two ionic liquids were increased 10-20 times compared with the case without any diluent. Indlekofer et al. have effectively developed a MF membrane reactor for effective retention of solid enzyme particles in an organic system [53]. Therefore, it is necessary and crucial to know the performance of MF membranes in organic media. One of the goals of this study is to initiate such a study using silica nanoparticles in water and study its filtration behavior in membranes previously soaked in ethanol and tri-n-octylamine (TOA). The microporous membrane of interest here is of ECTFE (ethylene chlorotrifluoroethylene). The relative usefulness of ECTFE material-based MF membrane vis-à-vis those of other fully fluorinated and partially fluorinated fluoropolymers has been discussed earlier. It is very useful to conduct a detailed study of the effects of a variety of organic solvents, pH variations and gamma radiation on the properties of microporous ECTFE membranes; comparison with polyvinylidene fluoride (PVDF) based membranes may also be carried out for selected properties.

In general, membrane thickness, porosity, nominal pore size, liquid entry pressure (LEP), bubble point pressure, maximum pore size etc. need to be characterized for a given membrane [54]. Moreover, the behavior or structure of membranes in severe environment such as organic solvents, caustic solutions and radiation exposure also needs to be considered. This thesis proposes to focus on the basic characterizations of microporous ECTFE membrane, as well as the changes of properties after exposure to severe environments such as aggressive organic solvents, pH variations and radiation exposure.

Some of the properties are to be compared also with membranes of another common fluoropolymer, PVDF. Microfiltration behaviors are also to be studied and analyzed.

1.4 Goal of the Dissertation

Microporous polymeric membranes with pore size in the range of 0.02 to 10 μm and usually identified as microfiltration (MF) membranes are used in a variety of industrial applications. The largest applications are usually limited to pore size no lower than 0.1 μm. These applications include separation, purification, concentration, sterilization and barrier applications; also included are sampling and analytical applications [27]. A particular MF membrane is selected for a particular use and therefore must possess the requisite properties. For example, complete bacterial retention by 0.22 μm rated MF membrane filter is essential for parenteral sterilization, aseptic processing, water for injection etc. For conventional MF applications, the membrane properties of pore size, porosity, and wetting behavior are of primary importance. In solvent-based MF applications, one would in addition look for membrane properties such as chemical resistance, sorption characteristics, thermal stability, mechanical strength, extractability etc. Membrane manufacturing considerations will emphasize ductility, processability and strength among others. In applications requiring sterilization of MF devices before use, the membrane must be stable to sterilization by steam, ethylene oxide (EtO) gas and γ-radiation.

A word about contact angle and hydrophobicity is important. Among MF membranes, PTFE membranes possessing high chemical and solvent resistance, are highly hydrophobic with a high contact angle; therefore, the value of liquid entry pressure (LEP) is high. This is a significant opportunity for a hydrophobic MF membranes having high

solvent and chemical resistance with a somewhat lower contact angle and easier wetting. Further recent applications of MF membranes for desalination by membrane distillation require inexpensive hydrophobic membranes with a reasonably high contact angle. This is useful for both direct contact membrane distillation (DCMD) and vacuum membrane distillation (VMD) [55, 56].

The changes in the properties of a flat ECTFE membrane exposed to a variety of environments were carried out in a variety of ways. In terms of solvent exposure, the tests carried out here included static solvent sorption studies and pH exposure studies. Exposure to specified radiation was followed by studies of morphological change and determination of changes in mechanical properties such as tensile strength/modulus. Liquid entry pressure was measured to evaluate pH-variation induced change. Maximum pore size was estimated by wetting properties including LEP and contact angle. Porous surface topology of virgin and solvent-soaked ECTFE membranes was investigated by atomic force microscopy (AFM).

This study focuses on the basic characterizations of microporous ECTFE membrane, as well as the changes of properties after exposure to severe environments such as aggressive organic solvents, pH variations and irradiations. Some of the properties were also compared with membranes of another common fluoropolymer, PVDF. The general questions addressed in this thesis are the following. How good is an ECTFE membrane under a variety of exposure conditions? How does its behavior compare with those of the commonly used PVDF membrane having the same mean pore size for selected properties? The interaction between solvents, especially TOA, and ECTFE membrane, as well as the effects of solvent-soaking of the membrane on the MF behavior of silica nanoparticle

suspension in a 25% mixture of an organic (ethanol) solution in water were also studied. These characterization are expected to facilitate use of microporous ECTFE membranes in selected applications.

CHAPTER 2

EXPERIMENTAL

2.1 Materials and Chemicals

Hydrophobic ECTFE membrane (3M, St. Paul, MN) with a nominal pore size of 0.2 μm and thickness of ~ 0.005 cm (0.002 in) was used in this study. Dense ECTFE sheets (3M, St. Paul, MN) with thickness between 0.05 cm (0.021 in) and 0.09 cm (0.035 in) were also used for specific experiments. Some tests included γ-irradiated ECTFE membranes (3M, St. Paul, MN) subjected to radiation strengths of 25 kGy, 35 kGy and 45 kGy. For a given series of tests, membrane samples were randomly taken from the same axial location in the membrane roll provided by 3M Corporation (St. Paul, MN). No consideration was made about the location of the sample across the roll width. Hydrophobic PVDF membranes with a nominal pore size of 0.2 μm provided by MilliporeSigma (Bedford, MA) were used to compare the solvent and thermal resistance as well as the wetting behavior with those of ECTFE membranes. Dense sheets of PVDF were provided by MilliporeSigma (Bedford, MA). Organic solvents methanol, ethanol, 2-propanol, 1-butanol, ethyl acetate, isopropyl acetate, acetone, heptane, toluene, THF, acetonitrile, p-xylene, chlorobenzene, TOA and sodium dodecyl sulfate (SDS) used as surfactant, were from Sigma-Aldrich (St. Louis, MO). Sodium hydroxide powder (Fisher Scientific, Pittsburgh, PA) was used to prepare NaOH solutions for caustic soaking treatment with ECTFE membranes. Aerosil 200 hydrophilic silica nanoparticles with primary size of 12 nm were from Evonik Corporation (Parsippany, NJ). During manufacturing, four such particles get fused together very often; therefore, the dominant primary size is 48 nm.

2.2 Membrane Treatment

Many solvents were used to study solvent sorption behavior of ECTFE membranes. Some of the solvents (methanol, ethanol, 2-propanol, 1-butanol, THF, toluene, acetonitrile, xylene, TOA and xylene80/TOA20-soaked (mixture of 80% (weight fraction) xylene and 20% TOA) were also selected to study their effect on membranes in so far as wetting, thermal and mechanical properties are concerned. In solvent related tests, unless otherwise noted, membranes were soaked in the desired solvent at room temperature for overnight; then they were taken out and left exposed in lab hood for at least three days for further study.

The pH effect on wetting properties (contact angle, liquid entry pressure and bubble point pressure) of ECTFE membranes were conducted by soaking ECTFE membranes at room temperature in 1M, 2M and 3M NaOH solutions (prepared by dissolving sodium hydroxide powder in deionized water) for three days. Then the membranes were dried completely for further study. Unless otherwise noted, each measurement was repeated at least three times.

2.3 Solvent Sorption Study

2.3.1 Solvent Sorption Tests of ECTFE Membranes

ECTFE membranes having dimensions of 2.54 cm x 5.08 cm (1 in x 2 in) were used in solvent sorption tests with methanol, ethanol, 2-propanol, ethyl acetate, isopropyl acetate, acetone, heptane, toluene, acetonitrile, p-xylene, THF, chlorobenzene and TOA for overnight soaking. The membrane weights before and after soaking were respectively recorded as m_1 and m_2; these were measured using a balance (Cole-Parmer PA 120, Vernon

Hills, IL). The formulas used to calculate the percent weight gain of microporous ECTFE membrane (W_p) are given below:

$$m_1 = (1 - \varepsilon)\, \rho_{\text{base material}}\, V \tag{2.1}$$

$$m_2 = m_1 + \varepsilon\, V \rho_{\text{solvent}} + m_s \tag{2.2}$$

$$W_p = \frac{m_s}{m_1} \text{ x } 100\% \tag{2.3}$$

Here, ε is the porosity of ECTFE membrane; $\rho_{\text{base material}}$ is the density of raw ECTFE polymer for fabricating ECTFE membrane; m_s is the weight gain due to solvent sorption. The value of the base material density has been mentioned in Section 2.4.1; the value of the porosity is reported in Section 3.2. This calculation method assumes that the porosity is unaffected by membrane swelling.

Sorption coefficient (S_{im}) or solubility coefficient is also a parameter illustrating the extent of solubility of a solvent species in a membrane. Equations (2.4-2.6) show the calculation of solubility coefficient for porous ECTFE membrane with various solvents.

$$V_s = \frac{m_s}{\rho_{\text{solvent}}} \tag{2.4}$$

$$V_m = V\,(1 - \varepsilon) \tag{2.5}$$

$$S_{im} = \frac{V_s}{V_m\, P_{vap}} \tag{2.6}$$

Here, V_s is the volume of solvent that is soaked in the solid membrane phase; V_m is the actual membrane volume; P_{vap} is the vapor pressure of each solvent at the testing temperature.

2.3.2 Solvent Sorption Tests of Nonporous ECTFE Membranes

Tests using dense ECTFE sheets having a diameter of 1.3 cm (0.5 in) were conducted using selected solvents including methanol, ethanol, 2-propanol, 1-butanol, THF, toluene, acetonitrile and TOA. The percent weight gain (W_d) for the nonporous ECTFE sheet was calculated from Equation (2.7) where m_1' and m_2' are the sample weights before and after soaking, respectively.

$$W_d = \frac{m_2' - m_1'}{m_1'} \text{ x } 100\% \qquad (2.7)$$

2.4 Membrane Characterization

2.4.1 Membrane Porosity

Membrane porosity is the ratio of the pore volume over the entire membrane volume. The porosity (ε) of ECTFE membrane was measured using Equations (2.8-2.9) [57]. A circular sample 47 mm in diameter (d) was cut out. Eight such membranes were placed one on top of another. The overall membrane thickness (t) and mass (m) were respectively measured using a caliper (Model No. CD-6" CSX, Mitutoyo, Japan) and a balance (Cole-Parmer PA 120, Vernon Hills, IL). The density of the base ECTFE polymer ($\rho_{base\ material}$) is 1.71 g/cm^3 [58] (1.68 g/cm^3 was found for Halar® ECTFE [22, 25]).

$$\rho_{sample} = \frac{m}{\frac{\pi}{4} d^2 t} \quad (2.8)$$

$$\varepsilon = \left(1 - \frac{\rho_{sample}}{\rho_{base\ material}}\right) \text{x } 100\% \quad (2.9)$$

2.4.2 Scanning Electron Microscopy (SEM)

LEO 1530 VP field emission scanning electron microscope (Carl Zeiss Inc., Peabody, MA) was used to study the membrane surface texture. Measurements were conducted on virgin and solvent-soaked ECTFE and PVDF membranes, as well as irradiated (25 kGy, 35 kGy and 45 kGy) ECTFE membranes under the kinetic energy of electron beam from 3 kV to 10 kV. In general, the higher the kinetic energy, the higher is the resolution of the image. All membrane samples were coated with carbon or Au/Pd (20/80) using a turbo-pumped sputter and carbon coater (EMS 150T ES, Hatfield, PA) prior to image collecting; this was done to improve the conductivity and prevent charging of the membrane surface.

2.4.3 Atomic Force Microscopy (AFM)

A NX 10 atomic force microscope (Park Systems Inc., Santa Clara, CA) was used to collect the topography images of virgin, ethanol-soaked and TOA-soaked ECTFE membranes with a silicon cantilever. The AFM images were collected in non-contact mode and analyzed via XEI data processing & analysis software (Park Systems Inc., Santa Clara, CA). It has to be mentioned that AFM provides a more real morphology than scanning electron microscope (SEM). This is due to the fact that before SEM image capture, polymeric membranes need to be coated with a conductive layer, which could cause the

membrane to become more vulnerable especially with residual solvents in membrane pores.

2.4.4 Wetting Properties

Contact angle (θ) or wetting angle is the angle between the liquid-vapor interface and the solid surface when a drop of water is placed onto a solid surface. In general, the larger the contact angle, the more hydrophobic is the solid surface. When θ equals to 0^o, it means the solid surface is super-hydrophilic; when θ is more than 150^o it indicates that the solid surface is super-hydrophobic. It is an easy and quick way to roughly estimate if the membrane surface is hydrophobic or hydrophilic. The contact angle for porous ECTFE and PVDF membranes, as well as nonporous ECTFE and PVDF films, were measured by an optical tensiometer (Model No. A 100, Rame-Hart Inc., Succasunna, NJ). Around 10 μL liquid was dropped on the membrane sample surface. The liquid drop was adjusted to be clearly observed in the eye lens. Even if there is no measuring device available, one can still add a drop of water on the solid surface to roughly estimate how hydrophilic or hydrophobic the solid surface is by looking at the shape of the bubble. It is a convenient way to tell if the solid surface is hydrophobic or hydrophilic.

Liquid entry pressure is the minimum pressure to force liquid to pass through the largest pores of a hydrophobic membrane. It can provide useful information such as, at what pressure or what liquid (the surface tension of such liquid supports the pressure drop across the vapor-liquid interface) can make the membrane get wet. With such information, undesired wetting in some membrane applications could be avoided as has been illustrated recently for VMD in great detail [56].

The apparatus for LEP measurement is shown in Figure 2.1 (a). The setup consists of a N_2 cylinder, a pressure gauge, a reservoir (Model No. 304L-HDF4-75, R.S. Crum & Company, Mountainside, NJ), and a measuring cell (Model No. XX4404700, MilliporeSigma, Bedford, MA). A membrane sample having a diameter of 47 mm was placed on top of an underdrain screen (Model No. 5614, MilliporeSigma, Bedford, MA) and a support screen (Model No. XX4204709, MilliporeSigma, Bedford, MA). Next, another underdrain screen was placed on top of the sample in the sample cell. The reservoir was filled with the desired liquid. Then, pressure was slowly increased stepwise until liquid came out at the bottom of the cell. Untreated ECTFE and PVDF membranes were measured using aqueous alkanol solutions, which were the same as used in the contact angle measurements. ECTFE membranes were also soaked in NaOH solutions with the concentration of 1M, 2M and 3M for three days to study the effect of pH variations on LEP. Each measurement was repeated at least three times.

Bubble point pressure is the minimum pressure at which a continuous stream of bubbles is observed downstream of a wetted membrane under gas pressure. It is a widely used method to determine the maximum pore size. It is a key indicator of the sterilization capability of the membrane. It has to be mentioned that this method is independent of the measuring liquid; however different liquids could provide different results probably due to wetting effects [59]. The apparatus for bubble point pressure measurement is shown in Figure 2.1 (b). A sample was cut out as a circle of diameter 47 mm. Pressure was increased slowly until a steady state (bubbles come out one by one continuously) was reached. Measurements were conducted on untreated ECTFE and PVDF membranes using aqueous ethanol and 2-propanol solutions. Irradiated ECTFE membranes were characterized using

pure ethanol and 2-propanol. ECTFE membranes were also soaked in NaOH solutions with the concentrations of 1M, 2M and 3M for three days to study the effect of pH variation on bubble point pressure. The accuracy of the pressure gauge was ± 0.1 psi (689 Pa). Each measurement was repeated at least three times.

The relationship between the bubble point pressure (P_{bp}) and the maximum pore diameter (d_{max}) is shown in Equation (2.10), where γ is the surface tension of the measuring liquid, θ is the contact angle of the liquid on the pore wall. Here, θ equals to 0 because 2-propanol perfectly wets ECTFE membranes; this is supported by previous liquid entry pressure measurements that 20% 2-propanol (80% water) is good enough to completely wet ECTFE membranes. It has to be noted that this method is independent of what measuring liquid is used; however, it may generate different pore diameters because of the different wetting effects of different solvents with the membrane. Here, the solvent effects on the P_{bp} and the d_{max} were studied.

$$d_{max} = \frac{4\gamma \cos\theta}{P_{bp}} \tag{2.10}$$

These indicators of wetting properties of untreated ECTFE and PVDF membranes were measured using aqueous ethanol, 2-propanol and 1-butanol solutions with different ratios of alkanols. These systems are useful because sometimes a membrane has to be used in an aqueous environment with alkanols or sometimes a membrane needs to be wetted in an aqueous environment, which could be achieved by adding some alkanols. Therefore, one needs to know what concentration of alkanol is the minimum concentration and what

pressure is the minimum pressure to wet the membrane. The irradiation effect on bubble point pressure was studied using pure ethanol and 2-propanol.

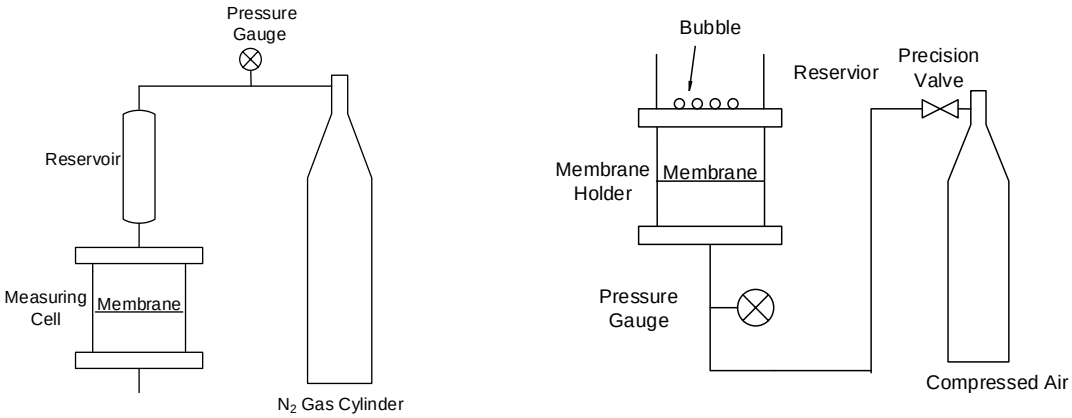

(a) (b)

Figure 2.1 Experimental set-ups for (a) LEP and (b) bubble point pressure measurements.

2.4.5 Thermal Properties

The effects of solvent and irradiation on thermal properties of ECTFE (and PVDF) membrane(s) were studied using differential scanning calorimetry (DSC, 4000, Perkin Elmer, Shelton, CT), thermogravimetric analysis (TGA, Pyris 1, Perkin Elmer, Waltham, MA) and dynamic mechanical thermal analysis (DMTA, IV, Rheometric Scientific, now TA Instrument, New Castle, DE).

The DSC technique measures the difference in heat flow between a sample and an inert reference as a function of temperature. In a DSC thermogram, the peak indicates the melting/crystallization temperature and the area of the peak indicates the melting/crystallization enthalpy. In the current study, a sample weighing 3 to 10 mg was placed and sealed in an aluminum pan and then heated/cooled under N_2 flow at a flow rate of 20 mL/min under heat-cool-heat cycle; the solvent effect was studied in the first heating and whether the corresponding effect was reversible or not was explored in the second

heating. For ECTFE membranes, the sample was first heated from 20°C to 280°C, then followed by cooling from 280°C to 20°C, which was followed by second heating from 20°C to 280°C. It has to be mentioned that the initial temperature for TOA-soaked ECTFE membrane was -60°C, instead of 20°C. For PVDF membranes, the sample was first heated from -60°C to 210°C, then followed by cooling from 210°C to - 60°C, and then followed by second heating from -60°C to 210°C. All heating and cooling rates were 10°C/min. Each measurement was repeated at least twice.

In addition, the degree of crystallinity (X_c) can be calculated from the data obtained from DSC, as shown in Equation (2.11):

$$X_c = \frac{(\Delta H_m - \Delta H_c)}{\Delta H_m^o} \times 100\% \qquad (2.11)$$

Here, ΔH_m and ΔH_c are the melting and crystallization enthalpies, respectively; ΔH_m^o is the melting enthalpy of the sample with 100% crystallinity.

In TGA studies, the thermal degradation of the membrane and whether there was residual solvent in membrane pores or not were tested. Virgin (porous and dense) and solvent-soaked ECTFE as well as PVDF membranes weighing from 3 mg to 10 mg were heated from 30°C to 370°C at a heating rate of 10°C/min under a 10 mL/min N_2 flow rate. It has to be mentioned that 370°C is not high enough to decompose either ECTFE or PVDF membranes. However, the degradation of fluorine-containing polymer would generate hazardous compound(s) so that measurements were ended at 370°C. It has to be mentioned that the length of the drying period for TOA-soaked membranes was the same as that in DSC analysis. Selected ECTFE membrane samples were heated to 800°C to study the full degradation behavior.

Solvent effect on glass transition temperature (T_g) was conducted via DMTA. Virgin and solvent-soaked ECTFE membranes were ramped from 0°C to 160°C with a ramping rate of 3°C/min. A strain of 1.0% and a frequency of 1 Hz were applied. The value of T_g can be determined from the peak point of tan δ vs. temperature curve where tan δ is defined as the ratio of loss modulus (E") over elastic modulus (E').

2.4.6 X-Ray Diffraction (XRD)

XRD analysis was conducted using a X-ray diffractor (Empyrean, Philips, Westborough, MA) equipped with Cu Kα (λ = 1.54 Å). Virgin, as well as solvent-soaked ECTFE and PVDF membranes were scanned from 5° to 50° with a step size of 0.02° under the operating condition of 45 kV and 40 mA. Each measurement was repeated at least twice. From the XRD pattern, the degree of crystallinity (X_c) can be calculated from the following equation:

$$X_c = \frac{A_{crystalline}}{A_{crystalline}+A_{amorphous}} \times 100\% \quad (2.12)$$

Here, $A_{crystalline}$ and $A_{amorphous}$ are the areas of the crystalline part and the amorphous part, respectively. It is an important parameter for a polymer sample or polymeric membrane. Samples with higher crystallinity would have better mechanical properties because the polymer chains are highly ordered. This would give liquid molecules a smaller chance to penetrate into when exposed to solvents.

2.4.7 Fourier Transform Infrared (FTIR) Spectroscopy

The interaction between solvent and membrane was investigated using a Nicolet ThermoElectron FTIR 560 spectrometer with a Miracle attenuated total reflectance (ATR)

platform assembly and a Germanium (Ge) plate. Each sample was measured with 32 scans in total within the range from 4000 to 600 cm^{-1}.

2.4.8 Raman Spectroscopy

The solvent effects on ECTFE membranes were also studied with Raman spectra collected using a Thermo Scientific Raman microscope (DXR, Waltham, MA) with a 532 nm laser. The laser power was set at 10 mW for all measurements.

2.4.9 Dielectric Relaxation Spectroscopy

Dielectric relaxation spectroscopy measurements were conducted using a broadband dielectric spectrometer (BDS-80 Novocontrol, Berlin, Germany). It measures the amplitude of the charge-density fluctuation of a sample under electric field. A membrane sample with a diameter of 1.9 cm (0.75 in) was placed between two electrodes in the low frequency module at room temperature. The complex dielectric permittivity (ε) of a material is expressed as $\varepsilon = \varepsilon' - i\,\varepsilon''$ where ε' is the real part or the dielectric constant, while ε'' is the imaginary part or energy loss. The effect of irradiation on ECTFE membrane was studied.

2.4.10 Tensile Test

Tensile tests were conducted using a texture analyzer (TA-XT2, Stable Micro Systems Ltd., Surrey, UK). Membrane samples with dimensions of 100 mm x 20 mm were pulled in the machine-driven direction at a strain rate of 0.0166%/s until break point was reached. Young's modulus was determined from the slope in a plot of the stress against the strain in the elastic region. Measurements were conducted on virgin, solvent-soaked, and irradiated ECTFE membranes. Each measurement was repeated at least four times.

2.5 Microfiltration Study

In general, there are two flow modes, (a) dead-end (DE) and (b) cross-flow (CF) in microfiltration (MF), as shown in Figure 2.2. The experimental set-up in Figure 2.2 (a) is the same as the one used in LEP measurements. In Figure 2.2 (b), the feed suspension was pumped through the CF cell using a peristaltic pump (Model No.: 7554-90, Cole Parmer, Vernon Hills, IL). The feed which cannot pass through the membrane, the retentate, will go back to the reservoir for recycling. Aqueous and organic silica nanoparticle suspensions were used in this study.

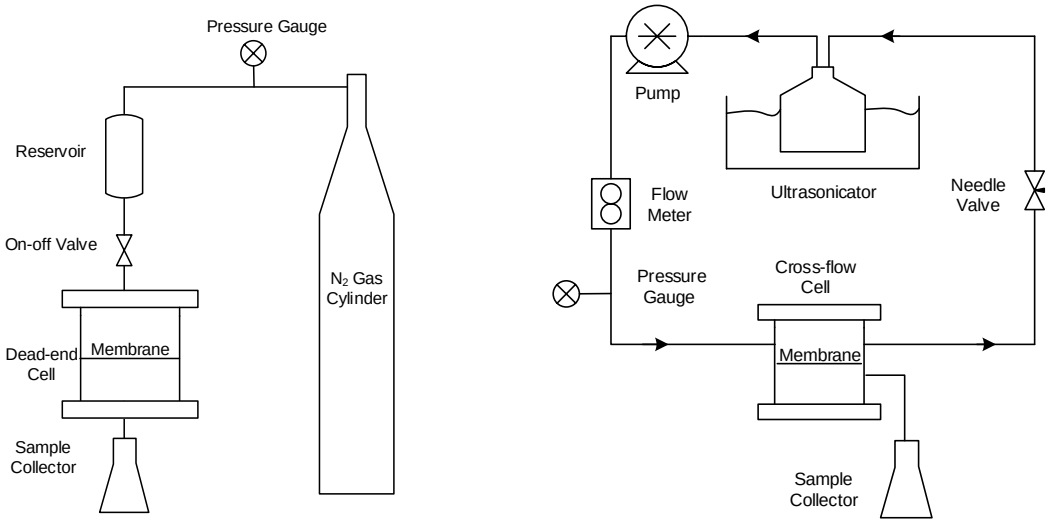

(a) (b)

Figure 2.2 Experimental set-ups for (a) dead-end and (b) cross-flow microfiltration.

2.5.1 Particle Size Distribution Measurement of Silica Suspensions

In dead-end microfiltration (DE-MF), the feed flows into the membrane perpendicularly, while in cross-flow microfiltration (CF-MF), the feed flows along the membrane tangentially. Based on the hydrophobicity of ECTFE membrane, aqueous silica suspension was used in DE-MF, whilst silica suspension in the media of organic or organic mixture

was used in CF-MF. Details of wetting properties of ECTFE membrane are discussed in Section 3.5.

Aqueous and organic silica suspensions were prepared in the same way. Preparation of 60 g of 3.8 ppm aqueous silica suspension is taken as an example to show how the silica suspension was prepared. Around 8 mg of silica was first added to 60 g deionized water (generally the solubility of silica in water is a very low value of 120-150 mg/L [60] based on different structures of silica) with 5 min sonication. This is added to prepare a solution saturated with dissolved silica. This will ensure that the size of silica nanoparticles added will not be affected by dissolution. Then 1 mg sodium dodecyl sulfate (SDS) and 0.23 g of silica nanoparticles were added in the earlier system of 60 g deionized water containing 8 mg silica. After that, the vessel containing the whole suspension was suspended in an ultrasonic cleaner (Model No. 0895-16, Cole-Parmer, Vernon Hills, IL) for 5-min sonication. Then, it was ready for MF test. It has to be mentioned that, the suspension-containing vessel was placed in an ultrasonicator in cross-flow MF measurement all the time to reduce aggregation of nanoparticles. Organic solvents such as ethanol were also used instead of deionized water to make silica suspensions for some of the measurements. In MF tests, samples were collected during a certain length of time. The particle size distribution (PSD) of the permeate was measured using a Malvern Zetasizer (Westborough, MA).

2.5.2 Particle Filtration in Dead-end Microfiltration

In DE-MF, the filtration flux (J in unit of g/(min-cm^2)) was determined using weight (m in unit of gram) divided by time (t in unit of min) and effective area (A in unit of cm^2) of the membrane, as shown in Equation (2.13). It has to be noted that the filtration flux is usually

expressed using volume e.g., L/m^2-h (LMH); however the density/concentration of each filtrate in this study is different. Therefore, it is more convenient to express the filtration flux using mass, instead of volume.

$$J = \frac{m}{A\,t} \tag{2.13}$$

The mechanism of membrane blocking has been previously studied as standard blocking, intermediate blocking and cake model [61-63] shown in Equation (2.14), where J is the filtration flux; J_o is the initial flux; t is the time interval; K and n are constants, which indicate different fouling mechanisms. These are schematically shown in Figure 2.3 [62]. The values of the constant n are 2, 1 and 0.5 for standard blocking, intermediate blocking and cake filtration [61], respectively. Here, a linear plot of $(J/J_o)^n$ against t was made to determine the constants K and n to find out which membrane blocking mechanism was governing.

$$\frac{J}{J_o} = (1 + Kt)^{-n} \tag{2.14}$$

The solvent effect on MF performance was studied based on the filtration flux and the PSD of the filtrate with virgin, ethanol-soaked and TOA-soaked ECTFE membranes. The rejection behavior of the particles is another way to characterize the membrane pore size. The results of PSD measurements for virgin, ethanol-soaked and TOA-soaked ECTFE membranes were obtained using a particle size analyzer (Malvern Zetasizer Nano series, Westborough, MA). It has to be mentioned that the spherical silica nanoparticles used have

a high tendency to agglomerate so that before PSD measurement, each sample was sonicated for 5 min to reduce the agglomeration.

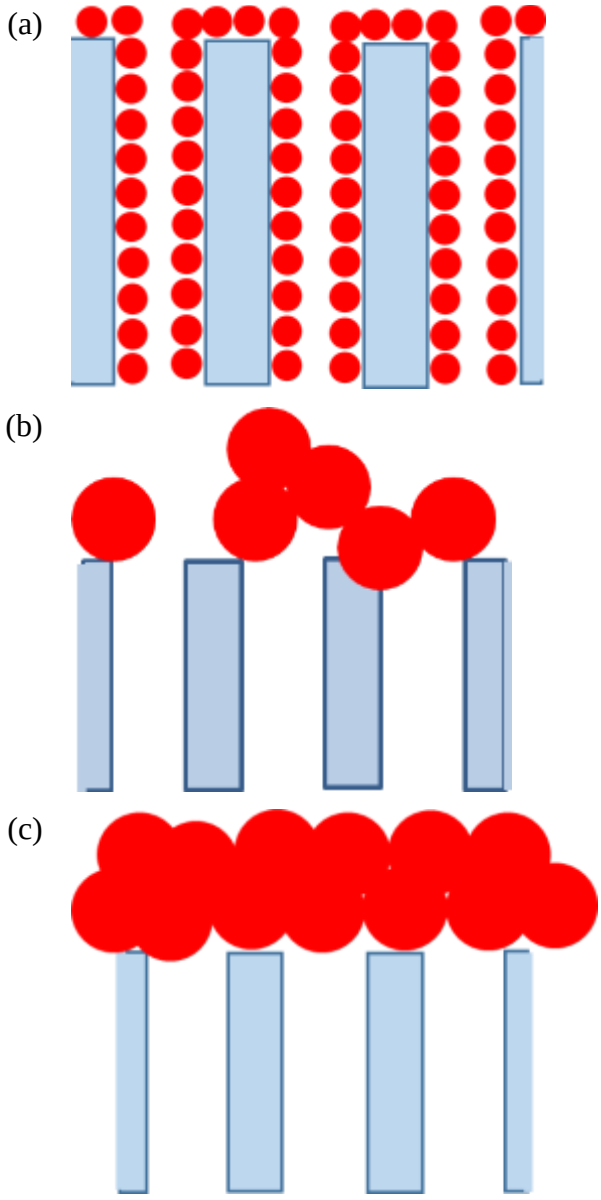

Figure 2.3 Schematic drawing of the fouling mechanisms for (a) standard blocking, (b) intermediate blocking and (c) cake filtration.
Source: [62].

2.5.3 Solvent Filtration in Dead-end Microfiltration

The solvent filtration tests were carried out with pure solvent in a dead-end cell (Model No.:XX4404700, MilliporeSigma, Bedford, MA). The solvents used were methanol, ethanol and 2-propanol. The diameter of the membrane sample was 47 mm, and the effective area (A) of the membrane was 13.8 cm^2. Experiments were conducted by applying N_2 at different pressures (1 psig (6.9 kPag), 2 psig (13.8 kPag), 4 psig (27.6 kPag), 8 psig (55.2 kPag) and 16 psig (110.3 kPag)). The permeates were collected every 30 min and weighed by a balance. The solvent flux (J) was calculated by Equation (2.13). It can also be written as Equation (2.15).

$$J = \frac{Q}{\delta} \Delta P \tag{2.15}$$

Here, ΔP is the applied pressure difference across the membrane; Q and δ are the permeability coefficient and the membrane thickness (~0.005 cm for virgin ECTFE membranes), respectively. The value of Q/δ is the permeability constant or permeance, which can be determined by the slope of a linear plot of J against ΔP.

2.5.4 Particle Filtration in Cross-flow Microfiltration

Due to the hydrophobicity of ECTFE membrane, an organic solvent such as ethanol was added to the suspension to "wet" the membrane. From LEP results of ECTFE membrane (See Section 3.5.2), 57.0 psig is the LEP value of pure water and 7.5 psig is the value of 25% ethanol (75% water). One needs 35% of ethanol to get the membrane wetted.

According to Darcy's law, the permeation flux of a feed across a membrane can be expressed as:

$$J = \frac{\Delta P}{\mu R_t} \tag{2.16}$$

Here, μ is the viscosity of the feed; R_t is the total hydraulic resistance over the entire membrane. For a microfiltration test using suspensions, R_t is usually the sum of three resistances: the resistance caused by membrane itself (R_m), that due to pore blocking (R_p) and the resistance of cake (R_c) [64]. Therefore, Equation (2.16) can be written in the following form:

$$J = \frac{\Delta P}{\mu (R_m + R_p + R_c)} \tag{2.17}$$

Flux decline is a major obstacle in microfiltration. As shown in Equation (2.17) the membrane itself, pore blocking and cake formation could cause fouling. According to Wiesner et al. [65] and Lim et al. [64], the permeation flux based on different fouling mechanisms can be summarized as:

Membrane-resistance-limited: $$\frac{1}{J} = \frac{1}{J_0} + K_m t \tag{2.18}$$

Pore blocking resistance-limited: $$\ln J = -K_p t + \ln J_0 \tag{2.19}$$

Cake resistance-limited: $$\frac{1}{J^2} = \frac{1}{J_0^2} + K_c t \tag{2.20}$$

Here, J_0 is the initial flux; K_m, K_p and K_c are the parameters that are respectively related to the resistance of the membrane itself, the pore blocking and the cake formation.

The reproducibility of CF-MF was examined by collecting the permeates at different time intervals, i.e. 2 min (I), 3 min (II) and 5 min (III) using 3.8 ppm silica suspension in the media of 25% ethanol solution in water. The filtration flux (calculated using Equation (2.13)) and the PSD were measured for each permeate. The effective area of measuring cell was 11.45 cm^2 (diameter = 1.5 in). Moreover, the effects of operating parameters such as transmembrane pressure and suspension concentration on the performance of ECTFE membrane in CF-MF were also conducted. The fouling phenomena of ECTFE membrane were captured via SEM.

CHAPTER 3

RESULTS OF CHARACTERIZATION OF MEMBRANE PROPERTIES OF ECTFE AND PVDF

3.1 Solvent Sorption Results

Solvent sorption results for porous ECTFE membranes and dense ECTFE sheets are summarized in Table 3.1 (a) – (b). The swelling behavior of ECTFE membranes by selected solvents is illustrated in Figure 3.1 (a). Alkanols show relatively lower values, while TOA generates the highest swelling of ECTFE membrane with chlorobenzene coming in next; this result is of significant interest in this thesis. The swelling behavior of porous ECTFE membrane in each solvent involves considerable complexity, such as volatility. Selected solvents can be grouped into polar protic solvent, polar aprotic solvent and nonpolar solvent. Figure 3.1 (b-e) shows the relationship between sorption coefficient and the critical temperature (T_c) based on the selected solvents. Generally, the higher the value of T_c, the higher is the solubility. Alkanols are usually very volatile so that the membrane samples start suffering solvent loss when they were taken out from the solvent while TOA was still present in membrane pores even after several months; this was confirmed later via DSC and TGA analyses. Different results were observed if samples were exposed to air after different intervals. Chapiro et al. [66] reported erratic issues of swelling measurement on PVDF films. Similar issues were observed in the current study.

(a)

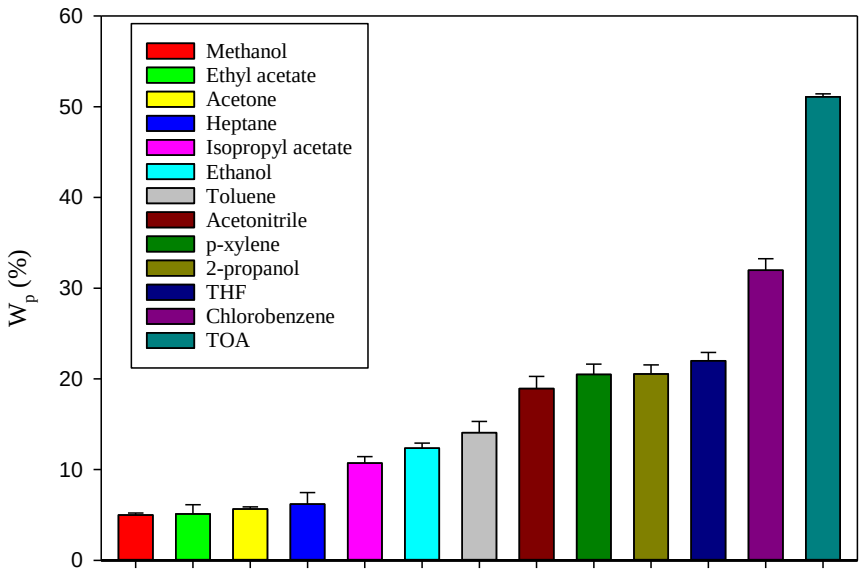

(b)

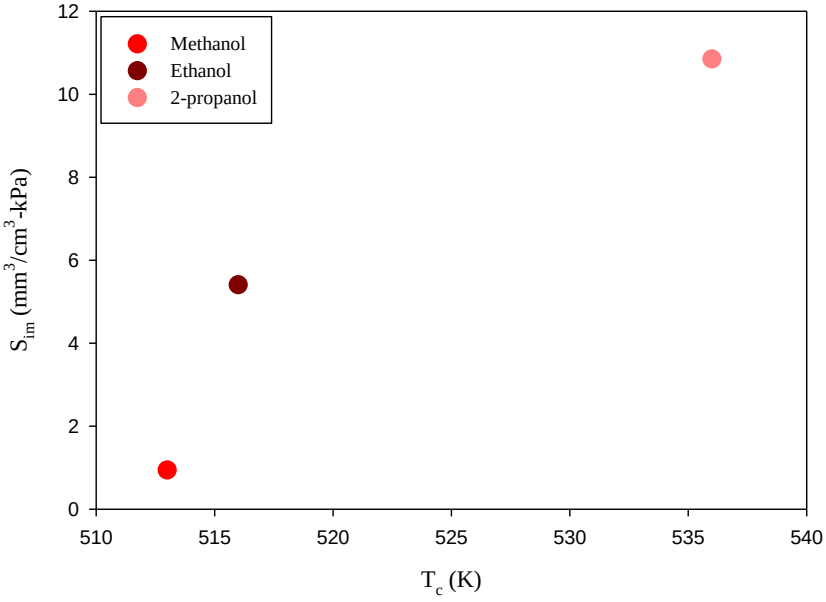

Figure 3.1 (a) Overview of solvent sorption results on ECTFE membranes and (b) the relationship of sorption coefficient with T_c for polar protic solvents (Continued).

(c)

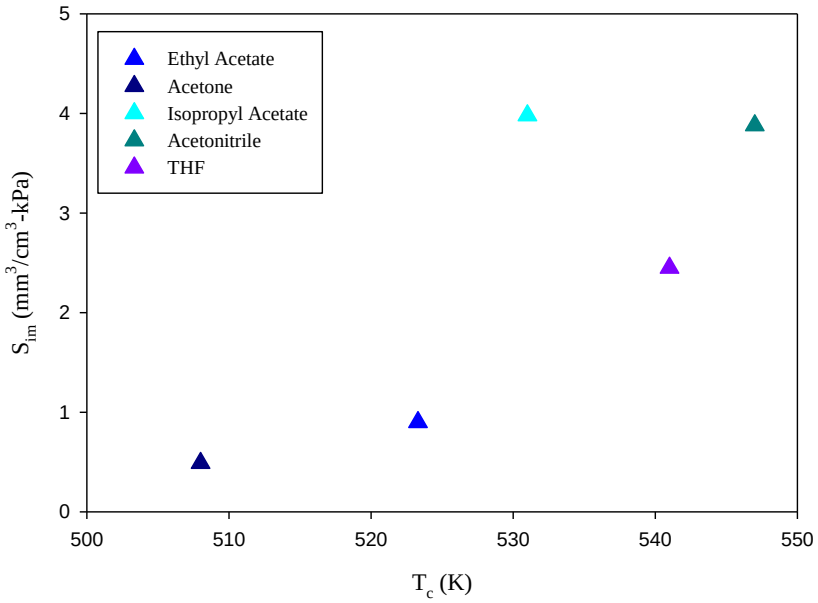

(d)

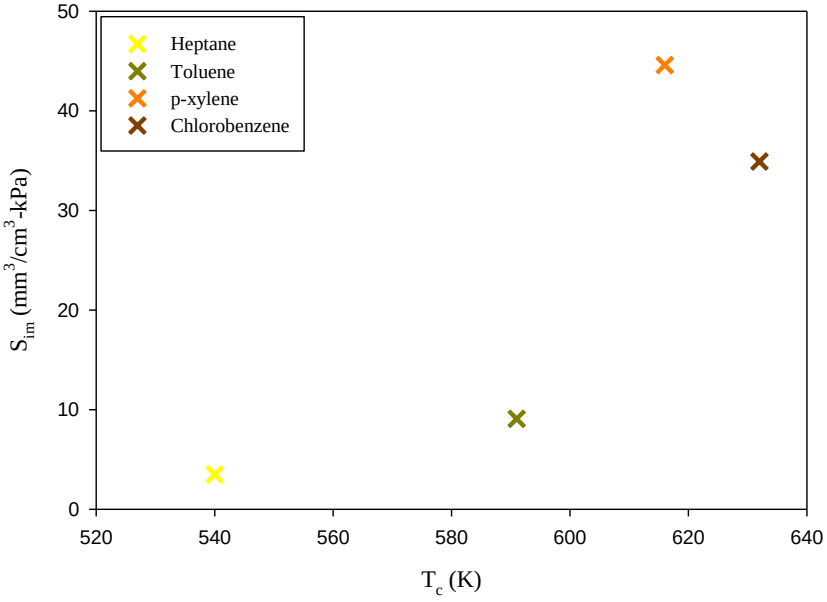

Figure 3.1 The relationship of sorption coefficient with T_c for (c) polar aprotic solvents (d) nonpolar solvents (Continued).

(e)

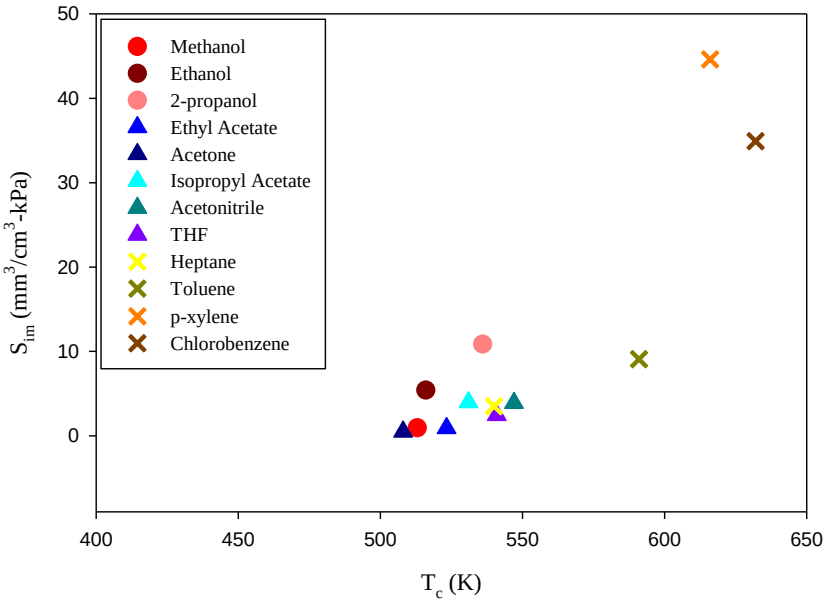

(f)

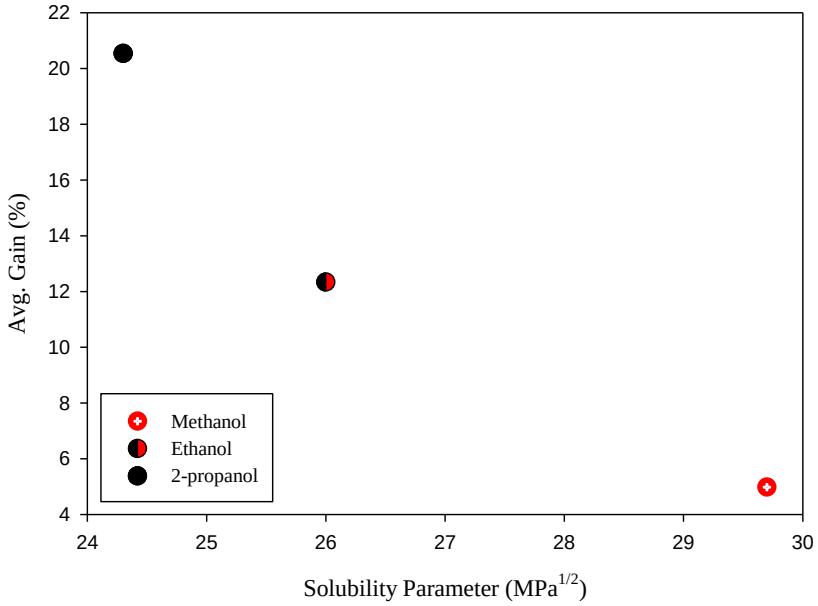

Figure 3.1 (e) An overview of all solvents as well as (f) the correlation of swelling behavior of polar protic solvents with Hansen solubility parameter (Continued).

(g)

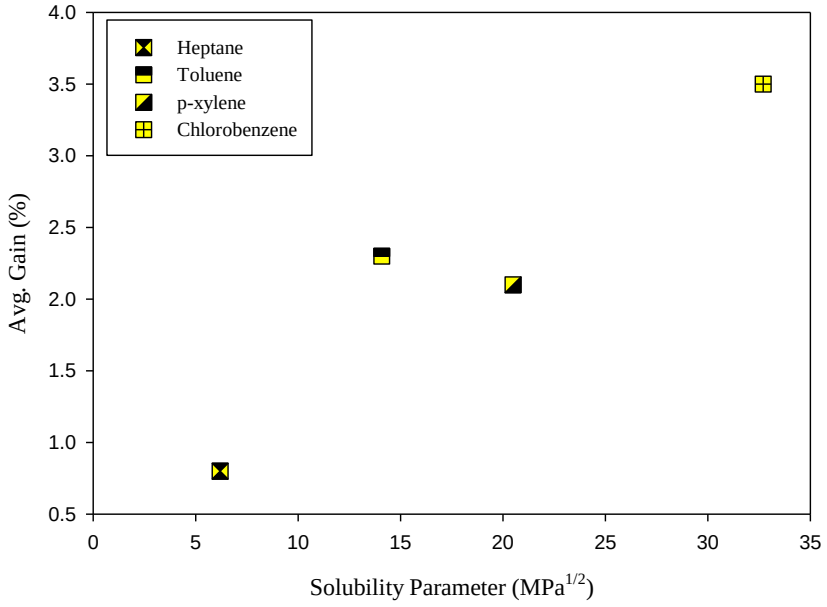

Figure 3.1 (Continued) (g) The correlation of swelling behavior of nonpolar solvents with Hansen solubility parameter.

In addition, the values of surface tension (γ) for selected solvents listed in Table 3.1 are smaller than the critical surface tension ($\gamma_{critical}$) of ECTFE membrane, 32 dyne/cm [67], which is discussed in Section 3.5.2. Only chlorobenzene is an exception in that its surface tension is close to $\gamma_{critical}$ of ECTFE. It is expected that the relatively lower surface tensions of the solvents will make the selected solvents wet ECTFE membrane pores easily. However, there could be some bubbles left in the pores. Moreover, viscosity of TOA is much higher than those of other solvents. Therefore, it is hard to entirely remove the extra TOA on the membrane surface. This could lead to a larger value of m_2 (see Equation (2.2)), which would cause m_s to be larger than its actual value. Thus, it is not a surprise that W_p of TOA is significantly large, whilst W_d of TOA is not (see Equation (2.7)).

Figure 3.1 (f-g) illustrates the relationship of membrane weight gain vs. solubility parameter for polar portic solvents and nonpolar solvents, respectively. Generally, Figure

3.1 (f) indicates that the higher the hydrophobicity of the solvent, the lower is the solubility parameter and the higher is the weight gain. On the other hand, Figure 3.1 (g) shows that alkanes and aromatic solvents having higher hydrophobicity and therefore lower solubility parameter have generally low weight gain. However, these two curves do not show clear trend as is shown in Figure 3.1 (e). Even though solubility parameter has been widely studied with solvent sorption behavior [68-72], all these studies were about the swelling of rubbers. In the current study, for nonpolar solvents, generally, the swelling behaviors of these solvents increase with Hansen solubility parameter [73]. Ebnesajjad reported that the extent of swelling of fluoropolymers, PTFE and FEP, by hydrogen-containing solvents is very limited (less than 1%); therefore, it does not depend on the solubility parameter [74]. Instead it depends on the chemical structure of the solvent; the higher the similarity of the solvent chemical structure and the fluoropolymer structure, the larger the swelling [74]. Moreover, the interaction of ECTFE and the solvents is only physical because the removal of certain halogenated solvents from ECTFE can bring the mechanical properties back to its original state [74].

For solvent sorption tests on nonporous ECTFE films, weight gain of samples in most solvents continues to increase very slowly even after 1 month. The data reported were collected over a 4-week period. It is clear that the swelling of ECTFE by alkanols was very limited. However, THF, toluene and TOA introduced significant swelling of nonporous ECTFE. The ECTFE membranes pores create a very high surface area shown in Figure 3.2. That allows relatively higher swelling with selected solvents.

Table 3.1 Summary of Solvent Sorption Results for (a) Porous and (b) Nonporous ECTFE Membranes

(a) Solvent	Methanol	Ethanol	2-propanol	Ethyl acetate	Isopropyl acetate	Acetone	Toluene
W_p (%)	4.98	12.3	20.5	5.11	10.7	5.53	14.1
STD (%)	0.18	0.46	0.81	0.83	0.58	0.22	1.01
γ (dyne/cm)	22.6	22.8	21.7	23.9	22.3**	23.7	28.5

(a) Solvent	Acetonitrile	Heptane	p-xylene	THF	Chlorobenzene	TOA
W_p (%)	18.9	6.19	20.5	22.0	32.2	51.1
STD (%)	1.09	1.03	0.93	0.74	0.93	0.27
γ (dyne/cm)	29.3	19.8**	28.4	25.0*	33.6	28.8**

(b) Solvent	Methanol	Ethanol	2-propanol	1-butanol	THF	Toluene	Acetonitrile	TOA
W_d (%)	0.20	0.06	0.12	0.16	8.37	4.18	1.36	2.14
STD (%)	0.01	0.01	0.02	0.05	0.10	0.03	0.03	0.12
γ (dyne/cm)	22.6	22.8	21.7	22.1	25.0*	28.5	29.3	28.8

Note: STD means standard deviation; * Taken from Reference [75]; ** Taken from Reference [76]; The rest of γ were taken from [77].

3.2 Membrane Porosity Results

The membrane porosity was measured for virgin and irradiated ECTFE membranes. The weight and the thickness of the eight-layer-membrane assembly were measured. The values of porosity calculated from Equations (2.8-2.9) for virgin and irradiated ECTFE membranes are all ~ 65%. It turns out that the irradiation up to 45 kGy does not have any effect on membrane porosity based on this measurement.

3.3 Scanning Electron Microscopy Results

3.3.1 Solvent Effect on ECTFE and PVDF Membranes

Scanning electron microscope is a useful tool to study the subject at submicrometer or nanometer scale. It is convenient to know what happened to the membrane such as swelling or dissolving, after solvent soaking. The surface textures of virgin and solvent-soaked ECTFE membranes are shown in Figure 3.2 (a) - (h), respectively. The scanning electron microscopy (SEM) images of virgin ECTFE membranes with different magnifications are shown in Appendix B. In Figure 3.2 (a) for virgin ECTFE membrane, only a very small amount of pores are observed to be ~ 0.2 μm. However, this is not in conflict with the nominal size of ECTFE membrane, 0.2 μm. The magnification of this SEM image is 20,000 so that the membrane shown in Figure 3.2 (a) is just a tiny piece in a membrane roll. The manufacturing method cannot guarantee that the diameter of every pore is 0.2 μm. The textures shown in Figure 3.2 (b)-(g) are very close to that in Figure 3.2 (a); this indicates the limited effect of these solvents brought about on ECTFE membranes.

However, the structure of TOA-soaked ECTFE membrane illustrated in Figure 3.2 (h) is apparently quite different from that of virgin ECTFE membrane shown in

Figure 3.2 (a). It has to be noted that, there is no apparent difference in surface texture for both sides of ECTFE membrane. During the image capture of TOA-soaked ECTFE membrane, the membrane surface was very vulnerable. It was getting burnt in several seconds after it was exposed to electron beams. The possible reason could be the defect (before SEM sample preparation) caused by TOA. This could also be explained by the interaction between the residual TOA and the coating material, carbon. Therefore, AFM was also used later to study the surface structure and solvent effect on ECTFE membrane; this technique can avoid the potential problem caused by the coating prior to SEM imaging. Similarly, only the texture of TOA-soaked PVDF membrane is different from that of virgin PVDF membrane as shown in Figure 3.3 (a) – (d); the SEM images of ethanol and THF-soaked PVDF membranes look similar to that of the virgin one. More consideration about the effect brought about by TOA on ECTFE and PVDF membranes will be provided during considerations on DSC, TGA, XRD, FTIR and Raman analyses. It has to be mentioned that except for TOA-soaked membrane, the SEM images of other solvent-soaked membranes are similar to those of virgin ECTFE/PVDF membranes. An additional SEM image which can indicate the ECTFE membrane pore size, 0.2 μm, is shown as Figure B1 (d) in Appendix B. There are variations within a roll of ECTFE membrane.

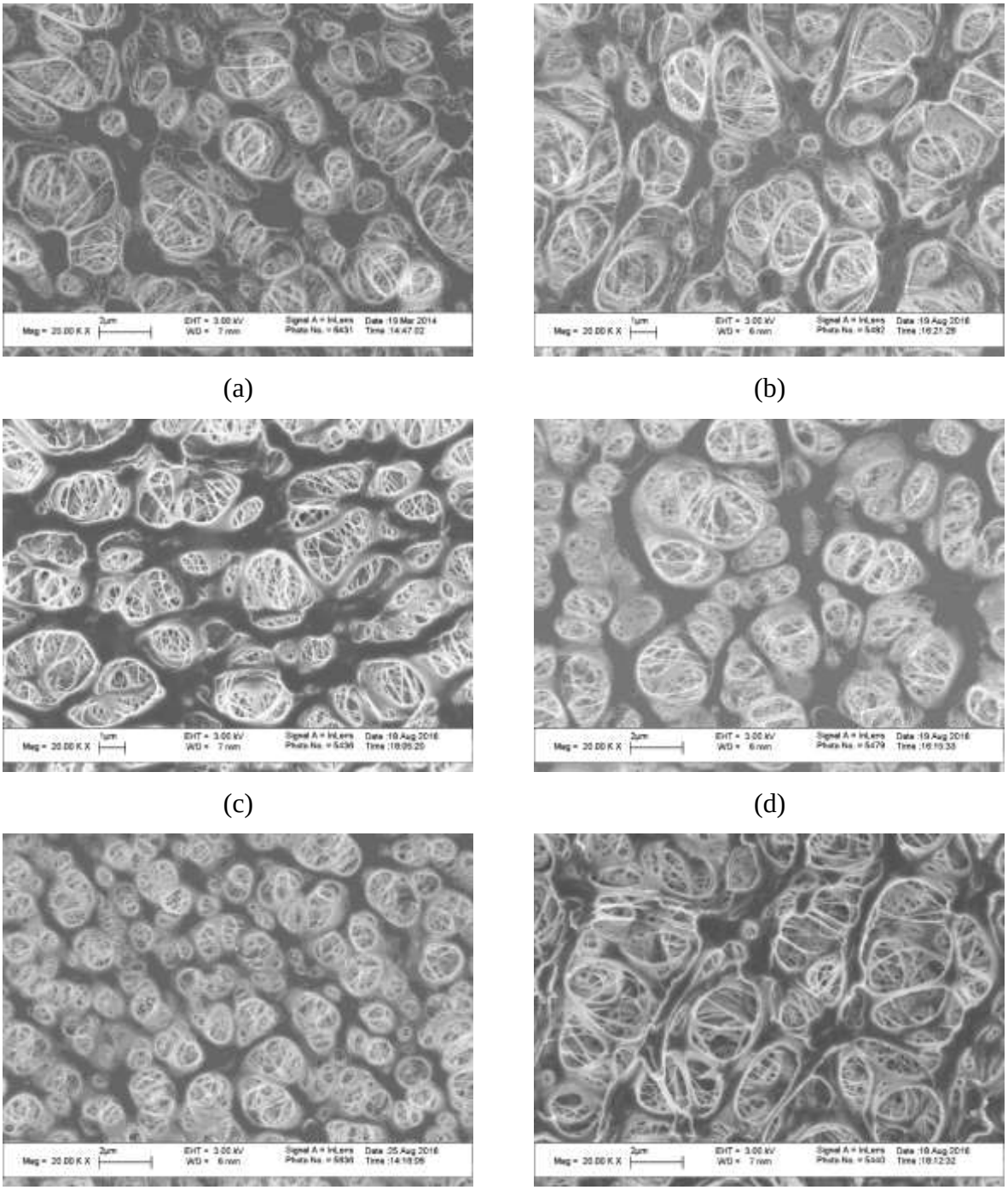

(a) (b)

(c) (d)

(e) (f)

Figure 3.2 SEM surface texture of (a) virgin, (b) methanol-soaked, (c) ethanol-soaked, (d) 2-propanol-soaked, (e) THF-soaked, (f) toluene-soaked ECTFE membranes (Continued).

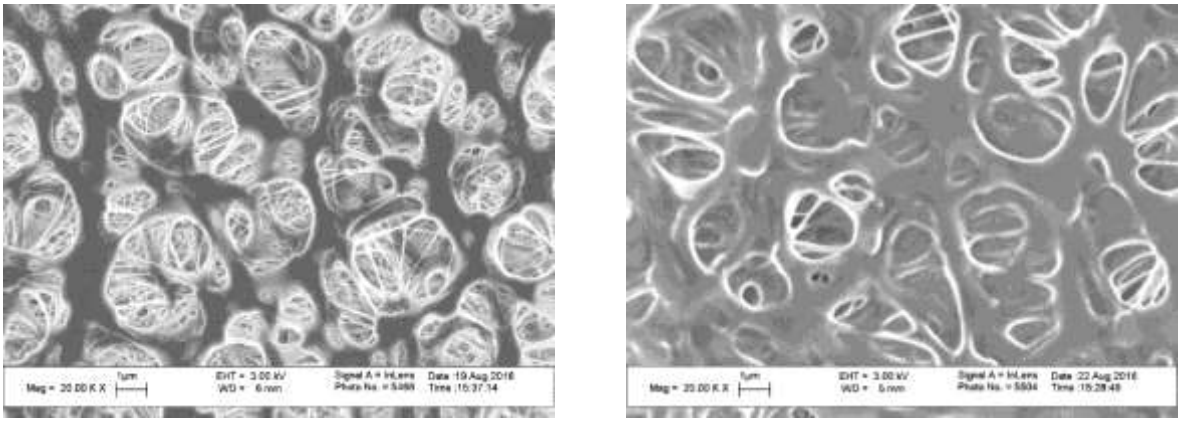

(g) (h)

Figure 3.2 (Continued) SEM surface texture of (g) acetonitrile-soaked and (h) TOA-soaked ECTFE membranes.

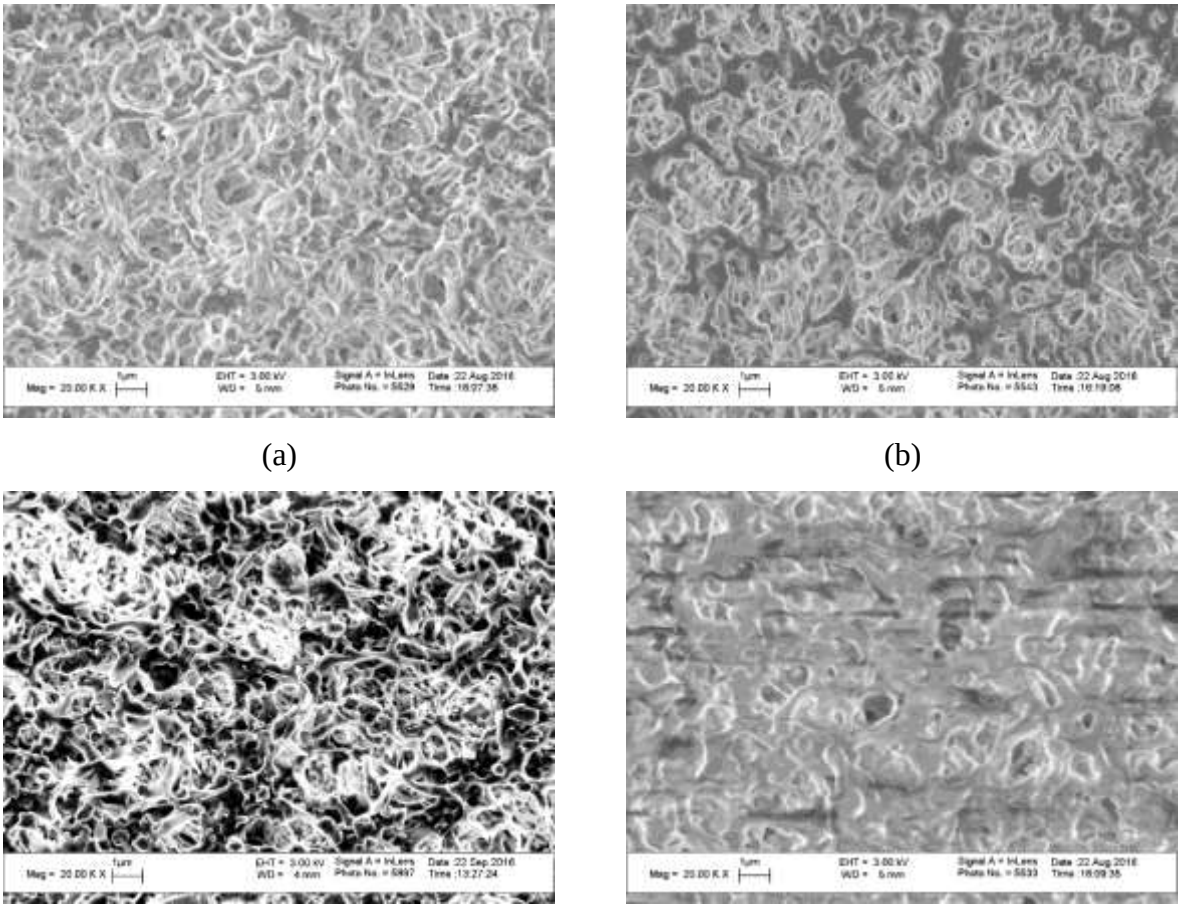

(a) (b)

(c) (d)

Figure 3.3 SEM surface texture of (a) virgin, (b) ethanol-soaked, (c) THF-soaked and (d) TOA-soaked PVDF membranes.

3.3.2 Irradiation Effect on ECTFE Membranes

The surface textures of γ-irradiated ECTFE membranes were also studied via SEM. The study of irradiation effect is important; irradiation has been used in space environments [15] and biomaterial science for sterilization [78]. The SEM images of irradiated ECTFE membranes with irradiation strengths of 25 kGy, 35 kGy and 45 kGy are respectively shown in Figure 3.4 (a)-(c). The morphologies of irradiated ECTFE membranes are very close to that of the virgin one. Therefore, γ-radiation up to 45 kGy did not bring about any defect on the morphology of ECTFE membrane; this is consistent with the membrane porosity results.

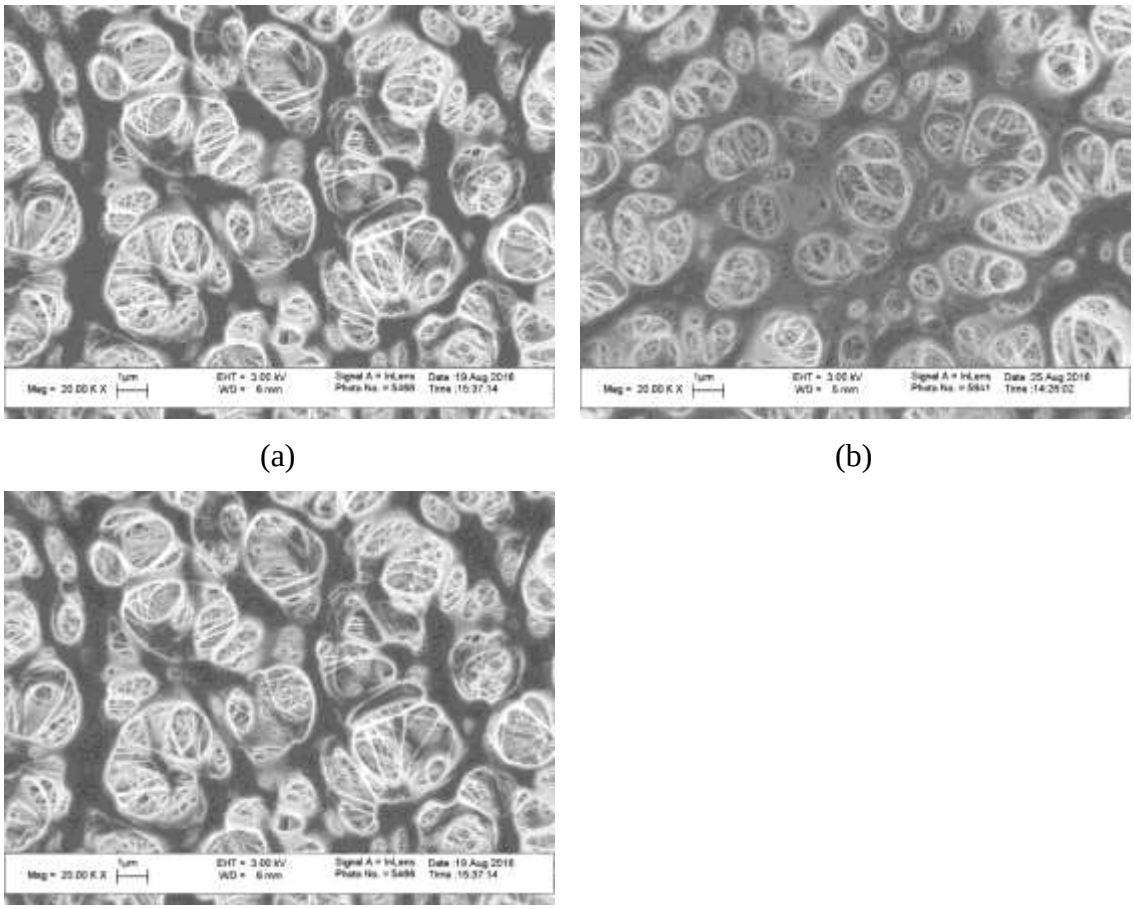

(a) (b)

(c)

Figure 3.4 SEM surface texture of ECTFE membranes subjected to irradiation strength of (a) 25 kGy, (b) 35 kGy and (c) 45 kGy.

3.4 Atomic Force Microscopy Results

Atomic force microscope (AFM) is often used to study surface structure, especially for rough surfaces. That is because the tip in AFM is capable of responding to small changes on the sample surface. Scanning electron microscope may not be as sensitive as AFM for rough surfaces. Moreover, as mentioned earlier, coating in the SEM would cause problems. Here, one does not have to worry about such problems.

The AFM images (10 μm x 10 μm) of virgin, ethanol-soaked and TOA-soaked ECTFE membranes are illustrated respectively in Figure 3.5 (a) – (c). The statistics of the membrane pore size from the corresponding images are shown in Figure 3.5 (d); the mean pore diameters for virgin, ethanol-soaked and TOA-soaked ECTFE membranes are 0.81 μm, 0.99 μm and 1.84 μm, respectively. It has to be noted that the sample size of membrane pores is around 60, a somewhat low value.

For the virgin ECTFE membrane, the highest frequency of the pore diameter (0.2 – 0.4 μm) is 23.1%, followed by the second largest frequency of the pore diameter (0 – 0.2 μm) at 21.5%. Generally, no pores with diameter larger than 2.6 μm are observed in Figure 3.5 (d). However, for the TOA-soaked ECTFE membrane, the highest frequencies of the pore diameter are 14.8% at two diameter ranges, namely 0 – 0.2 μm and 2.2 – 2.4 μm. In addition, pore diameters can be as large as 4.8 μm and 7.8 μm. Thus, it is clear that membranes after soaking in TOA developed larger pores and wider pore size distribution. Moreover, the membrane pores became larger as well after soaking in ethanol; but they are not as large as the pores of the TOA-soaked ECTFE membrane. These results will be especially useful in explaining the particle size distributions in the permeate from membranes having exposure to different solvents.

The roughness estimation of virgin, ethanol-soaked and TOA-soaked ECTFE membranes based on the pixel of these images is shown in Figure 3.5 (e), where a larger number of pixels at 0 nm are observed for virgin ECTFE membranes; thus, virgin ECTFE membranes are flatter than the rest. On the other hand, at 0 nm, the pixels of the TOA-soaked ECTFE membrane are the least, which means that this membrane is the roughest among others. It is clear that for ECTFE membranes, the surface became rougher after soaking in ethanol, and they became much rougher after soaking in TOA; this indicates that solvents, especially TOA, may have introduced defects in ECTFE membranes. Roughness of the membrane surface may lead to increased fouling.

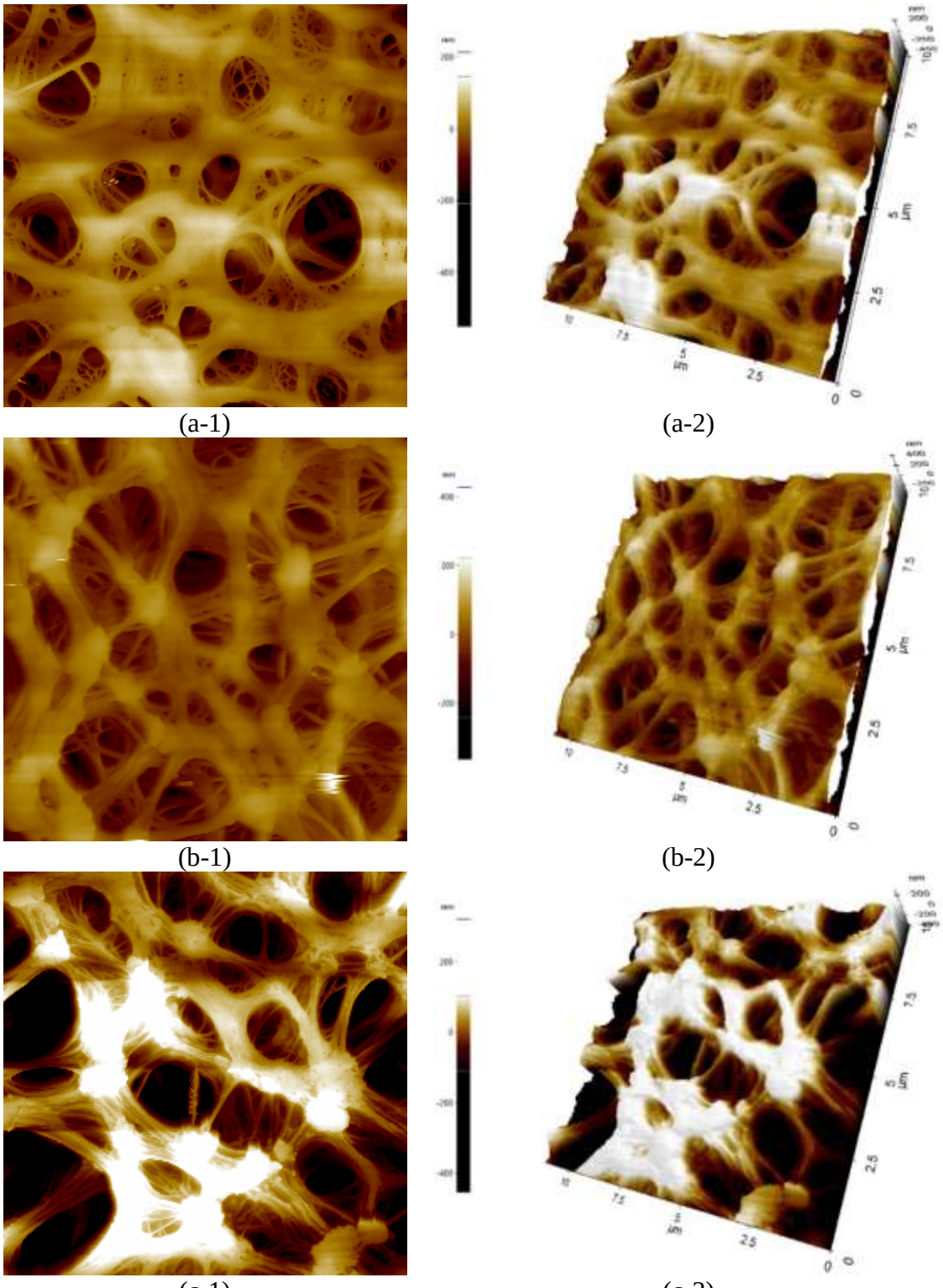

(a-1) (a-2)

(b-1) (b-2)

(c-1) (c-2)

Figure 3.5 AFM image (10 µm x 10 µm) of (a) virgin, (b) ethanol-soaked and (c) TOA-soaked ECTFE membranes ((a-1), (b-1) and (c-1): 2D images; (a-2), (b-2) and (c-2): 3D images) (Continued).

(d)

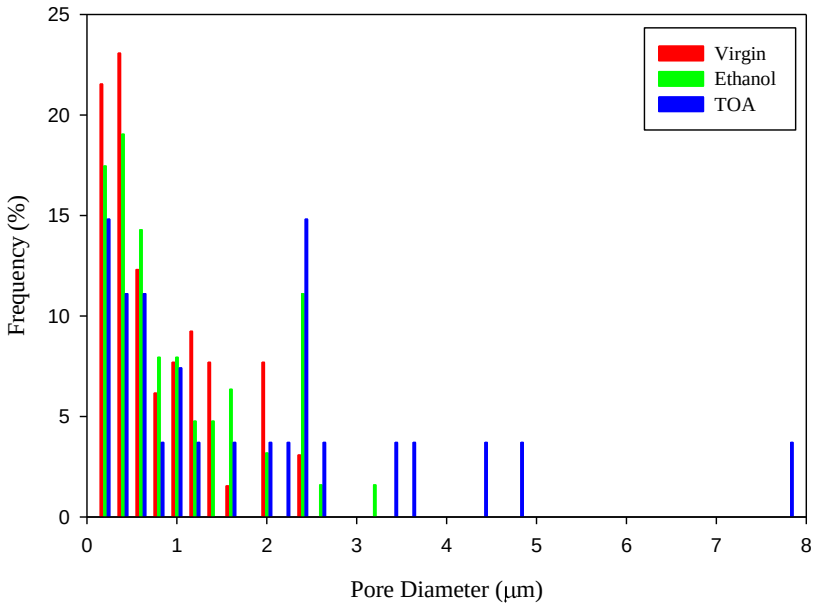

(e)

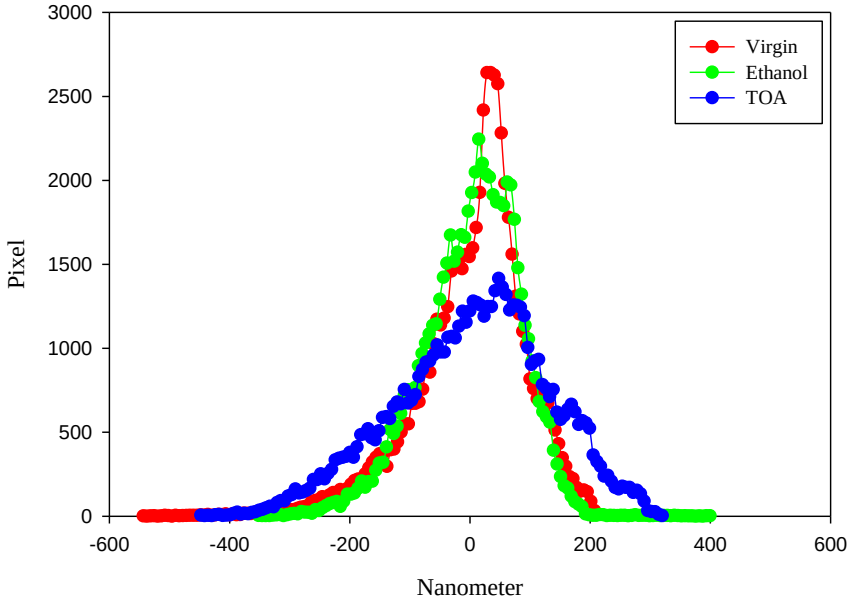

Figure 3.5 (Continued) The resulting (d) pore size distribution and (e) roughness estimation.

3.5 Wetting Property Results

3.5.1 Contact Angle Results

The results of contact angle measurements for nonporous ECTFE and PVDF films as well as microporous ECTFE and PVDF membranes are illustrated in Figure 3.6 (a) – (c) using aqueous ethanol, 2-propanol and 1-butanol solutions, respectively. The contact angle was measured on both sides of virgin ECTFE membranes and the results are identical regardless of the side. The average value of the contact angle for virgin ECTFE membrane is 114^{o}, which is somewhat similar to the results obtained by Drioli et al. [25], namely, 92^{o} on the smooth top-layer surface and 113^{o} on the rough bottom-layer surface of the Halar® ECTFE flat-sheet membrane. It needs to be mentioned that roughness may affect the values of contact angle. For dense membranes, the contact angle of ECTFE is larger than that of PVDF at each alkanol concentration except for 3.96% 1-butanol. These results indicate that nonporous ECTFE film is more hydrophobic than nonporous PVDF film. For porous membranes, however, PVDF membrane seems to be more hydrophobic than ECTFE membrane at low alkanol concentrations. Interestingly, the contact angles measured using PVDF membranes drop faster compared with those on ECTFE membranes as alkanol concentration increases. Thus, ECTFE membrane displays a stronger wetting resistance at higher alkanol concentrations than PVDF membrane. The contact angle results measured using NaOH solutions (1M, 2M and 3M) soaked ECTFE membranes were in the range of 104^{o} – 109^{o}. Clearly, ECTFE membrane is hydrophobic regardless of the NaOH concentration.

(a)

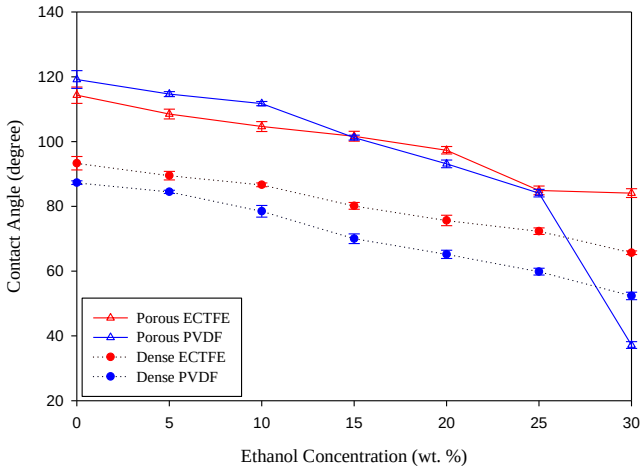

(b)

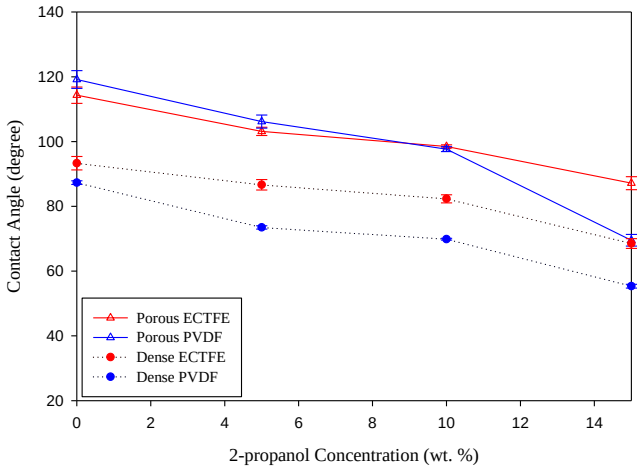

(c)

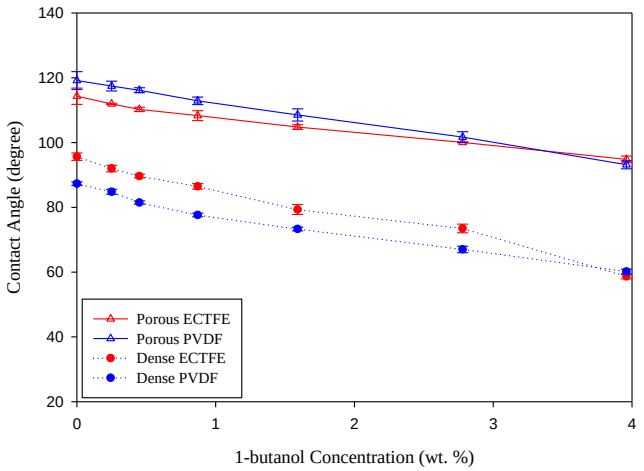

Figure 3.6 Contact angle values measured with different alkanol concentrations on dense as well as porous ECTFE and PVDF membranes for (a) ethanol, (b) 2-propanol and (c) 1-butanol.

3.5.2 Liquid Entry Pressure Results

Liquid entry pressure values are very useful in various microfiltration applications. The results for LEP values of ECTFE and PVDF membranes are listed in Table 3.2 using aqueous ethanol, 2-propanol and 1-butanol solutions. It is obvious that LEP for ECTFE membrane is larger than that of PVDF membrane at every concentration for each aqueous solution, which indicates that PVDF membrane is more easily wetted by adding an alkanol. These results are consistent with the contact angle results measured on ECTFE and PVDF membranes. In addition, 35% ethanol concentration is needed to wet ECTFE membrane spontaneously, while only 25% ethanol concentration is needed to wet PVDF membrane. Similar results are observed for 2-propanol and 1-butanol in that somewhat higher alkanol concentrations are needed to wet ECTFE membrane compared to most for PVDF membranes. Therefore, higher alkanol concentrations are needed to wet the ECTFE membrane completely as compared with PVDF membranes. The ability of PVDF to maintain the hydrophobicity is somewhat weaker compared with that of ECTFE. The LEP measured using 1M NaOH solution soaked ECTFE membrane was almost identical to that of virgin ECTFE membrane. Variation in NaOH concentration appears to have very little effect on LEP. A higher concentration, 3M NaOH, reduces the value of LEP by around 13.8 kPag (2 psig).

Table 3.2 LEP Values* for Alkanol-Water Mixtures for ECTFE and PVDF Membranes

Ethanol (wt. %)		0	5	10	15	20	25	30	35
γ_L (dyne/cm)**		72.8	56.4	48.1	42.7	38.6	36.1	33.5	32.1
LEP kPag (psig)	ECTFE	393 (57.0)	254 (36.8)	194 (28.2)	134 (19.5)	93.1 (13.5)	51.7 (7.5)	17.2 (2.5)	0
	PVDF	243 (35.3)	146 (21.2)	105 (15.2)	68.9 (10.0)	27.6 (4.0)	0	-	-
2-propanol (wt. %)		0	5	10	15	20			
γ_L (dyne/cm)**		72.8	50.3	41.2	35.3	31.2			
LEP kPag (psig)	ECTFE	393 (57.0)	216 (31.3)	117 (17.0)	24.8 (3.6)	0			
	PVDF	243 (35.3)	112 (16.3)	24.1 (3.5)	0	-			
1-butanol (wt. %)		0	0.25	0.45	0.87	1.59	2.78	3.96	
γ_L (dyne/cm)***		72.1	64.7	59.8	53.0	45.8	38.6	33.3	
LEP kPag (psig)	ECTFE	393 (57.0)	341 (49.5)	305 (44.3)	236 (34.2)	174 (25.3)	106 (15.3)	3.4 (0.5)	
	PVDF	243 (35.3)	208 (30.2)	179 (26.0)	143 (20.7)	103 (15.0)	15.9 (2.3)	0	

Note: * The accuracy of pressure gauge is ± 1 psi (6.9 kPa); **Taken from Reference [79]; *** Taken from Reference [80].

García-Payo et al. [81] pointed out that the correlation between LEP for a porous membrane and the surface tension is shown below:

$$\mathrm{LEP} = \frac{2}{r_{max}}(\gamma_L - \gamma_L^W) \tag{3.1}$$

Here, r_{max} is the maximum pore radius of the membrane sample; γ_L is the surface tension of the liquid; γ_L^W is the wetting surface tension, which is defined as $2\sqrt{\gamma_S^d \gamma_L^d}$. Here, γ_S^d and γ_L^d are the dispersion component of surface tension for the solid and liquid, respectively. Equation (3.1) is valid for alcohol solutions only if γ_L^d is constant [81]. Figure 3.7 illustrates how LEP varies with surface tension [79, 80] for ECTFE and PVDF membranes. From this plot, r_{max} can be calculated using the slope, $\frac{2}{r_{max}}$. γ_L^W can be calculated from the intercept $-\frac{2\gamma_L^W}{r_{max}}$ if r_{max} is known. The results obtained for r_{max} and γ_L^W are summarized in Table 3.3. Values of γ_L^W for PVDF membranes measured using ethanol and 2-propanol are in good agreement with those calculated by García-Payo et al. [81]. The results of maximum pore size are consistent with those from the SEM and AFM images.

It has to be mentioned that the critical surface tensions ($\gamma_{critical}$) of Halar® ECTFE and PVDF are 32 dyne/cm and 25 dyne/cm, respectively [67]. Based on the results from Table 3.2, the critical surface tension of ECTFE membrane should be between 31.2 dyne/cm and 33.3 dyne/cm, which is close to the literature value of the other varieties of ECTFE. From these experiments, the critical surface tension for PVDF membrane is in the range of 36.1 dyne/cm and 33.3 dyne/cm, which is different from the literature value, 25 dyne/cm. It is probably caused by some additives which make the membrane less hydrophobic. Additionally, the estimated $\gamma_{critical}$ for ECTFE and PVDF membranes are in good agreement with γ_L^W (Table 3.3) for those calculated from Equation (3.1).

Kim and Harriott [82] studied the relationship between critical entry pressure ($\Delta P_{critical}$) for liquid-air systems as shown in Equation (3.2). It suggests a linear plot of $\Delta P_{critical}$ against $-\gamma \cos \theta$, where γ is the surface tension of the liquid and θ is the liquid-

solid contact angle. A similar study was conducted on ECTFE and PVDF membranes, which also provides a linear plot as shown in Figure 3.8:

$$\text{LEP} = \Delta P_{\text{critical}} = -\frac{2\gamma_L \cos\theta}{r_{max}} \qquad (3.2)$$

The values of r_{max} calculated from Equation (3.2) are close to those estimated from Equation (3.1). Moreover, the pore size results of ECTFE membrane estimated from both equations (Equations (3.1 - 3.2)) show similarities to the dimensions visually detected in the SEM image of untreated ECTFE membrane shown in Figure 3.2 (a) as well as the AFM image shown in Figure 3.5 (a).

Table 3.3 Summary of r_{max} and γ_L^W Estimated from LEP and Surface Tension Correlation (Equations (3.1 - 3.2))

Membrane	Solvent	r_{max}(μm)*	γ_L^W (dyne/cm)*	r_{max} (μm)**
ECTFE	Ethanol	1.4	30.2	1.2
	2-propanol	1.5	30.1	1.2
	1-butanol	1.4	29.5	1.0
PVDF	Ethanol	2.2	33.8	2.2
	2-propanol	2.0	36.0	1.9
	1-butanol	2.1	32.7	1.7

Note: * Calculated from Equation (3.1); ** Calculated from Equation (3.2).

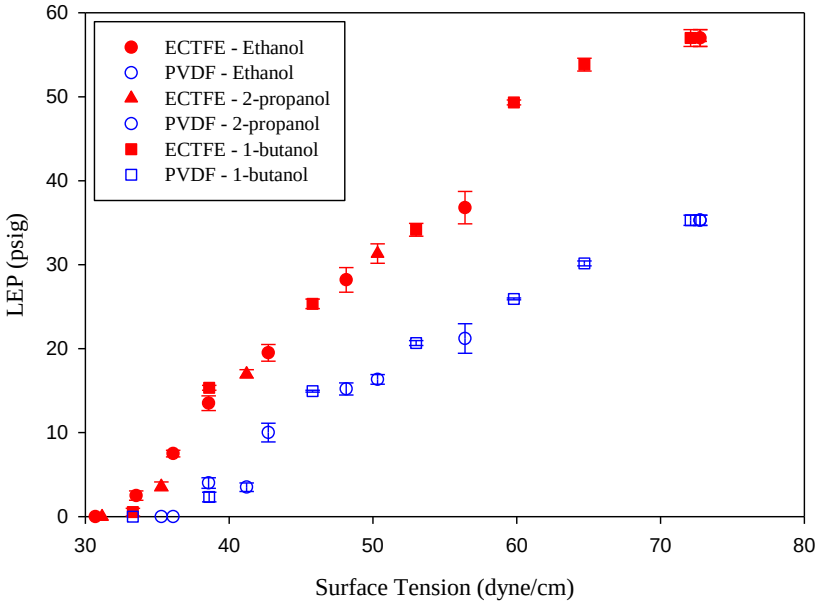

Figure 3.7 Plot of LEP against surface tension for ECTFE and PVDF membranes.

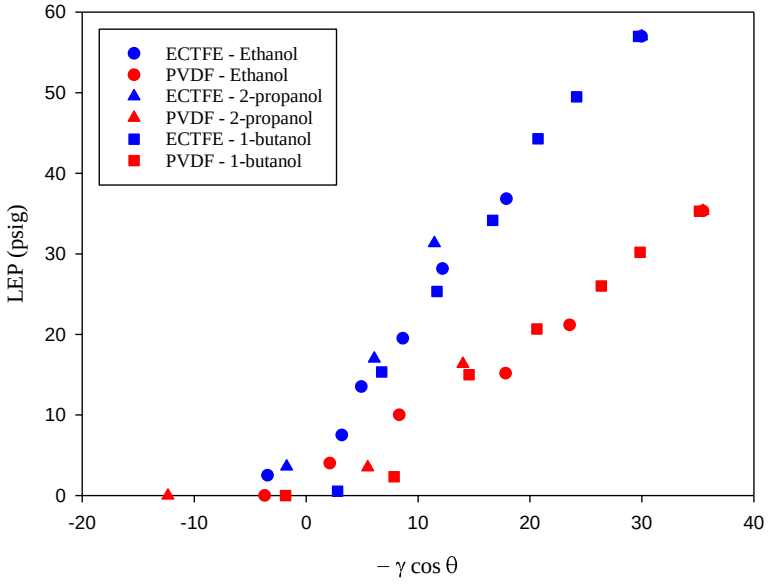

Figure 3.8 Variation of LEP with surface tension and contact angle on ECTFE and PVDF membranes.

3.5.3 Bubble Point Pressure Results

Bubble point value is a very important membrane property for microfiltration applications. The bubble point pressure results of irradiated ECTFE membranes are shown in Figure 3.9. The ECTFE membrane untreated by γ-radiation (0 kGy) provides the largest value. The results for irradiated ECTFE membranes are a bit lower compared to that of a virgin ECTFE membrane regardless of which solvent was used in the measurement. The difference is larger with heavier radiation strength. Therefore, irradiation has some effect on the bubble point values of ECTFE membranes. It has to be mentioned that the effect on ECTFE membrane brought about by irradiation is small since it was not visually detected via SEM.

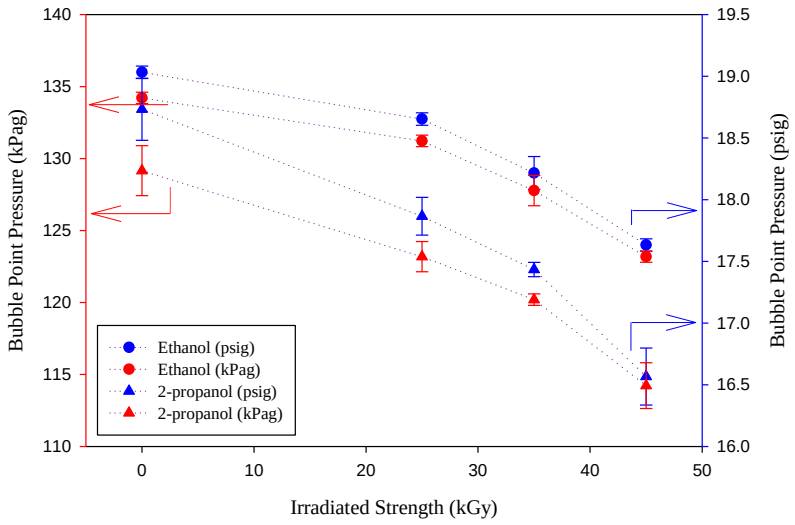

Figure 3.9 Bubble point pressure results for irradiated ECTFE membranes measured using pure ethanol and 2-propanol.

The bubble point pressure was also determined for untreated ECTFE and PVDF membranes using aqueous ethanol and 2-propanol solutions with alkanol concentration varying from 60% to 100%. The variations between LEP and bubble point pressure with

alkanol concentration for ethanol and 2-propanol are plotted in Figure 3.10 (a) – (b), respectively. The relationship between bubble point pressure and alkanol concentration is linear so that after a few measurements, the bubble point pressure for a certain alkanol concentration can be estimated. Similar relationship is observed for LEP and alkanol concentrations.

(a)

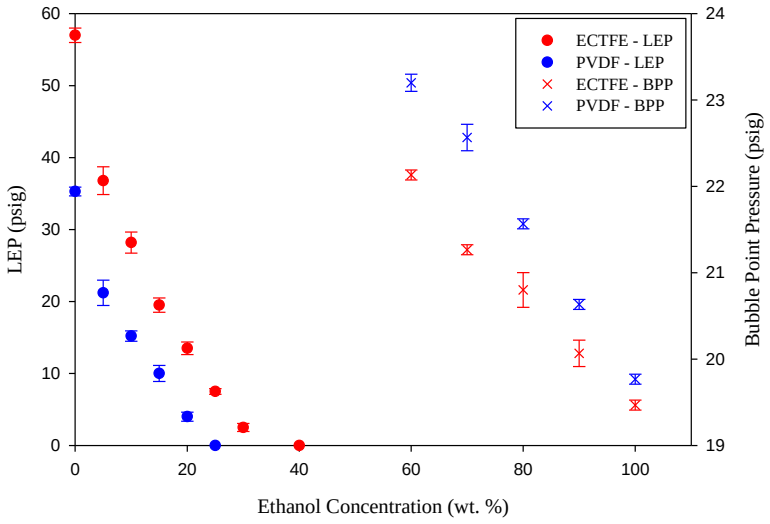

(b)

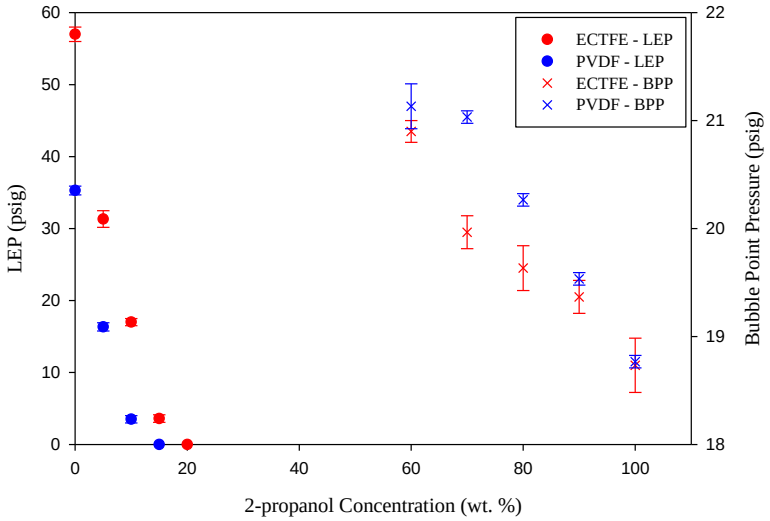

Figure 3.10 Variation of LEP and bubble point pressure (BPP) with (a) ethanol and (b) 2-propanol concentrations.

The bubble point pressure results measured using NaOH solution-soaked ECTFE membranes were very close to that of virgin ECTFE membrane. This is consistent with contact angle results measured using NaOH solution-soaked ECTFE membranes. However, the higher concentration (3M) of NaOH solution reduced the value of LEP by ~13.8 kPag (2 psig), which indicates a small effect on ECTFE membrane. Corrosion resistance has been studied by Leivo et al. [22] using salt spray test, H_2SO_4 (pH = – 0.7) and NaOH (pH = 14) solution with fully fluorinated and partially fluorinated polymers including Halar® ECTFE. ECTFE coating corroded a little in caustic solutions, which does not show high corrosion resistance as compared with fully fluorinated polymers. That is because fully fluorinated polymers have strong bond between fluorine and carbon atoms [22]. But it has to be mentioned that the soaking solutions were very aggressive.

The maximum pore size of ECTFE membrane is also estimated using the bubble point method. The value of the largest pore size in solvent-treated membranes will influence the size of the particles and particle agglomerates which slip through the membrane pores. To that end, the results of bubble point pressure (P_{bp}, kPag) and the maximum pore diameter (d_{max}, µm) for virgin and solvent-soaked ECTFE membranes (here, membranes were treated with ethanol, xylene and TOA) are shown in Figure 3.11. The P_{bp} and d_{max} for virgin ECTFE membrane are 127.3 ± 1.4 kPag and 0.67 ± 0.001 µm, respectively. It has to be noted that the d_{max} obtained here is actually the "pore-throat", not the "pore-mouth" on the membrane surface; it was schematically shown by Yu et al. [83] about the non-cylindrical characteristics of a pore tunnel in membranes. On the other hand, the pores shown in the AFM images are actually the "pore-mouth". Therefore, it is not

surprising that the values of the d_{max} obtained from the AFM images and the bubble point method are somewhat different.

The solvent effects on d_{max} are obvious: membranes after soaking in all these solvents developed larger pores. The membrane pore size ranges are: $d_{max,\ TOA} > d_{max,\ Xylene/TOA} > d_{max,\ Xylene} > d_{max,\ Ethanol} > d_{max,\ Virgin}$, which is in good agreement with the pore size ranges of virgin, ethanol-soaked and TOA-soaked ECTFE membranes obtained by the AFM analysis. Moreover, the value of d_{max} for the TOA-treated (xylene80/TOA20 and pure TOA) membranes may be smaller than their actual values; that is because the residual TOA is extremely hard to remove from the membrane pores, and the surface tension of TOA (γ_{TOA}, 28.8 dyne/cm [77]) is larger than that of 2-propanol ($\gamma_{2\text{-propanol}}$, 21.2 dyne/cm [79]). Thus, γ_{TOA} could generate larger values of d_{max} for the membranes that were treated with TOA.

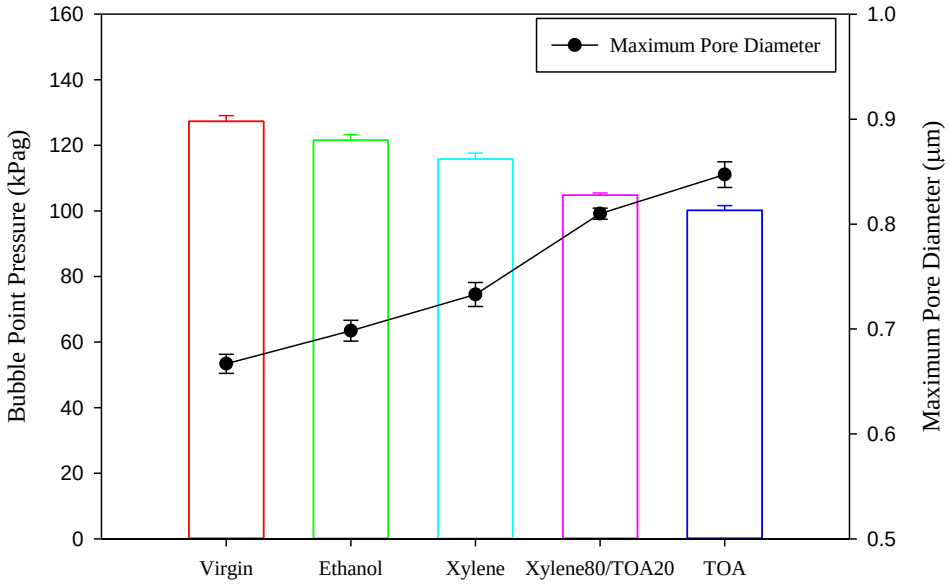

Figure 3.11 The results of the P_{bp} and the d_{max} for virgin and solvent-soaked ECTFE membranes.

3.6 Thermal Property Results

3.6.1 Differential Scanning Calorimetry Results

Differential scanning calorimetry (DSC) is a very useful and easy-handling tool to study the amorphous and crystalline behavior of a polymer or polymeric membrane sample. The crystalline part is an important factor for the sample's physical properties such as integrity, hardness, diffusion etc., which are useful information in membrane applications. Moreover, DSC can measure the glass transition temperature (T_g), which is the temperature where a polymer transitions from a glassy (stiff) state to a rubbery (soft) state or vice versa depending on the direction of temperature change. Differential scanning calorimetry can also measure the melting temperature (T_m) where the polymer sample starts to melt. These information would the guidance for applications that have to be operated at higher temperatures. However, the DSC instrument used in current study cannot determine T_g due to the lower heating rate. Thus, a dynamic mechanical thermal analyzer is used later to determine the T_g of virgin and solvent soaked ECTFE membranes.

Thermal properties obtained from DSC measurements resulting from 1st heating and 2nd heating are illustrated in Figure 3.12 (a) - (b) for virgin and solvent-soaked ECTFE membranes. In the 1st heating of ECTFE membranes, it is clear that except for the membranes treated with TOA (pure TOA and TOA/xylene mixture), the thermograms of other solvent-soaked ECTFE membranes are very similar to that of virgin ECTFE membrane. The melting temperatures (T_m) of these membrane samples are ~239.5^{o}C, which is very close to that of the virgin one; this indicates that the effect caused by these solvents on ECTFE membranes is very limited. However, in the thermogram of TOA-soaked ECTFE membrane, the melting peak at around – 40^{o}C indicates melting of TOA.

This confirms that TOA was present in membrane pores before DSC test. Moreover, the residual TOA introduced crystallization which is displayed as a small exothermic peak at around –5^{o}C. This recrystallization indicates the enhanced mobility of molecular chains [84, 85] caused by TOA.

In the range of 200 – 250^{o}C, there are additionally two melting peaks, which could be explained by different crystalline structures [86]. Part of the structure is similar to that of virgin ECTFE membrane; other segments, somehow different, were introduced by TOA-soaking. Occelli et al. [87] reported that TOA generated crystals. The double-peak phenomenon has also been explained by Vázquez-Torres et al. [88] as the result of recrystallization effect and morphological effect. It needs to be mentioned that T_m of TOA-soaked ECTFE membranes, ~230^{o}C, is reduced compared to that of the virgin one; this indicates an increase in the amount of lattice defects [89]. Similar to the TOA-soaked ECTFE membrane, in the xylene80/TOA20-soaked ECTFE membrane, there are also two melting peaks, i.e. at -40^{o}C and 230^{o}C. This corresponding melting enthalpy at -40^{o}C is smaller; it is because the amount of TOA left in the xylene80/TOA20-soaked ECTFE membrane is less compared with that in the pure TOA-soaked ECTFE membrane. Unlike the TOA-soaked ECTFE membrane, this limited amount of residual TOA did not cause any recrystallization and bring about different crystalline structures.

In the 2nd heating of ECTFE membrane shown in Figure 3.12 (b), the thermograms of TOA-soaked ECTFE membrane provide significantly reduced values of melting temperature (T_m) and melting enthalpy (ΔH_m), which indicate less energy is required to melt the sample compared with that for virgin ECTFE membrane. Similarly, the ΔH_m of xylene80/TOA20-soaked membrane is also reduced, however, the reduced amount is not

as much as that for the TOA-soaked ECTFE membranes. The values of T_m and ΔH_m for other solvent-soaked ECTFE membranes are almost identical to those of virgin ECTFE membrane even though slight difference of ΔH_m was observed in the first heating.

Singh et al. [20] reported that the heat of fusion calculated by group contributions method for perfectly crystalline ECTFE is ~166.25 J/g, which was used in this study. Results of crystallinity for ECTFE membranes calculated from 1st and 2nd heating via Equation (2.11) are illustrated in Figure 3.12 (c). The crystallinities of TOA-soaked and xylene80/TOA20-soaked ECTFE membranes were reduced to different levels according to the amount of TOA left in the membrane samples, which indicates some defects caused by TOA. Berens and Hodge [90] also observed weaker endotherms when heating poly(vinyl chloride) treated with CH_3Cl vapor. Moreover, the defect caused by TOA on ECTFE membrane is irreversible since only TOA reduced the value of crystallinity in the 2nd heating.

(a)

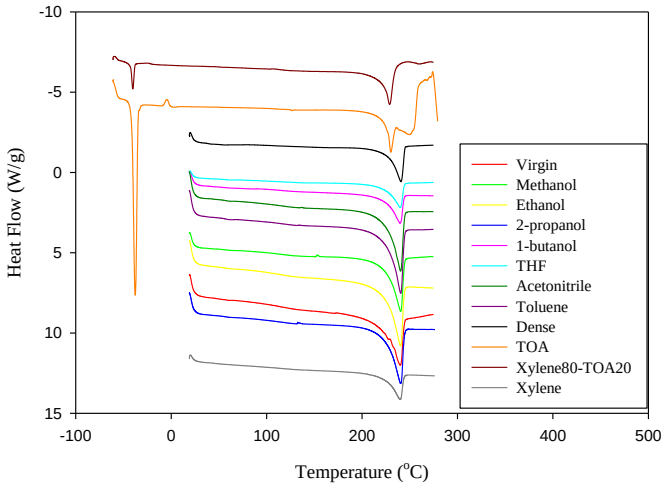

(b)

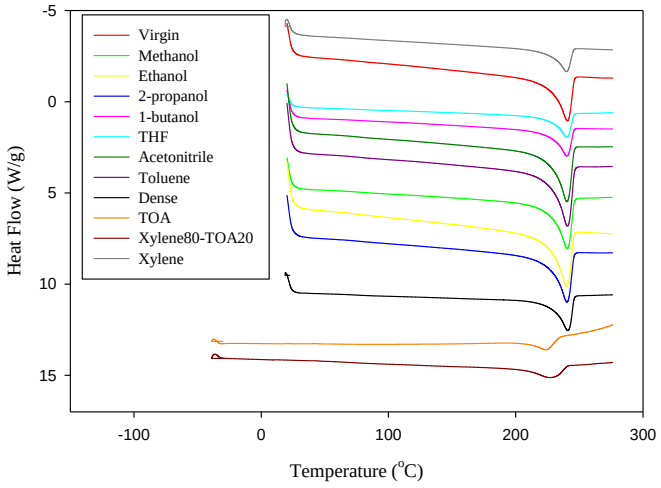

(c)

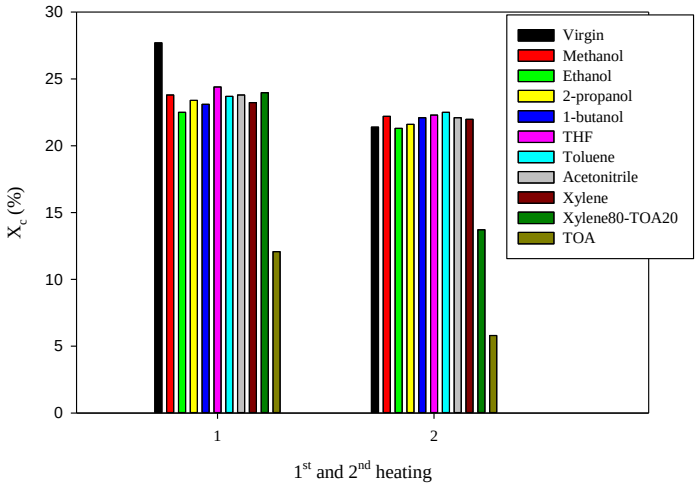

Figure 3.12 DSC results of (a) 1st heating, (b) 2nd heating and (c) corresponding values of crystallinity for virgin and solvent-soaked ECTFE membranes.

For virgin and solvent-soaked PVDF membranes, similarly, only the thermogram of TOA-soaked PVDF membrane is different from that of virgin PVDF membrane. Details are shown in Figure 3.13 (a) - (b). In the thermogram of TOA-soaked PVDF membrane, the existence of TOA in PVDF membrane pores was confirmed by the melting peak at around – 40^{o}C in the 1st heating. The melting enthalpies occurring at ~ 165^{o}C are reduced in both 1st and 2nd heatings compared with those of virgin PVDF membrane. That is because TOA brought about defects in PVDF membrane. The thermograms of irradiated ECTFE membranes are illustrated in Figure 3.14 (a) – (b). The reduced melting enthalpies of irradiated ECTFE membranes in both 1st and 2nd heatings indicate defects caused by irradiation. Singh et al. [20] also observed thermal degradation of ECTFE caused by heavy ion (lithium, carbon, nickel and silver) irradiation. Therefore, irradiation leads to a certain level of defects in ECTFE membrane.

(a)

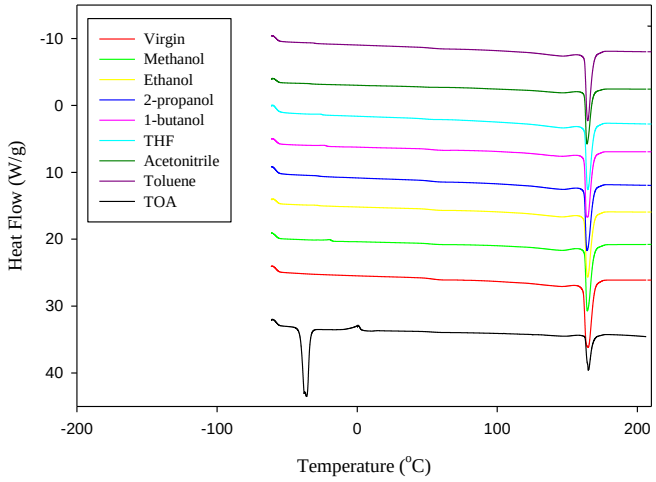

Figure 3.13 DSC results of (a) 1st heating for virgin and solvent-soaked PVDF membranes (Continued).

(b)

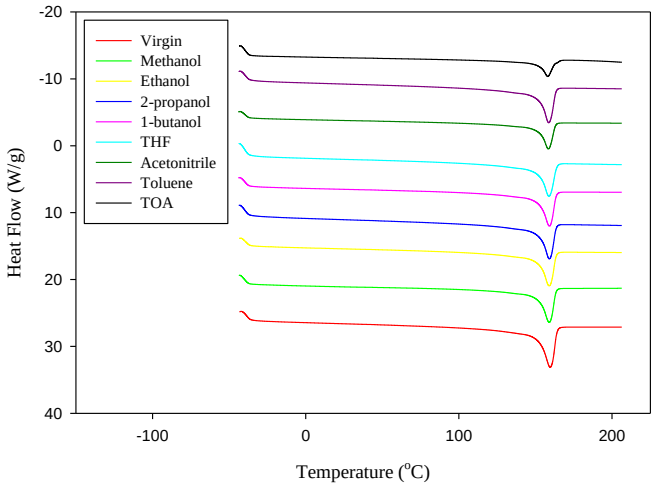

Figure 3.13 (Continued) DSC results of (b) 2nd heating for virgin and solvent-soaked PVDF membranes.

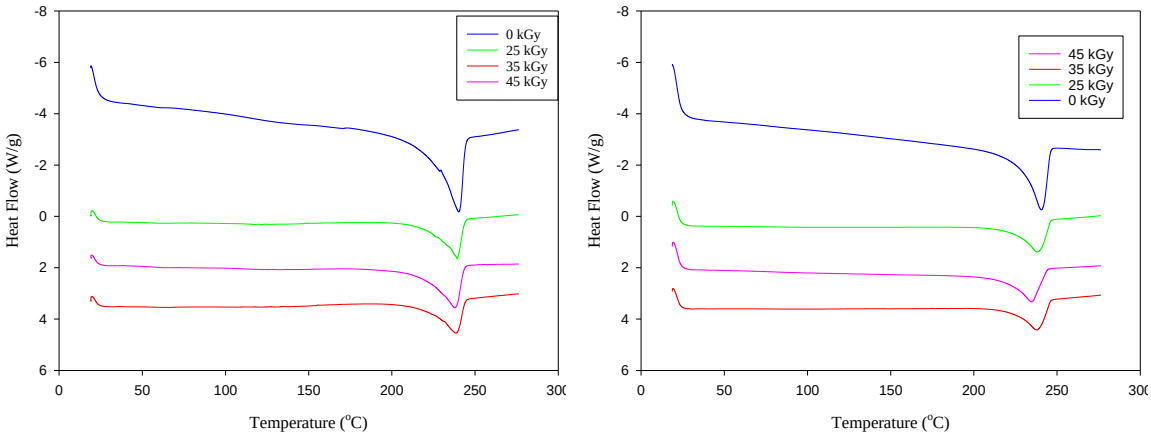

(a) (b)

Figure 3.14 DSC results of (a) 1st heating and (b) 2nd heating for irradiated ECTFE membranes.

3.6.2 Thermogravimetric Analysis Results

The TGA results of virgin and solvent-soaked ECTFE and PVDF membranes are shown in Figure 3.15 (a) – (b), respectively. For solvent-soaked ECTFE membranes except in the case of TOA, the weight loss started at ~250°C, which is similar to that of the virgin sample.

However, the weight loss of TOA-soaked ECTFE membrane began earlier at ~115^{o}C; this reflects the loss of TOA (boiling point 365 – 367^{o}C). Similar results are observed for virgin and solvent-soaked PVDF membranes as shown in Figure 3.15 (b). Only TOA-soaked PVDF membrane started weight loss earlier when it was heated to ~142^{o}C, while weight loss of virgin and other solvent-soaked PVDF membranes was from ~268^{o}C. It has to be mentioned that different initial temperatures of weight loss for TOA-soaked ECTFE and PVDF membranes indicate different levels of interactions between TOA and the two kinds of membranes. Additionally, PVDF membranes have better thermal resistance than that of ECTFE membranes namely, ECTFE membranes start weight losss earlier (~260^{o}C) than that of PVDF membranes (~272^{o}C). When both kinds of membranes were heated up to 350^{o}C, the weight losses of ECTFE and PVDF membranes are 23% and 4%, respectively.

In order to study the full thermal degradation behavior of ECTFE membranes, selected membrane samples were heated to 800 ^{o}C. These TGA results for virgin and solvent-soaked ECTFE membranes are illustrated in Figure 3.16 (a). For the virgin ECTFE membrane, two stages of the degradation are obvious: the first stage starts from ~260 ^{o}C to ~400 ^{o}C, followed by the second stage ranging from ~400 ^{o}C to ~525 ^{o}C. This two-stage thermal degradation was also reported by Toniolo et al. [91] for Halar® high clarity ECTFE films. In general, solvent treatments slightly weaken the stability of ECTFE membranes; the comparison of virgin and TOA-soaked membranes is shown in Figure 3.16 (b). More details about the comparisons of virgin and solvent-soaked ECTFE membranes are illustrated in Figure C.1 in Appendix C. The degradation behaviors of ethanol-soaked and xylene-soaked ECTFE membranes look similar to that of the virgin one.

However, for the membranes treated with TOA, there is an earlier weight loss (at ~115 ^{o}C), which is due to the loss of TOA (boiling point 365 ^{o}C - 367 ^{o}C), as mentioned earlier. To be more specific, just before the ECTFE membrane itself starts losing weight (at ~260 ^{o}C), the weight loss is ~39% for the TOA-soaked ECTFE membrane and ~21% for the xylene80/TOA20-soaked ECTFE. After 260 ^{o}C, the weight loss was contributed by both ECTFE membrane and the residual TOA until the temperature reached the boiling point of TOA. Moreover, Fanti et al. [92] reported the mechanism of thermal degradation of alternating ECTFE copolymers: the dehydrohalogenation started when polymer samples were suffering the weight loss by the elimination of HCl and HF. During the weight loss of ECTFE membrane itself, virgin, ethanol-soaked and xylene-soaked ECTFE membranes show stronger stabilities than those of TOA-soaked and xylene80/TOA20-soaked ECTFE membranes; e.g., the residue at 450 ^{o}C: ~19.5% for virgin, ethanol-soaked and xylene-soaked ECTFE membranes; ~16.5% for the xylene80/TOA20-soaked ECTFE membrane; ~14% for the TOA-soaked ECTFE membrane. Therefore, the existence of TOA in membrane pores is confirmed by TGA tests; the residual TOA is somehow weakening the stability of ECTFE membranes.

(a)

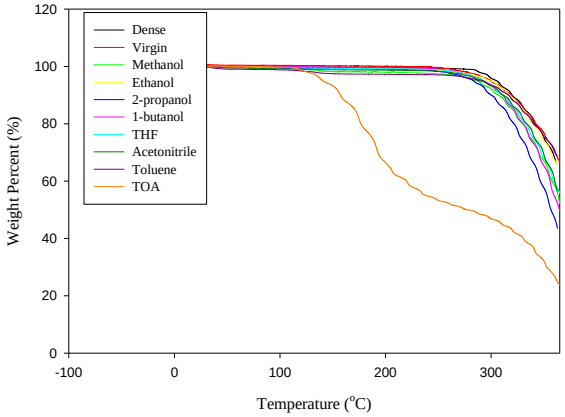

(b)

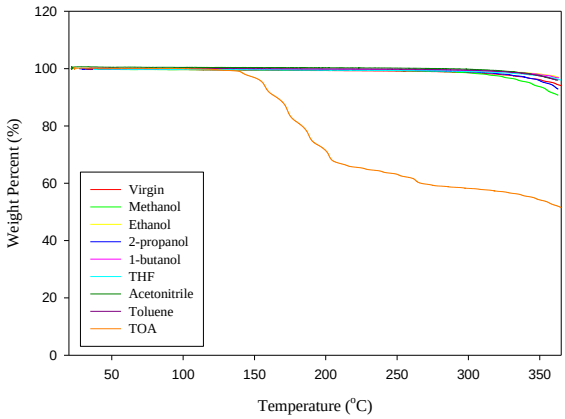

Figure 3.15 Thermogravimetric analysis of virgin and solvent-soaked (a) ECTFE and (b) PVDF membranes.

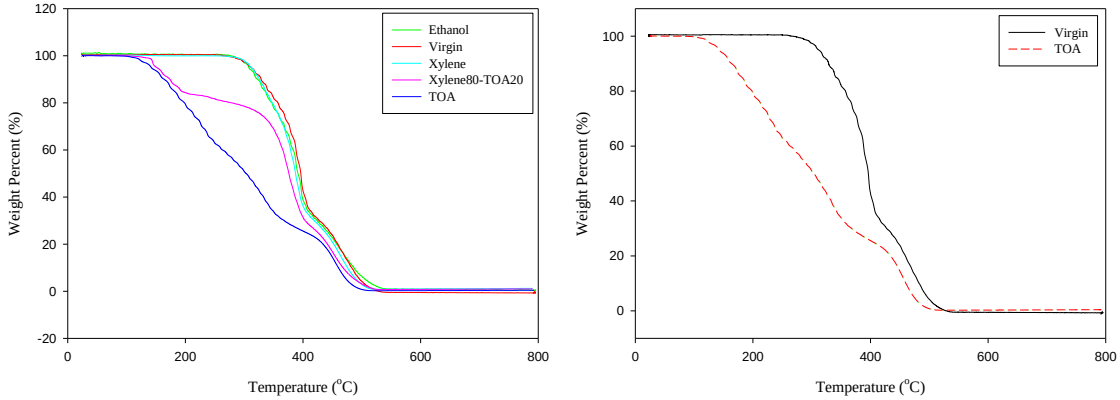

(a) (b)

Figure 3.16 (a) Thermogravimetric analysis (up to 800 ºC) of virgin and solvent-soaked ECTFE membranes and (b) the comparison of virgin and TOA-soaked ECTFE membranes.

3.6.3 Dynamic Mechanical Thermal Analysis Results

Dynamic mechanical thermal analysis (DMTA) is a combination of mechanical and thermal analyses. During the measurement, a sinusoidal stress is applied on the sample and the elongation (strain) of the sample is recorded so that the dynamic modulus can be determined. Based on the properties of the sample and the measuring goal, the sample can be heated simultaneously during the stress application. Dynamic mechanical thermal analysis is used to measure the T_g of virgin and solvent-soaked ECTFE membranes in the current thesis. The value of T_g for solvent-soaked membranes is used for membranes that will be used in the environment. The phenomenon of reduced T_g caused by organic solvent is called plasticizer effect, in which the solvent penetrates into the chains of the sample. The physical properties of membrane sample would change due to the plasticizer effect. It is not favorable. Therefore, knowledge of T_g for solvent-soaked ECTFE membranes is important and necessary for membranes to be used in organic environments.

The values of T_g for virgin and solvent-soaked ECTFE membranes are shown in Figure 3.17 (a-b). The T_g of virgin ECTFE membrane is 116.7 ± 0.6^oC. The T_g results of solvent-soaked ECTFE membranes are very close to that of virgin one, as shown in Figure 3.17 (b). Lin et al. [93] observed that T_g was reduced for Eudragit acrylic films caused by adding organic esters. The plasticizer effect on polymer glass transition behavior was also theoretically studied by Chow [94]. In his study, molecular weight, size, concentration, number of lattice sites and transition isobaric specific heat increment had effect on the T_g of polymer-diluent mixtures [94]. Results obtained from this study appear to indicate that the changes of T_g due to solvents are quite limited so that selected solvents do not have much effect on the mobility of polymer chains or the amorphous part of this

semi-crystalline membrane. Therefore, ECTFE membrane has a strong ability to resist plasticization by solvents. It has to be mentioned that the values of thermal properties were measured at least twice; they were highly reproducible.

(a)

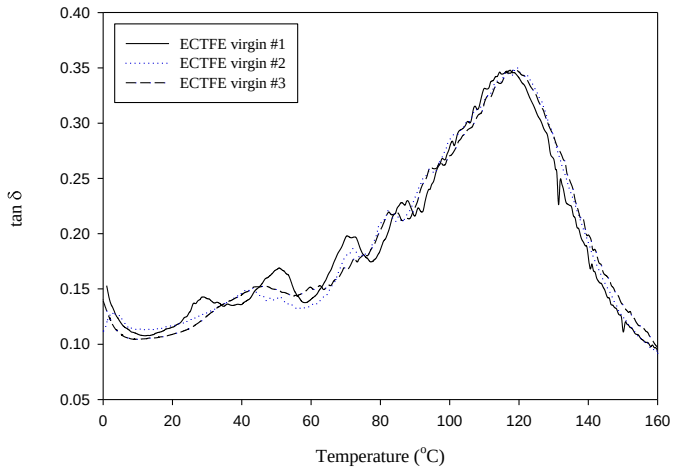

(b)

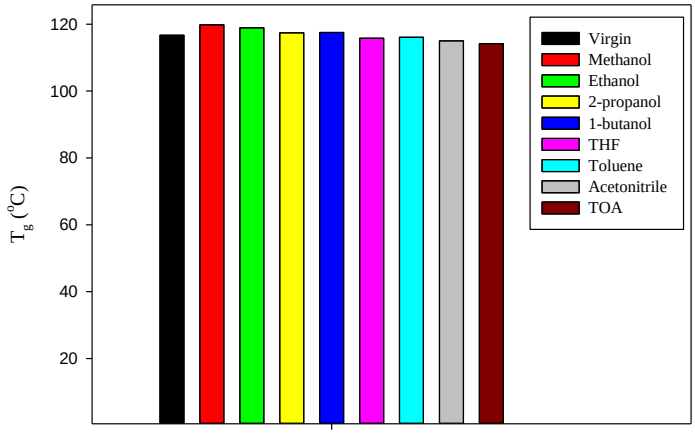

Figure 3.17 (a) Values of T_g for virgin ECTFE membrane and (b) comparison of T_g for virgin and solvent-soaked ECTFE membranes.

3.7 X-Ray Diffraction Results

The XRD patterns for virgin and solvent-soaked ECTFE and PVDF membranes are illustrated in Figure 3.18 (a) – (b), respectively. All XRD patterns show the characteristics of semi-crystalline structure.

(a)

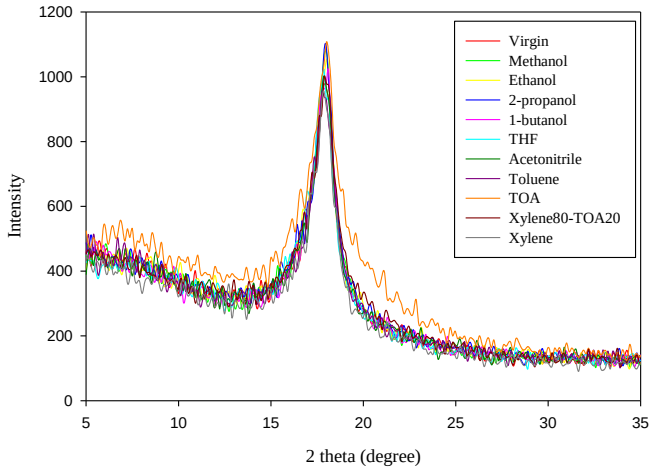

(b)

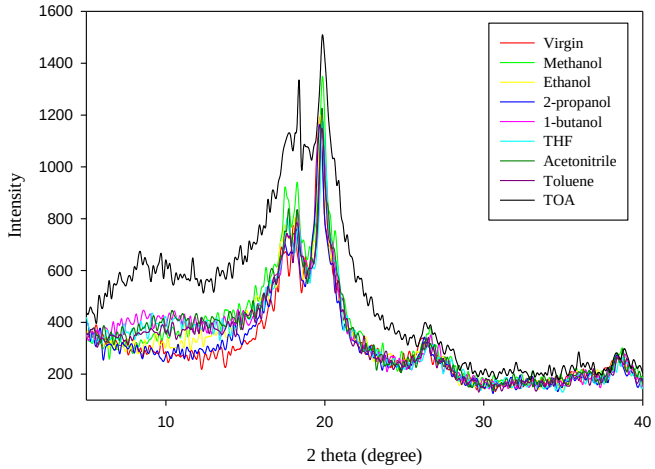

Figure 3.18 XRD patterns for virgin and solvent-soaked (a) ECTFE and (b) PVDF membranes.

In Figure 3.18 (a), the XRD pattern of virgin ECTFE membrane is almost identical to those of solvent-soaked ones except for TOA-soaked ECTFE membrane. It has to be noted that the XRD pattern of xylene80/TOA20-soaked ECTFE membrane looks identical to that of the virgin one. In the XRD pattern of TOA-soaked ECTFE membrane, the halo pattern (amorphous part) increases more than the sharp peak (crystalline part) so that the crystallinity of TOA-soaked ECTFE membrane defined by Equation (2.12) is reduced. The difference between TOA-soaked ECTFE membrane and the rest (virgin and other solvent-

soaked membranes) illustrates the defect brought about by TOA in ECTFE membrane. The solvent effect characterized by XRD is consistent with the DSC results. Similar results of solvent effects are observed for PVDF membranes as shown in Figure 3.18 (b). Additionally, in the XRD pattern of TOA-soaked ECTFE and PVDF membranes, the halo pattern of PVDF membrane increased significantly more than that of ECTFE membrane, which indicates more defect brought about by TOA in PVDF membranes.

3.8 Fourier Transform Infrared Spectroscopy Results

The FTIR results of virgin and solvent-soaked ECTFE membranes are illustrated in Figure 3.19. The FTIR spectra of ethanol-soaked and xylene-soaked ECTFE membranes look almost identical to those of the virgin one. However, for TOA-treated (xylene 80-TOA 20 and pure TOA) ECTFE membranes, there are two strong peaks at 2925.0 cm^{-1} and 2854.7 cm^{-1} which are contributed by C-H stretching vibrations [95, 96] of CH_3 and CH_2 groups. It has to be mentioned that there is no CH_3 group in ECTFE so that it must be from TOA. Even though there are no specific functional groups in tertiary amine reported [97], the strong peaks at the range of 3000 – 2800 cm^{-1} were observed in most tertiary amines [98], including TOA [96, 98]. Therefore, TOA is confirmed to exist in ECTFE membrane pores before the FTIR tests. This is consistent with earlier DSC and TGA results. Additionally, there is a small shoulder peak shown at ~1470 cm^{-1} (indicated by an arrow on the bottom right in Figure 3.19) where there is no absorption for tertiary amines or their salts [99]; this small shoulder peak is probably due to CH_3 deformation [100, 101], which results from TOA. The strong-to-medium peaks observed from all spectra within the range

of 1200 – 900 cm^{-1} contribute to the stretching of C-F [102-104]. Therefore, even though TOA introduced additional bands, it did not destroy the structure of ECTFE membranes.

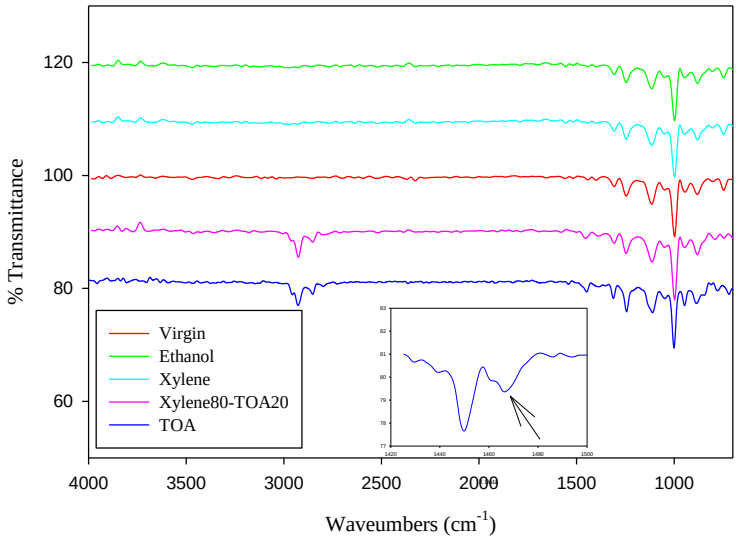

Figure 3.19 FTIR spectra of virgin and solvent-soaked ECTFE membranes.

3.9 Raman Spectroscopy Results

The Raman spectra of virgin and solvent-soaked ECTFE membranes are shown in Figure 3.20. Generally, the peaks in all spectra at 2986 cm^{-1} and 2961 cm^{-1} result from contributions by medium-strong and medium symmetric CH_2 stretching [101]. In addition, the spectra of ethanol-soaked and xylene-soaked ECTFE membranes are almost the same as those of the virgin one. But, there are additional peaks (at 2900 cm^{-1} and 2860 cm^{-1}) shown in the spectrum of the TOA-soaked ECTFE membrane; these peaks are contributions from medium-strong symmetric CH_3 and CH_2 stretching [101]. This additional medium-strong symmetric CH_3 stretching must result from TOA because there is no CH_3 group in ECTFE, which is in good agreement with the FTIR results. In all spectra, the peaks shown at 1441 cm^{-1} and 414 cm^{-1} respectively are contributions from medium-

strong CH_2 deformation [103] and C-F deformation [103, 104]. However, the spectrum of the TOA-soaked ECTFE membrane shows reduced Raman intensities at these Raman shifts; this indicates the defect of such ECTFE membrane caused by TOA. Interestingly, the spectrum of the xylene80/TOA20-soaked ECTFE membrane looks like the combination of those of the xylene-soaked and the TOA-soaked ECTFE membranes, especially in the range of 2800 – 3050 cm^{-1}. Thus, the effect brought about by TOA on the ECTFE membrane is obvious: the higher the amount of TOA is left, the larger is the difference shown in the Raman spectra compared with those of the virgin membrane.

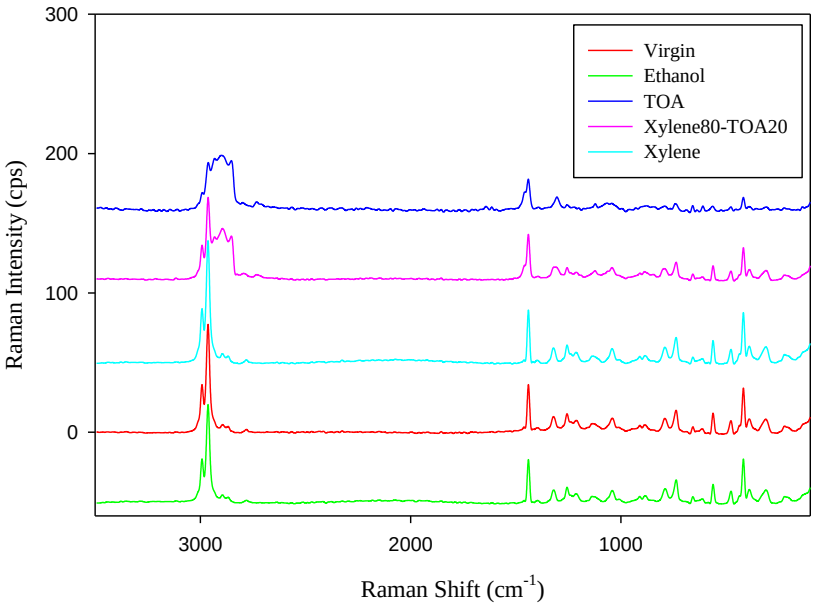

Figure 3.20 Raman spectra of virgin and solvent-soaked ECTFE membranes.

In general, based on the FTIR and Raman spectra, it can be concluded that ethanol and xylene bring about a limited effect in the ECTFE membrane; however, TOA introduced C-H stretching and deformation respectively shown in the ranges of 3000 – 2800 cm^{-1} and 1500 – 1400 cm^{-1}. There is no additional band indicating any chemical

reaction. Therefore, the interaction between TOA and ECTFE is only physical, as was mentioned in Section 3.1.

3.10 Dielectric Relaxation Spectroscopy Results

Dielectric relaxation spectroscopy measures the dielectric properties of a material as a function of frequency. The use of cables in network performance would have cable attenuation issue due to the generated heat; therefore, insulating materials are needed for the network [23] to reduce the problem of cable attenuation. The dielectric constant and energy loss at room temperature for irradiated ECTFE membranes are plotted in Figures 3.21 (a) and 3.22 (a), respectively. It has to be noted that the values shown in Figure 3.21 (a) are averaged values of three measurements. Changes due to irradiation are non-monotonous. The values of dielectric constant are free of electrode polarization and frequency independent within the whole frequency range of the measurement. Thus, the average value of dielectric constant for each sample is taken over the whole frequency range; this is shown in Figure 3.21 (b) with the consideration of measurement variance. Lin and Curilla [23] reported similar observations in the frequency range of 1 kHz to 300 MHz. However, the values of dielectric constant are a bit different since ECTFE polymers are from different sources. Moreover, only 45 kGy irradiation reduced the value of the dielectric constant; the dielectric constant values of irradiated ECTFE membranes treated with 25 kGy and 35 kGy are very close to that of the virgin one. In this case, these two treated membranes could be a candidate for cable usage. Regarding the results of energy loss, irradiation increased the minimum value by about 15%, which indicates some attenuation [23] of ECTFE membrane. In addition, the comparison of energy loss for virgin

and irradiated ECTFE membranes with statistical information is shown in Figure 3.22 (b-d). Therefore, irradiation has some effects on the dielectric constant and energy loss.

(a)

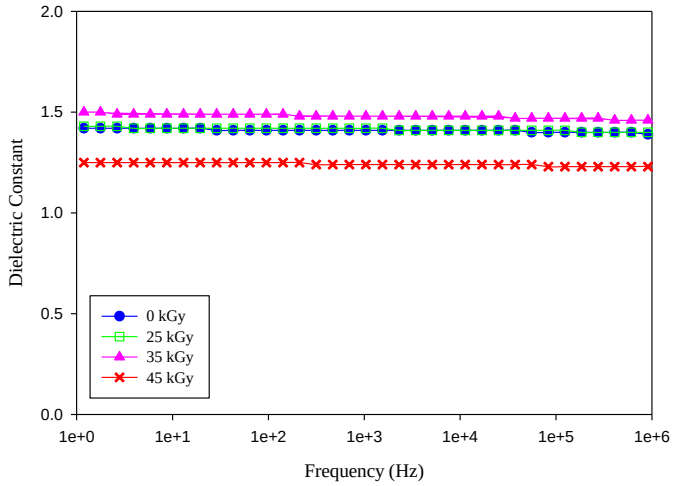

(b)

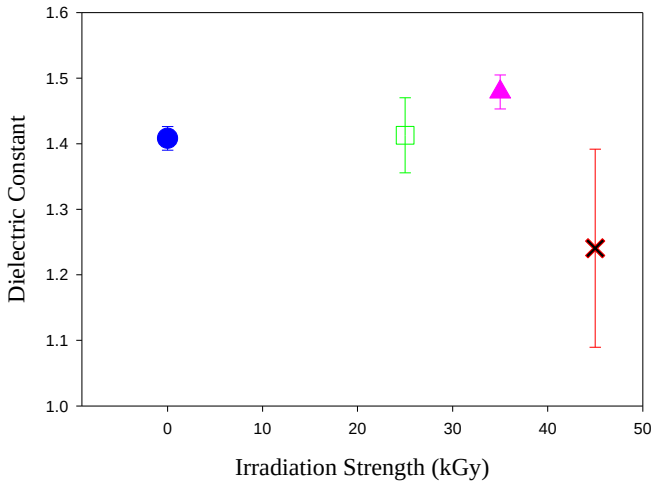

Figure 3.21 Results of (a) dielectric constant for irradiated ECTFE membranes and (b) their average values over the whole frequency.

(a)

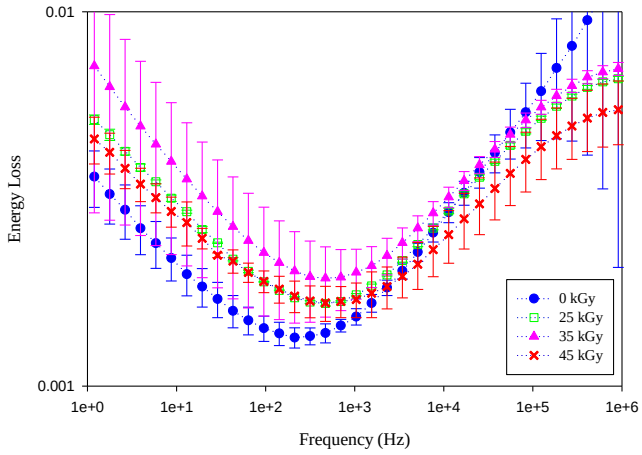

(b)

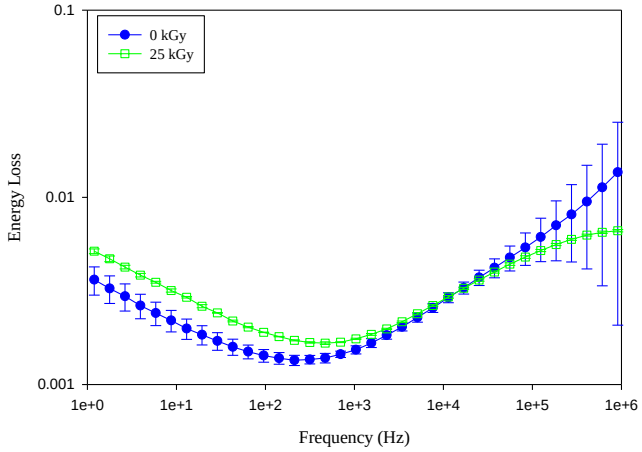

(c)

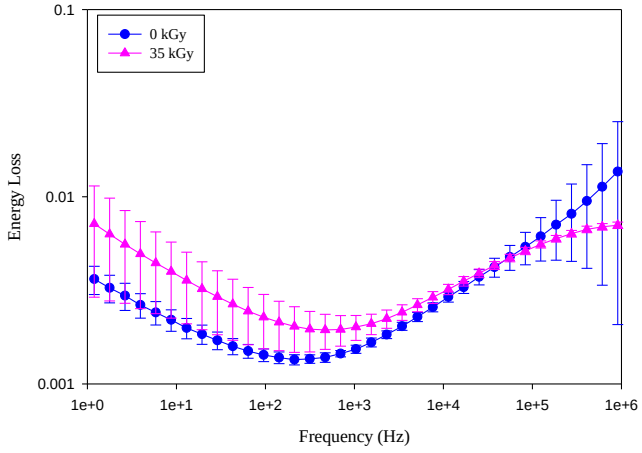

Figure 3.22 Results of (a) energy loss for virgin and irradiated ECTFE membranes as well as the comparison of virgin and irradiated ECTFE membranes with the radiation strength of (b) 25 kGy, (c) 35 kGy (Continued).

(d)

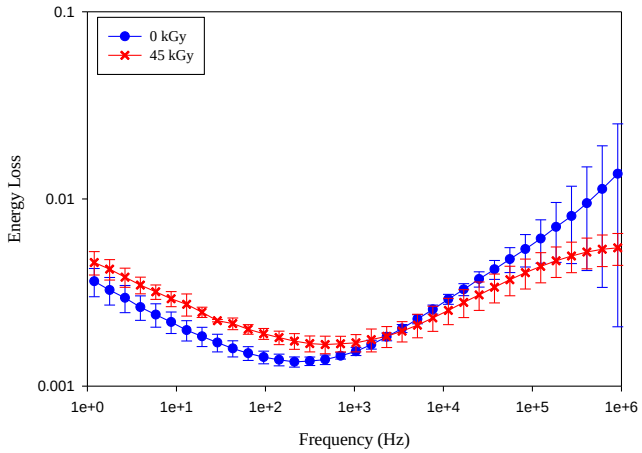

Figure 3.22 (Continued) (d) The comparison of virgin and irradiated ECTFE membranes with the radiation strength of 45 kGy.

3.11 Tensile Test Results

Membranes with excellent mechanical properties can be used for fabricating filter cartridges [11-13]. It is also a very important factor for long-term membrane usage. Besides Young's modulus, the values of stress and strain at break are useful as well. However, the texture analyzer used in current study cannot guarantee reproducibility. Results for Young's modulus of virgin, solvent-soaked and γ-irradiated ECTFE membranes are illustrated in Figure 3.23. The values of alkanol-soaked ECTFE membranes are very similar to that of virgin ECTFE membrane, which appears to indicate absence of any effect on ECTFE membrane. However, THF, toluene, acetonitrile and TOA reduce the value of Young's modulus by ~ 30%, 6%, 9% and 15%, respectively. These could be explained by the swelling of ECTFE membranes caused by the solvents. The values of irradiated ECTFE membranes are very similar to that of virgin ECTFE membrane regardless of the irradiation strength. Similar conclusions have been made by Dargaville et al. [15]. In their tests, the irradiation level of at least 200 kGy seems to have no effect on the mechanical properties,

i.e. stress and strain at break. Therefore, the radiation strength, 45 kGy, seems not to be high enough to reduce Young's modulus of ECTFE membranes. Therefore, ECTFE membranes have the ability to maintain its elastic property when they are exposed to alkanols and γ-radiation up to 35 kGy.

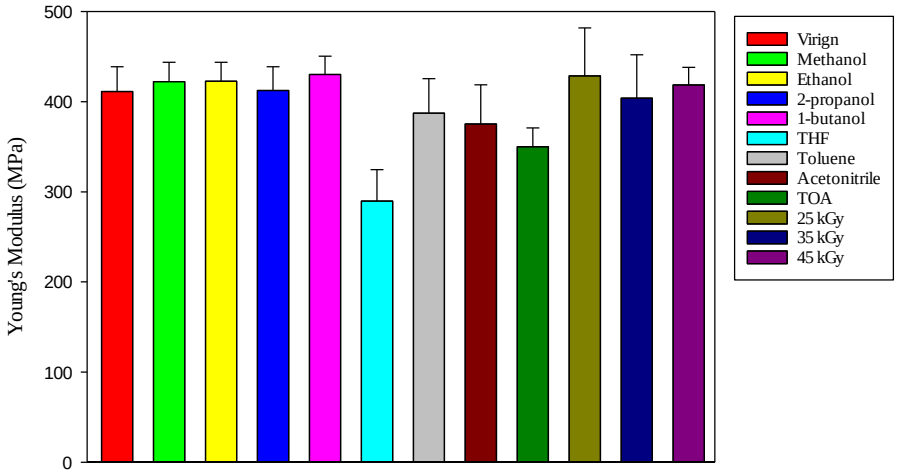

Figure 3.23 Summary of Young's modulus for virgin, solvent-soaked and irradiated ECTFE membranes.

CHAPTER 4

MICROFILTRATION STUDY OF ECTFE MEMBRANES

4.1 Particle Filtration in Dead-end Microfiltration

Solvent effect on dead-end microfiltration (DE-MF) was studied using aqueous silica suspention. The relationship between the filtration flux and time is shown in Figure 4.1 for virgin, ethanol-soaked and TOA-soaked ECTFE membranes. The initial flux of the TOA-soaked ECTFE membrane is extremely high due to the residual TOA (confirmed earlier by thermal analysis) and TOA–water emulsion (when water in the suspension gets in touch with the TOA-soaked membrane) makes the membrane wet easily. The surface tension of TOA is 28.8 dyne/cm, which is much lower than that of water, 72.75 dyne/cm [105]. Moreover, TOA could form hydrogen bonds with water, which also facilitates the wetting of ECTFE membranes. After five minutes, the filtration flux of these three membranes are close. It is because the silica nanoparticles were deposited on the surface of these membranes, and a cake layer was building up on the membrane surface.

The filtration results plotted using Equation (2.14) are illustrated in Figure 4.2 (a-c), and the regression equations are summarized in Table 4.1. It needs to be mentioned that the values of J used here are the average of three measurements. For the virgin ECTFE membrane, the value of R^2 (it measures how close the data are to a statistical model) of the cake filtration ($(J/J_0)^{0.5}$) equation is 0.9812, which is close to 1.0; therefore, the governing mechanism of the virgin ECTFE membrane is cake filtration. The mechanism of intermediate blocking is also acceptable since such R^2 is 0.9693. For ethanol-soaked ECTFE membranes, the intermediate blocking and the standard blocking well fit with the

filtration results. However, for TOA-soaked ECTFE membranes, only the intermediate blocking mechanism can describe its fouling behavior; the other two are not good fits.

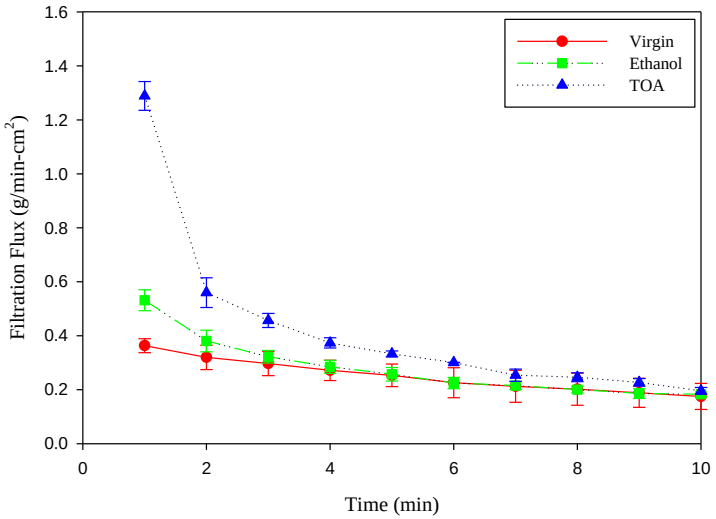

Figure 4.1 The relationship between the filtration flux and the time measured using virgin, ethanol-soaked and TOA-soaked ECTFE membranes.

Table 4.1 Regression Equations of Membrane Blocking Mechanism for Virgin, Ethanol-Soaked and TOA-Soaked ECTFE Membranes

Mechanism / Membrane	Cake filtration $(J/J_0)^{0.5}$	Intermediate blocking $(J/J_0)^1$	Standard blocking $(J/J_0)^2$
Virgin	y = 0.0427x + 1 R^2 = 0.9812	y = 0.1x + 1 R^2 = 0.9693	y = 0.2822x + 1 R^2 = 0.9260
Ethanol	y = 0.0789x + 1 R^2 = 0.9473	y = 0.2052x + 1 R^2 = 0.9762	y = 0.7372x + 1 R^2 = 0.9705
TOA	y = 0.1687x + 1 R^2 = 0.9054	y = 0.5516x + 1 R^2 = 0.9764	y = 3.4734x + 1 R^2 = 0.9219

(a)

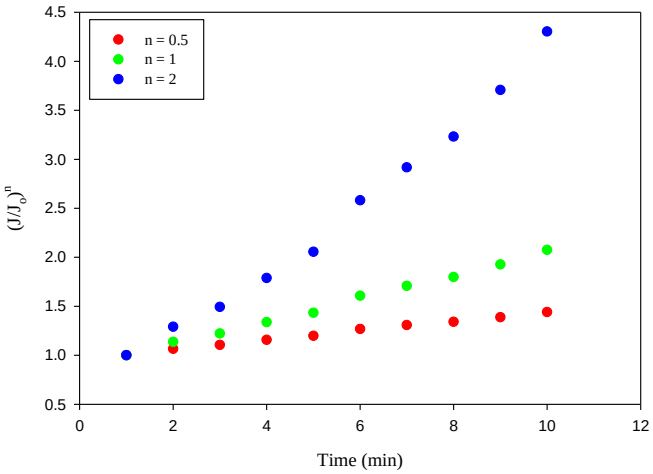

(b)

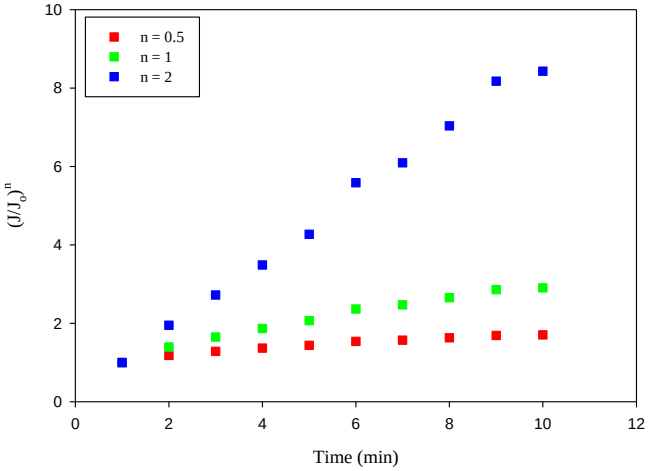

(c)

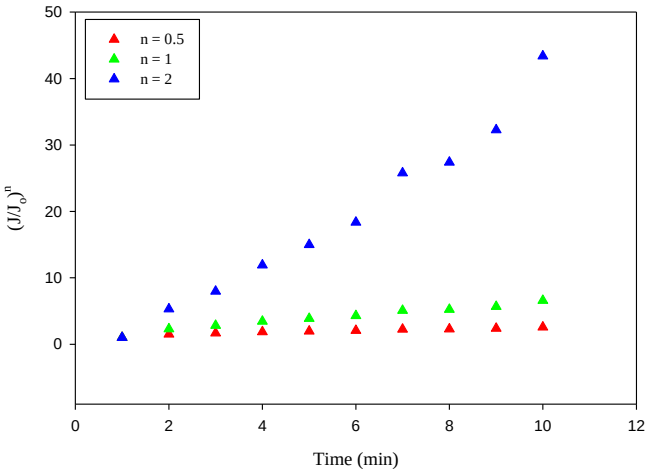

Figure 4.2 Plot of the filtration data based on the membrane blocking mechanism for (a) virgin, (b) ethanol-soaked and (c) TOA-soaked ECTFE membranes.

The PSD measurement was conducted with the filtrate collected every minute. It has to be noted that hardly any particle can pass through the virgin ECTFE membrane after ~five min, which is shown in Figure 4.3 (a). It is because the silica nanoparticles get embedded in the membrane pores; the embedded silica nanoparticles and the growing filtration cake essentially blocked the membrane pores completely. In other words, the membrane allows only the solvent to pass after five min; therefore, there was no point to continue the measurement after five min. This is especially relevant if one is interested in allowing smaller particles to go through the pores. Interestingly, for TOA-soaked ECTFE membranes, the PSD results shown in Figure 4.3 (b) indicate that after the filtration cake was developed (~five min), the separation ability of such a membrane became similar to that of the virgin membrane for the first five minutes. Here, the PSD in the second minute shows a larger size distribution than that of the feed; it is probably due to the aggregation of silica nanoparticles. After effective sonication, the large aggregates would fall apart. Moreover, with respect to the filtration mechanisms discussed earlier, the performances of the virgin and ethanol-soaked ECTFE membranes can be explained by two different governing equations; the reason could be the shorter time of each measurement. In the measurements conducted by Herrero et al. [61] on the filtration behavior (5000 seconds) of bovine serum albumin, the initial steps of fouling fitted to the standard model, while the final steps of the fouling fitted the intermediate model. Regardless, the TOA-soaked ECTFE membrane behaves differently compared with the virgin one.

The results for virgin, ethanol-soaked and TOA-soaked ECTFE membranes in the first four minutes are shown in Figure 4.4. It is clear that fouling occurs as time goes on so that the particles which can pass through the membranes are smaller and smaller.

Compared with the separation performance of virgin ECTFE membrane, some larger particles with size as large as 300 nm can pass through the ethanol-soaked ECTFE membrane; some larger particles with size as large as 400 nm can pass through the TOA-soaked ECTFE membrane. This is in good agreement with the pore size distribution results from AFM analysis and d_{max} in the P_{bp} measurements that ECTFE membranes after soaking in ethanol developed larger pores, but not as large as the pores of TOA-soaked ECTFE membranes.

(a)

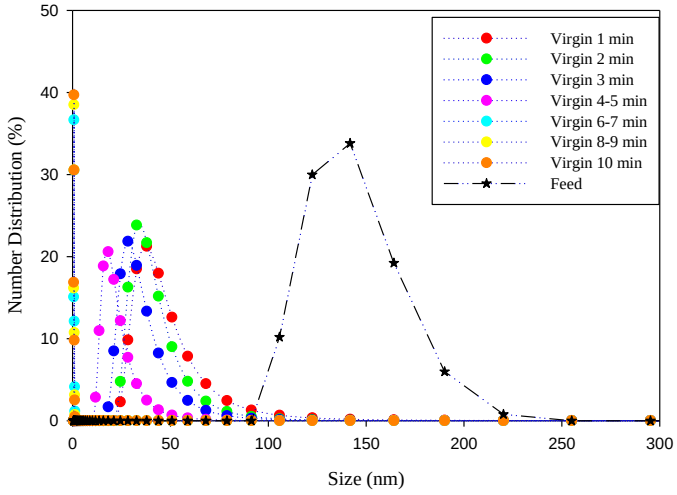

(b)

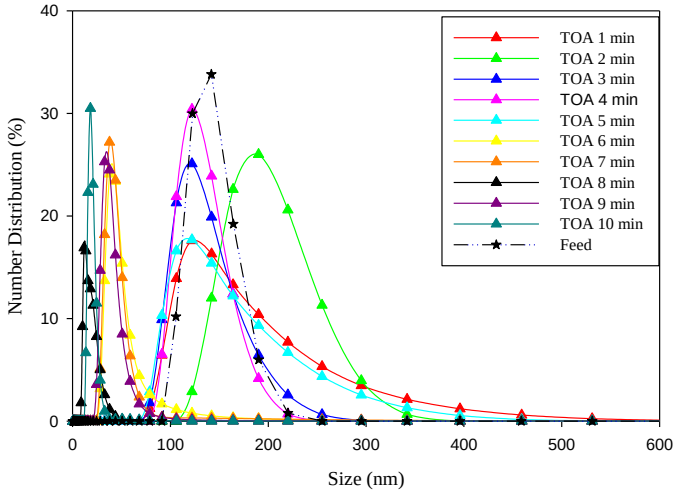

Figure 4.3 PSD results of the filtrates collected in the DE-MF of an aqueous suspension of silica nanoparticles using (a) virgin and (b) TOA-soaked ECTFE membranes.

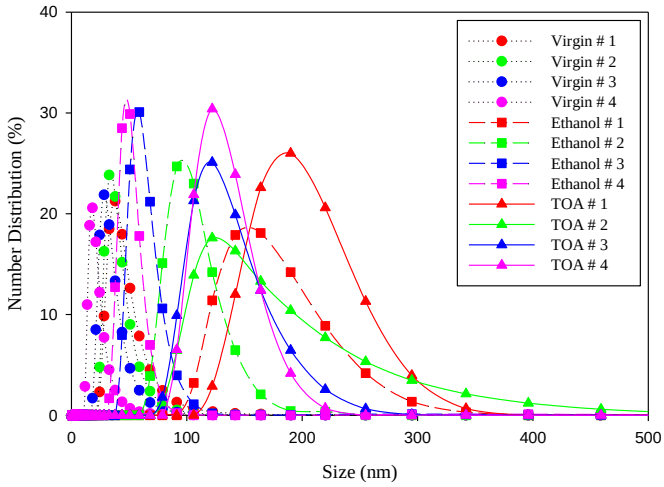

Figure 4.4 PSD results of the filtrates collected in the DE-MF using virgin, ethanol-soaked and TOA-soaked ECTFE membranes for aqueous suspensions of silica nanoparticles (Note: the sample number # was labeled as time goes by).

4.2 Solvent Filtration in Dead-end Microfiltration

The selected solvents are methanol, ethanol and 2-propanol, whose basic characteristics are summarized in Table 4.2. Based on the combination of Equations (2.13) and (2.15), the permeability constant (i.e. permeance) can be determined. The results of solvent flux vs. pressure and the permeability constant are respectively shown in Figure 4.5 and Table 4.2.

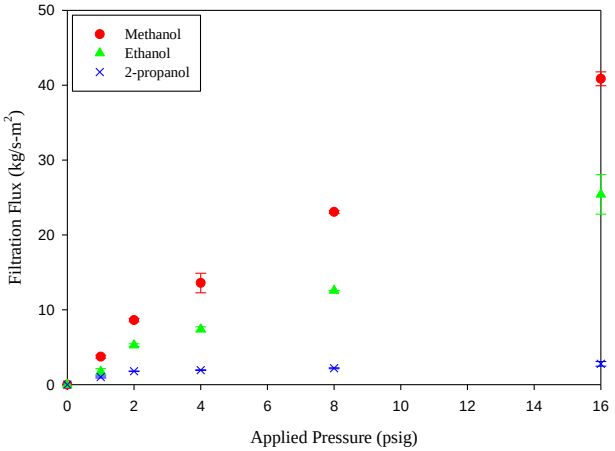

Figure 4.5 The results of the solvent flux at different pressures.

In all tests, the permeate flux increased linearly with an increased pressure. At all testing pressures, $J_{methanol}>J_{ethanol}>J_{2\text{-propanol}}$. Ursino et al. also reported the similar solvent flux results of methanol and ethanol [73]. The permeability constant of these three solvents also perform in the same order as filtration flux. These can be explained by the different molecular weights and the viscosities of these three solvents [73, 106] namely, the molecular weight and the viscosity of methanol are smaller than those of the rest two solvents.

Table 4.2 Characteristics of the Solvents Used in Filtration Flux Measurements

Solvent	Molecular weight (g/mol)	Density (kg/m^3)	Surface tension* (dyne/cm)	Viscosity** (cP)	Permeability constant (kg/m^2-s-kPa)
Methanol	32.04	791	22.51	0.585	0.39
Ethanol	46.07	789	21.82	1.201	0.23
2-propanol	60.1	786	21.22	2.428	0.03

Note: * adapted from Reference [79]; ** adapted from Reference [77].

4.3 Particle Filtration in Cross-flow Microfiltration

Three runs with filtrate samples collected every 2 min (I), 3 min (II) and 5 min (III) have been carried out using a suspension of 3.8 ppm silica in 25% ethanol solution at 15 psig (103 kPag). A comparison of filtration fluxes is illustrated in Figure 4.6 showing that the runs were reproducible in terms of flux vs. time. The PSD results are shown in Figure 4.7 (a-c) for these three runs. Figure 4.8 (a-b) illustrates the PSD comparison of three different runs at around 10 min and 20 min, respectively. It appears that the three runs were quite similar (Figure 4.8 (b)). In addition, it seems that the particles with size larger

than 200 nm cannot go through the membrane as far as Figure 4.7 (a-c) is concerned. This suggests that the nominal membrane pore size is 0.2 μm, as was known earlier.

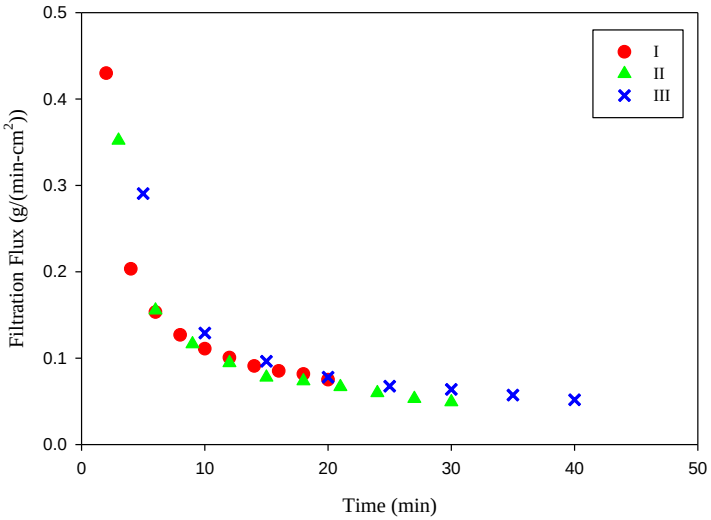

Figure 4.6 Filtration flux comparison of cross-flow microfiltration at 15 psig.

(a)

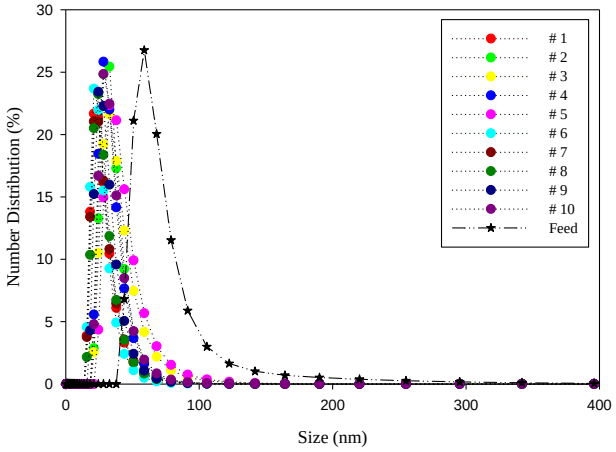

(b)

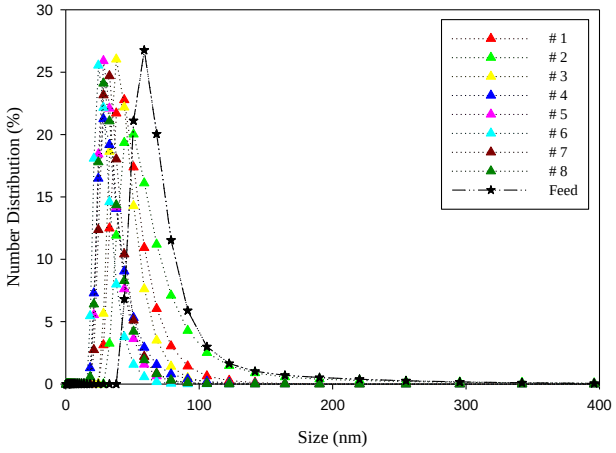

(c)

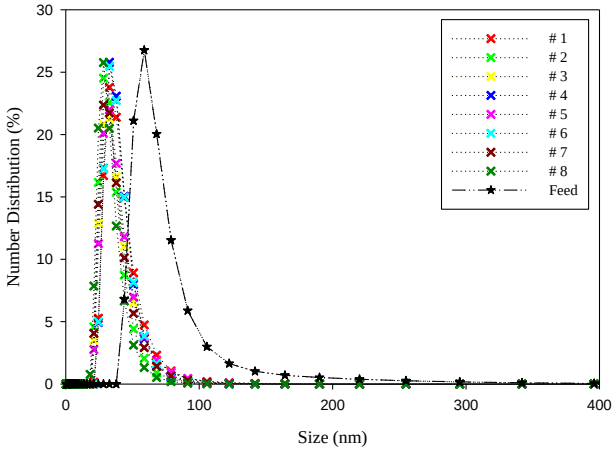

Figure 4.7 The PSD results of filtrates collected every (a) 2 min, (b) 3 min and (c) 5 min.

(a)

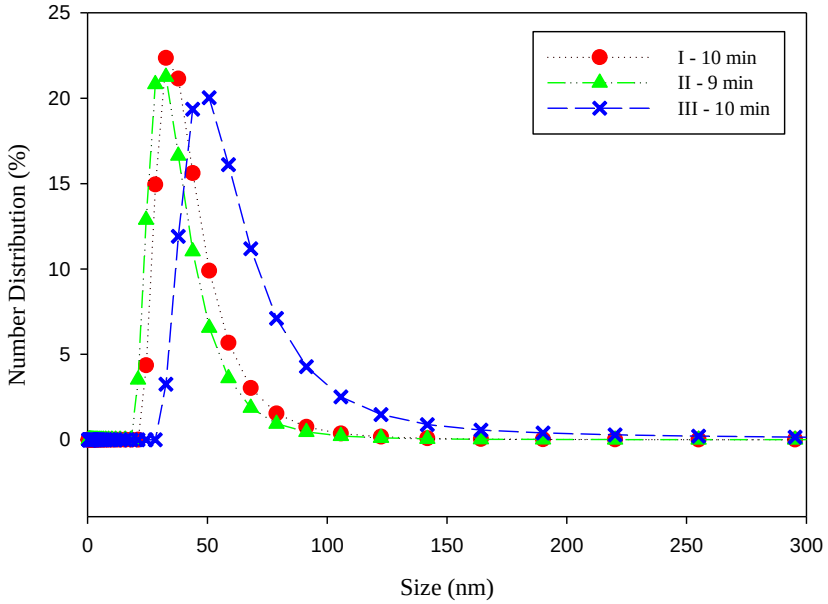

(b)

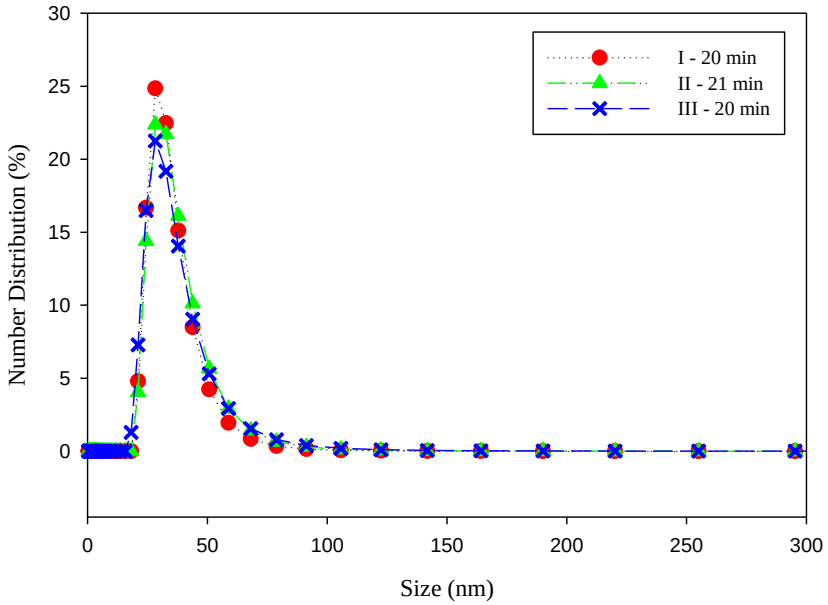

Figure 4.8 The PSD comparison of three runs at around (a) 10 min and (b) 20 min for CF-MF with 3.8 ppm silica suspension in aqueous-ethanol solution.

The effects of feed concentration and operating pressure were also studied. The feed flow rate was 30 mL/min for all tests. Figure 4.9 illustrates the relationship between filtration flux and time operated at different pressures using 3.8 ppm and 1.9 ppm silica-ethanol suspensions. In Figure 4.9, the flux operated under 1 psig using 3.8 ppm suspension had as expected the lowest flux value. Generally, the flux of all six runs shows the highest values and the highest decline rate at the beginning, and then the flux drops down gradually towards a plateau at the end. At the last 20 min, the flux values compare as follow: $J_{1.9\ ppm\ -\ 4\ psig} > J_{1.9\ ppm\ -\ 2\ psig} > J_{1.9\ ppm\ -\ 1\ psig} > J_{3.8\ ppm\ -\ 4\ psig} > J_{3.8\ ppm\ -\ 2\ psig} > J_{3.8\ ppm\ -\ 1\ psig}$ as shown in the small inset figure in Figure 4.9. Less fouling is observed in the case where the filtration is operated under 4 psig using 1.9 ppm suspension. The filtration results of these six runs were also plotted using Equations (2.18-2.20) to find out the governing fouling mechanism. The regression equations are shown in Table 4.3. The governing fouling mechanism for the experiments which was operated using 3.8 ppm at 1 psig and 2 psig is pore blocking. These two runs have the lowest values of the filtration flux at the last 20 min. The governing mechanism for the remaining four runs are membrane resistance. Less particles get embedded in membrane pores in the experiments operated using suspensions with lower concentrations or somehow higher concentration with a higher transmembrane pressure. When the operating pressure is lower, the shear rate is lower. Therefore, more particles would get embedded in membrane pores. The cake formation mechanism is not the governing mechanism for any run. It reflects the intrinsic characteristics of cross-flow mode that the high shear rate would lead to deposition of less particles.

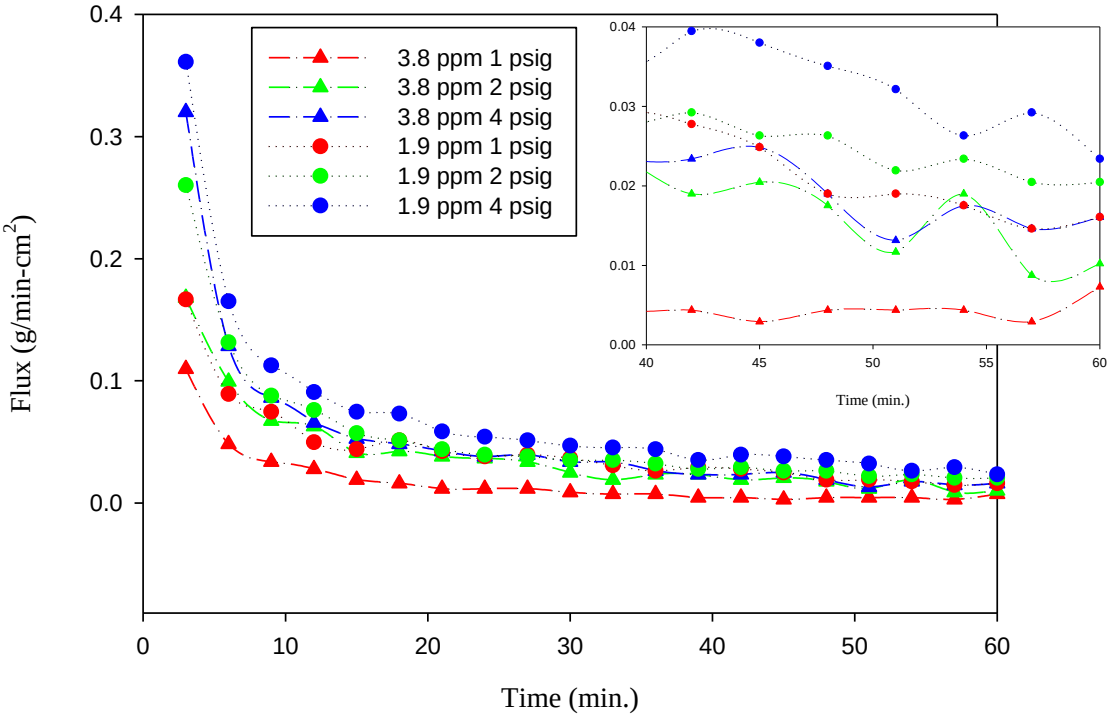

Figure 4.9 The relationship between filtration flux and time operated at different pressures using different silica aqueous-ethanol suspensions.

Table 4.3 Regression Results of Membrane Fouling Mechanisms

Test Condition	Mechanism		
	Membrane resistance-limited	Pore blocking resistance-limited	Cake resistance-limited
3.8 ppm – 1 psig	y = 4.9354x - 14.707 R^2 = 0.7364	y = -0.0497x - 3.0313 R^2 = 0.8153	y = 1477.6x - 16835 R^2 = 0.5307
3.8 ppm – 2 psig	y = 1.4753x - 3.2098 R^2 = 0.8247	y = -0.04x - 2.2737 R^2 = 0.8959	y = 150.56x - 2081.3 R^2 = 0.6051
3.8 ppm – 4 psig	y = 1.1084x - 0.3161 R^2 = 0.9211	y = -0.041x - 2.0245 R^2 = 0.8521	y = 81.334x - 965.86 R^2 = 0.7653
1.9 ppm – 1 psig	y = 0.953x + 3.4637 R^2 = 0.936	y = -0.0328x - 2.3242 R^2 = 0.8985	y = 68.521x - 747.03 R^2 = 0.8188
1.9 ppm – 2 psig	y = 0.7483x + 4.8144 R^2 = 0.9809	y = -0.034x - 2.1167 R^2 = 0.8277	y = 41.467x - 329.53 R^2 = 0.9479
1.9 ppm – 4 psig	y = 0.5849x + 3.1675 R^2 = 0.9602	y = -0.0342x - 1.8334 R^2 = 0.8294	y = 25.579x - 232.94 R^2 = 0.8645

The plots of fouling mechanisms are shown in Figure 4.10 (a-d). At the beginning of the six runs, it seems that membrane itself has more impact on the permeate flux, as shown in Figure 4.10 (a) and (c). In this case, the clean membrane would be the major resistance. However, as time goes by, more and more particles get embedded in membrane pores. Thus, pore blocking mechanism plays an more important role, as shown in 4.10 (b) and (d). This is consistent with the results reported by Lim et al. [64].

(a)

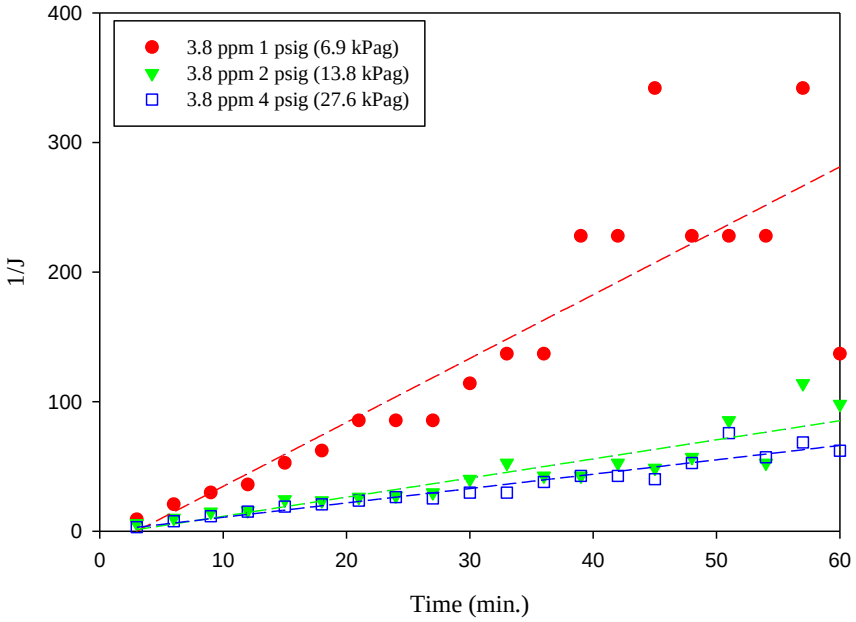

(b)

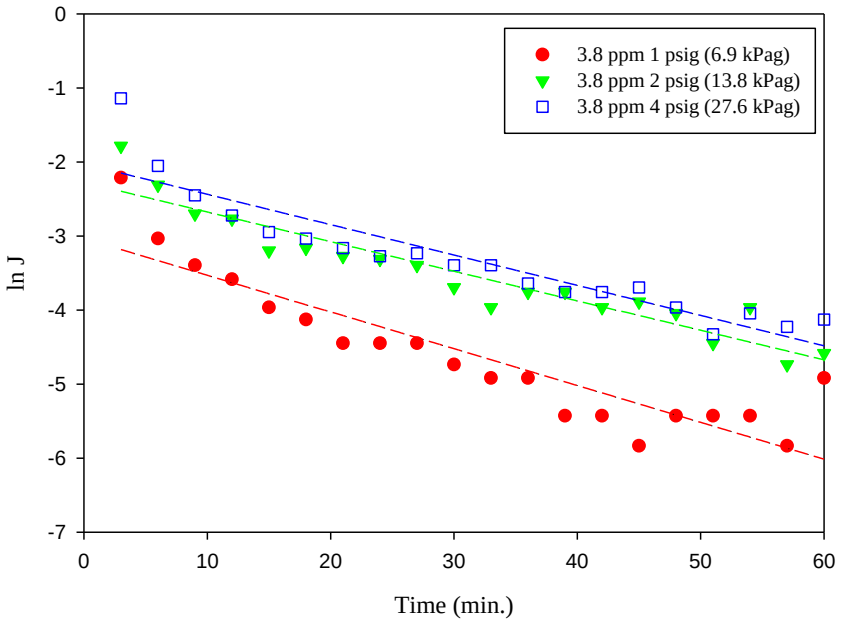

Figure 4.10. Plots of fouling mechanisms: (a) membrane-limited model and (b) pore-blocking model for 3.8 ppm suspension (Continued).

(c)

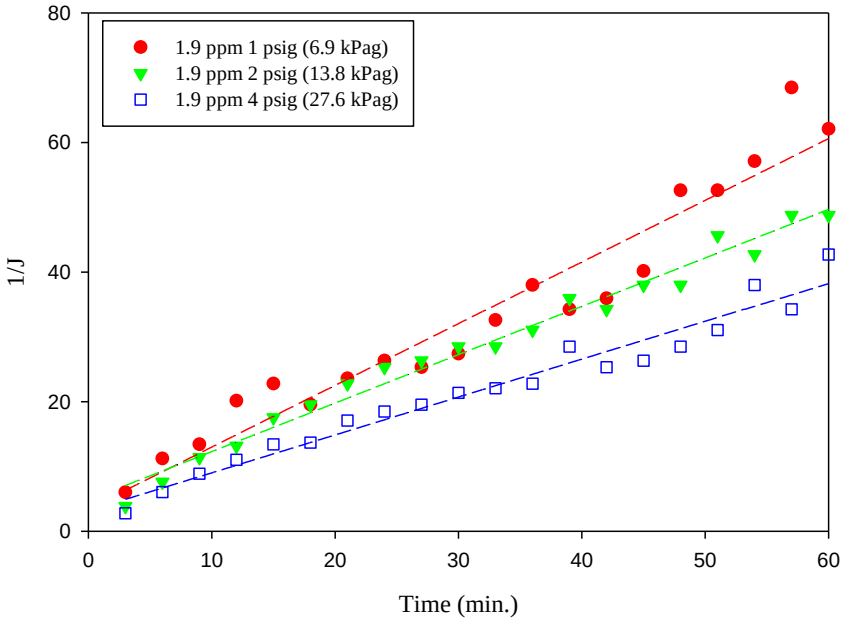

(d)

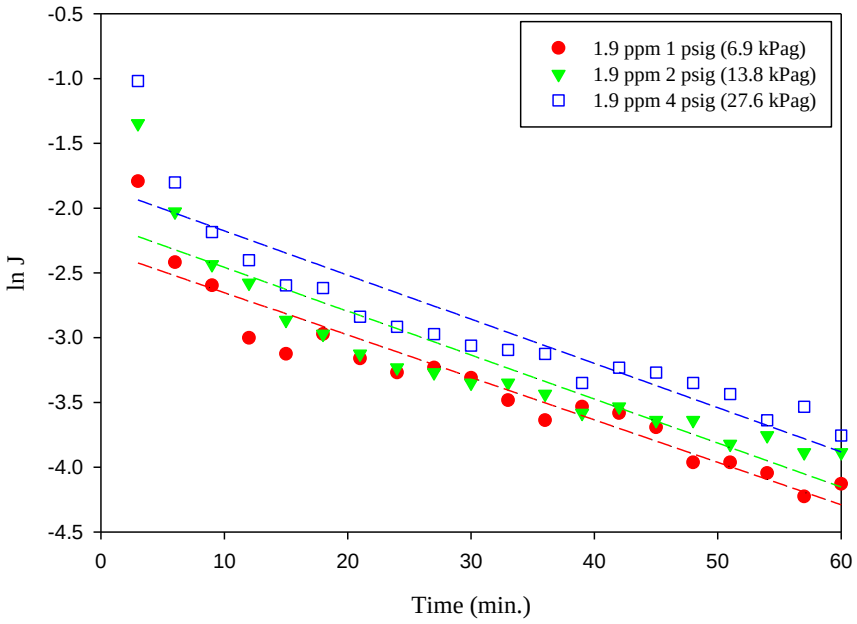

Figure 4.10. (Continued) Plots of fouling mechanisms: (c) membrane-limited model and (d) pore-blocking model for 1.9 ppm suspension.

Figure 4.11 illustrates SEM images of ECTFE membrane after microfiltration tests using 3.8 ppm silica-ethanol suspension at different pressures. All of these images show that particles were deposited on the membrane surface or embedded in membrane pores. Therefore, the particle size in the permeates was smaller than that of the feed as shown in Figure 4.6. Moreover, less particles were observed in Figure 4.11 (a-b). In this case, the membrane is cleaner than those of the other two. This is in good agreement with earlier results that the governing fouling mechanism for the experiment using 3.8 ppm at 4 psig is membrane resistance while for the tests that operated at 1 psig and 2 psig are pore blocking. Therefore, it is clear that the higher the operating pressure, the lower is the fouling of the membrane sample.

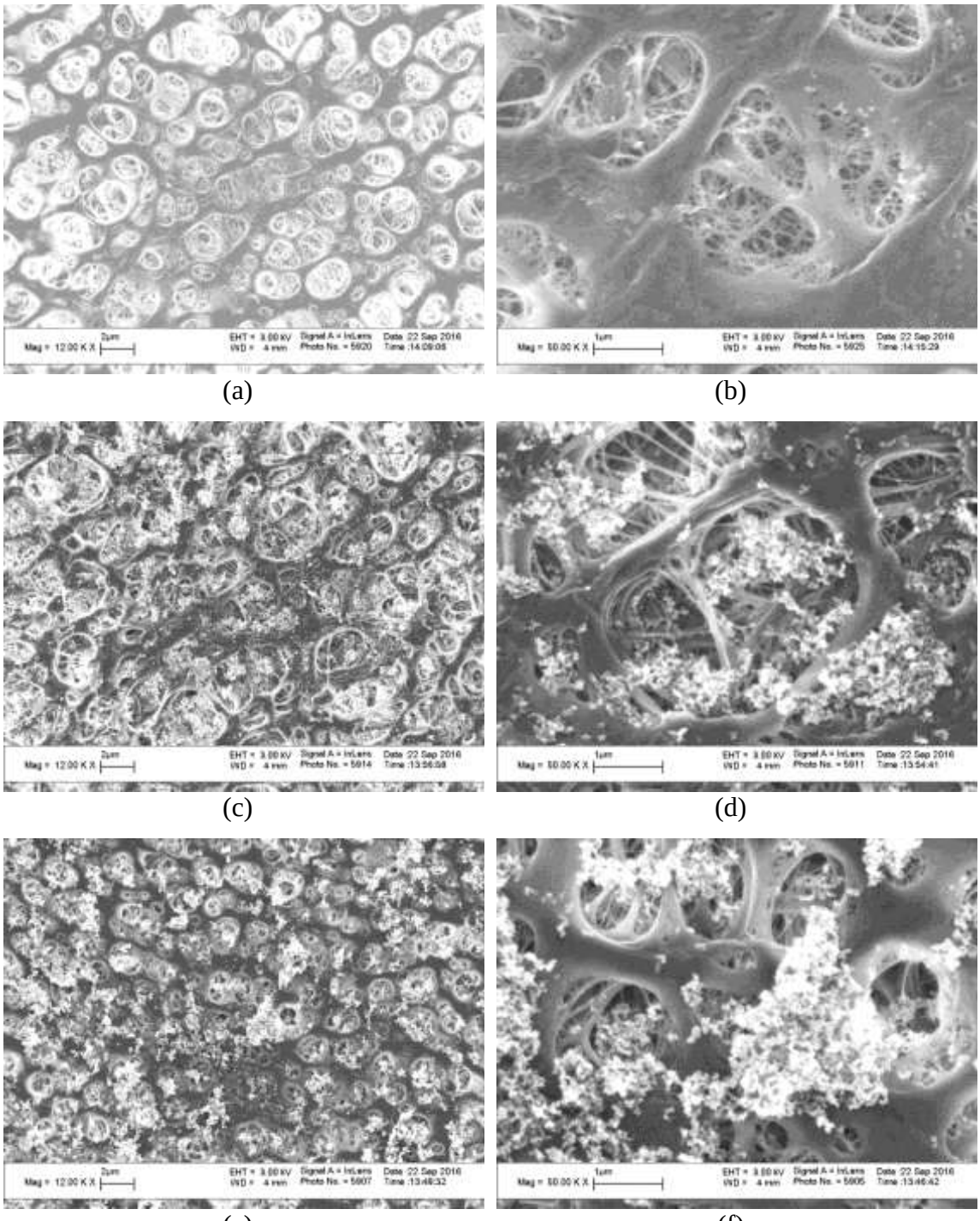

Figure 4.11 SEM images of ECTFE membrane after CF-MF that operated under (a, b) 4 psig, (c, d) 2 psig and (e, f) 1 psig using 3.8 ppm silica aqueous–ethanol suspension.

CHAPTER 5

CONCLUDING REMARKS AND RECOMMENDATIONS

5.1 Concluding Remarks

Microfiltration membranes are widely used for particle removal from process fluids including organic solvents and bases in semiconductor processing. Microfitration membranes also routinely used for sterilization in beverage, biotechnology and pharmaceutical industries are themselves subjected to sterilization by γ-irradiation among others. Partially fluorinated polymers with better radiation resistance are of special interest. The effects of exposure to a variety of liquid media and radiation treatment on various properties of new MF membranes of the partially fluorinated polymer ECTFE were determined via a variety of characterization techniques. Limited comparison was carried out with PVDF membranes. Swellings of porous ECTFE membranes by methanol, ethanol, 2-propanol, THF, toluene, acetonitrile and TOA were much larger than those of nonporous ECTFE films due to the significantly larger surface area of porous membrane. In γ-irradiated ECTFE membranes, the membrane structures characterized by SEM, porosity and tensile properties appeared to be very similar to those of virgin ECTFE membrane. Only the membrane samples subjected to irradiation strength of 45 kGy indicated some effect: the defects introduced by variations were observed in the measurements of dielectric constant and energy loss. In addition, a small decrease in percent of crystallinity and bubble point pressure were observed in ECTFE membranes after exposure to γ-irradiation. Caustic soaking showed essentially similar results in the values of contact angle and bubble point

pressure. Only the higher concentration (3M) of NaOH solution reduced LEP by 13.8 kPag (2 psig).

Variations of T_g for solvent-soaked ECTFE membranes were limited. It appears that the mobility of polymer chains was almost the same with and without organic solvent treatment. However, the crystallinity of TOA-soaked ECTFE membrane was reduced, as shown in the DSC and XRD results. Additionally, roughness estimation from AFM images indicates that ECTFE membrane became rougher after soaking in TOA.

A comparison was carried out with PVDF membranes widely used now. ECTFE membranes showed greater hydrophobicity, stronger wetting resistance as well as better ability to maintain hydrophobicity compared with PVDF membranes. More significant defects on PVDF membranes were observed by XRD analysis in the solvent treatment with TOA. Moreover, the presence of residual TOA in the membrane pores was confirmed by DSC and TGA analyses for both ECTFE and PVDF membranes.

Further, there are potential applications in membrane solvent extraction with TOA in the presence of diluents. Knowledge of membrane resistance to such solvents in such applications is of great interest. Additional characterizations were therefore carried out on ECTFE membranes which were either virgin, or soaked in ethanol, or xylene or xylene80/TOA20 or pure TOA. In tests using FTIR, Raman spectroscopy, thermal analysis and XRD analysis, ECTFE membranes showed excellent solvent resistance to ethanol and xylene; however, TOA did bring out some effects. Moreover, some of the characterization techniques are sensitive enough to catch different levels of effects caused by different levels of TOA in the treating solvents.

The mean pore size and maximum pores size of ECTFE membranes estimated from morphology studies and wetting property indicated that ECTFE membranes developed larger pores after soaking in TOA. This was also confirmed by PSD measurements of the filtrates in the DE-MF test. In the regression study of fouling mechanisms, the filtration behavior of virgin ECTFE membrane fitted well with the cake filtration mechanism, whilst that of the TOA-soaked ECTFE membrane could be described by the intermediate blocking mechanism.

FTIR and Raman spectra demonstrated that ethanol and xylene brought about a limited effect in ECTFE membranes; on the other hand, TOA introduced extra bands indicating C-H stretching and deformation. Interestingly, Raman spectra of xylene80/TOA20-soaked ECTFE membrane were a combination of those of xylene and pure TOA. In the thermal analysis carried out via DSC and TGA, the membranes after treatment by TOA with/without diluent xylene behaved differently compared with the virgin one namely, the melting temperature and thermal stability were reduced. It was due to increasing defects in the lattice structure caused by TOA. The thermograms of xylene80/TOA20-soaked and pure TOA-soaked ECTFE membranes were different; it is due to different amounts of TOA in the treating solvent. In other words, the higher the amount of TOA left in membrane pores, the more defects on the lattice structure and the less stability in such membranes. However, the XRD pattern of xylene80/TOA20-soaked ECTFE membrane looked close to that of the virgin one. Therefore, X-ray diffraction is not sensitive enough to capture the small lattice structure change caused by 20% TOA in xylene.

Moreover, the surface roughness estimation from the AFM images led to the conclusion that the membrane surface became somewhat rougher after soaking in ethanol, and it became much rougher after soaking in TOA. This is a reflection of the defects caused by such solvents.

In DE-MF, fouling mechanisms behaved differently for virgin and TOA-soaked membranes; filtrate particle size distributions agreed well with estimated pore size of ECTFE membranes namely 0.2 μm. In CF-MF, less fouling is observed in the case where the filtration was operated under a higher pressure using a more dilute suspension. The effect of suspension concentration on fouling was confirmed via SEM.

Based on characterization results after exposure to irradiation, caustic solutions and organic solvents as well as its microfiltration behaviors, ECTFE membrane has a high potential for use in severe environments.

5.2 Recommendations

The major goal of this study was to evaluate how good the ECTFE membrane is. This membrane is expected to be used in severe environments and can be an alternative for other polymeric membranes in some aspects such as utilization of ECTFE membrane in radiation sterilization instead of using PTFE in such environment. Therefore, the performance of ECTFE membranes treated by higher levels of γ-radiation or ion radiation need to be studied more extensively. For example, how does the radiation-treated ECTFE membrane perform when it is exposed to heat, solvent and pH variations.

Microfiltration is one of the most expected applications of ECTFE membranes. Silica nanoparticles and pure solvents were used in the current study. This application is

expected to be useful in different activities such as pharmaceutical manufacturing, chemical processing, electronics industry, auto assembly, food processing etc. Therefore, MF studies of paint suspensions, beer, oil, buffer solutions, bacteria-contaminated solutions etc. are of further interest. Extensive MF studies need to be conducted with organic solvents.

APPENDIX A

DERIVATION OF YOUNG-LAPLACE EQUATION

The Young-Laplace equation is useful and important for surface tension analysis or capillary effects of fluids. The deviation of Equation (2.12) is shown below. For an increased interfacial area (dA), Equation (A.1) shows the amount of work (dW) needed. Here, γ is the surface tension. A surface with radii R_1, R_2 and side lengths x and y is considered. The increased area (dA) is calclulated by Equation (A.2). As illustrated in Figure A.1, the small and the large surfaces are the initial and final surfaces, respectively. The distance between the two surfaces is dz. The amount of work shown in Equation (A.1) is also associated with a corresponding change of pressure (ΔP), as shown in Equation (A.3). Equation (A.4) is the result of the conbination of Equations (A.1) and (A.3).

$$dW = \gamma\, dA \tag{A.1}$$

$$dA = (x + dx)(y + dy) - xy = xdy + ydx \tag{A.2}$$

$$dW = \Delta\, P\, x\, y\, dz \tag{A.3}$$

$$\gamma\, dA = \Delta\, P\, x\, y\, dz \tag{A.4}$$

Comparing similar triangles, it is easy to get Equations (A.5-A.6).

$$dx = \frac{x\,dz}{R_1} \tag{A.5}$$

$$dy = \frac{y\,dz}{R_2} \tag{A.6}$$

Substituting Equations (A.2, A.5 and A.6), Equation (A.7) can be obtained. For a spherical drop, namely R_1 equals to R_2 or R and Equation (A.7) can be written as Equation (A.8).

$$\Delta P = \gamma \left(\frac{1}{R_1} + \frac{1}{R_2}\right) \tag{A.7}$$

$$\Delta P = \frac{2\gamma}{R} \tag{A.8}$$

Figure A.2 (b) illustrates the schematic drawing of an interface of two phases in a cylindrical tube. Here, R is the radius of the meniscus that is formed by the two phases; θ is the contact angle; a is the radius of the cross-section of the tube. According to the triangle rule, it is easy to get Equation (A.9). It has to be mentioned that for bubble point pressure measurement, phase I is the gas phase and phase II is the liquid phase. The Young-Laplace Equation can be obtained by combining Equations (A.8 and A.9), as shown in Equation (A.10). However, for LEP measurement, phase I is the liquid and phase II is the gas. The surface tension forces support the pressure drop across the liquid-vapor interface. That is why there is a negative in LEP calculation, as shown in Equation (3.2).

$$R = \frac{a}{\cos\theta} \tag{A.9}$$

$$\Delta P = \frac{2\gamma\cos\theta}{a} \tag{A.10}$$

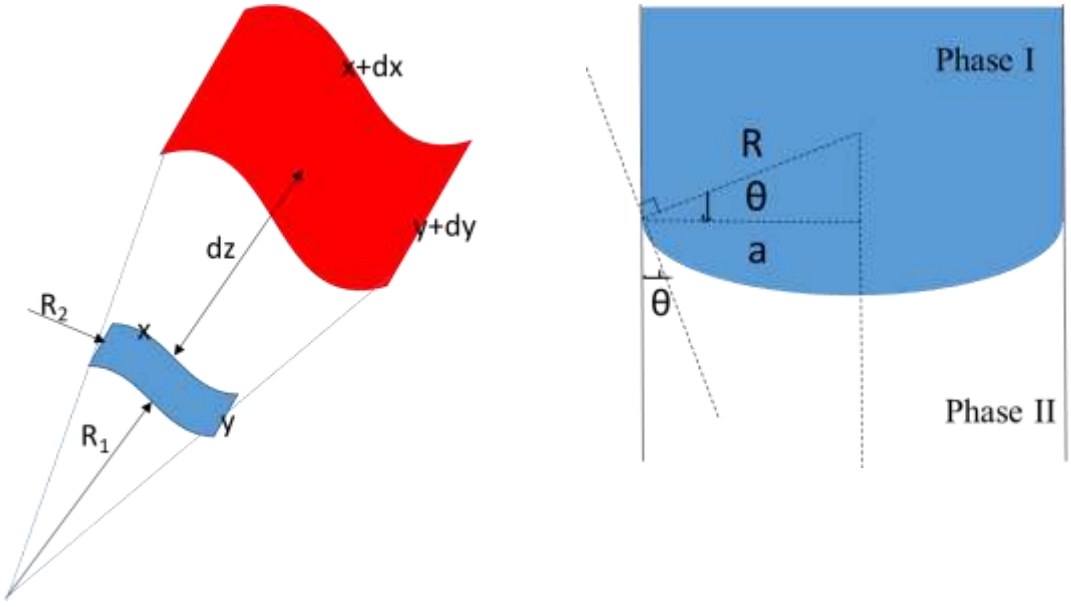

(a) (b)

Figure A.1 Schematic drawing of (a) an increased interfacial area and (b) interface of two phases in a cylindrical tube.

APPENDIX B

SEM IMAGES OF VIRGIN ECTFE MEMBRANES

Figure B.1 (a-d) shows virgin ECTFE membranes with different magnitudes as described in Section 3.3.

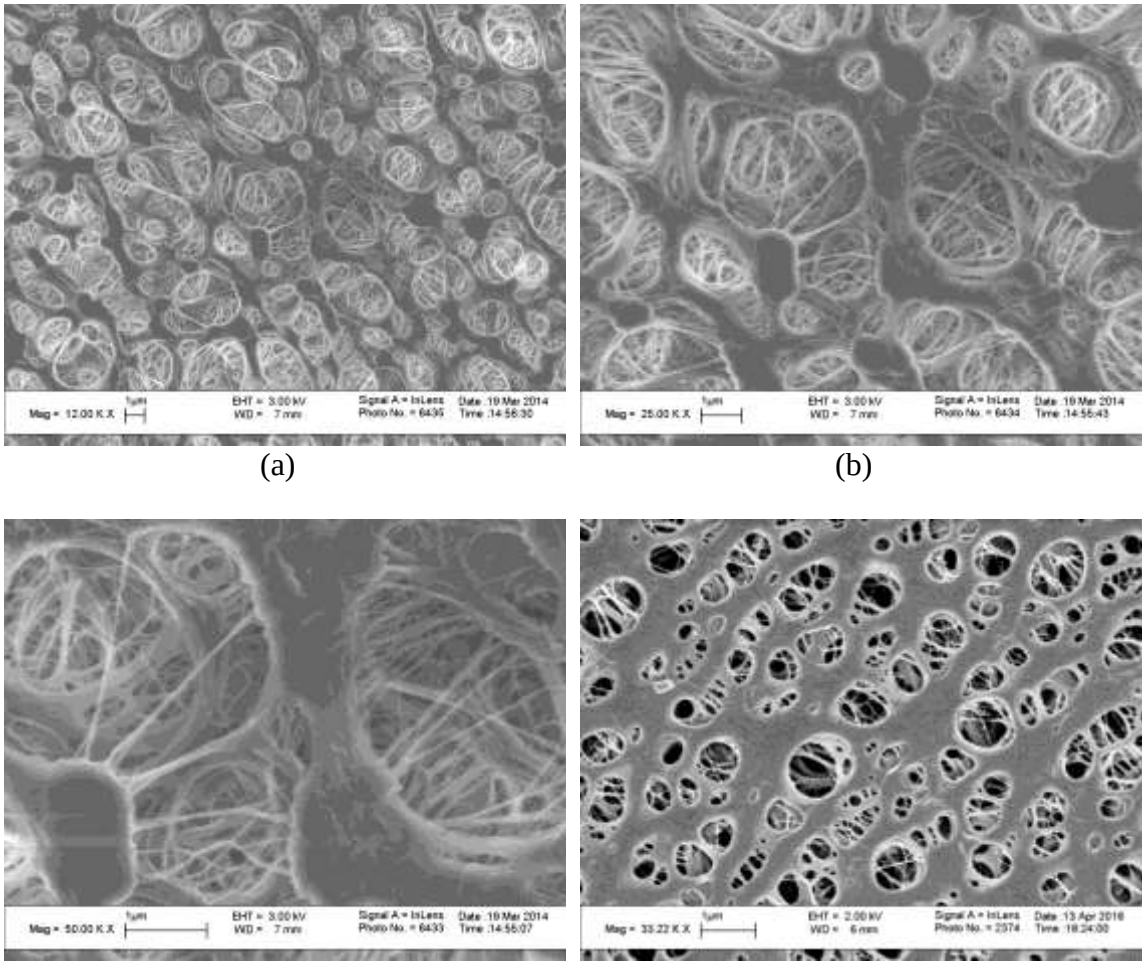

(a) (b)

(c) (d)

Figure B.1 SEM images of virgin ECTFE membranes with the magnification of (a) 12000, (b) 25000 and (c) 50000 as well as (d) membrane sample indicating most pores with size of 0.2 µm.

APPENDIX C

TGA RESULTS OF VIRGIN AND SOLVENT-SOAKED ECTFE MEMBRANES

Figure C.1 (a-c) illustrates the comparison of virgin and solvent-soaked ECTFE membranes as described in Section 3.6.2.

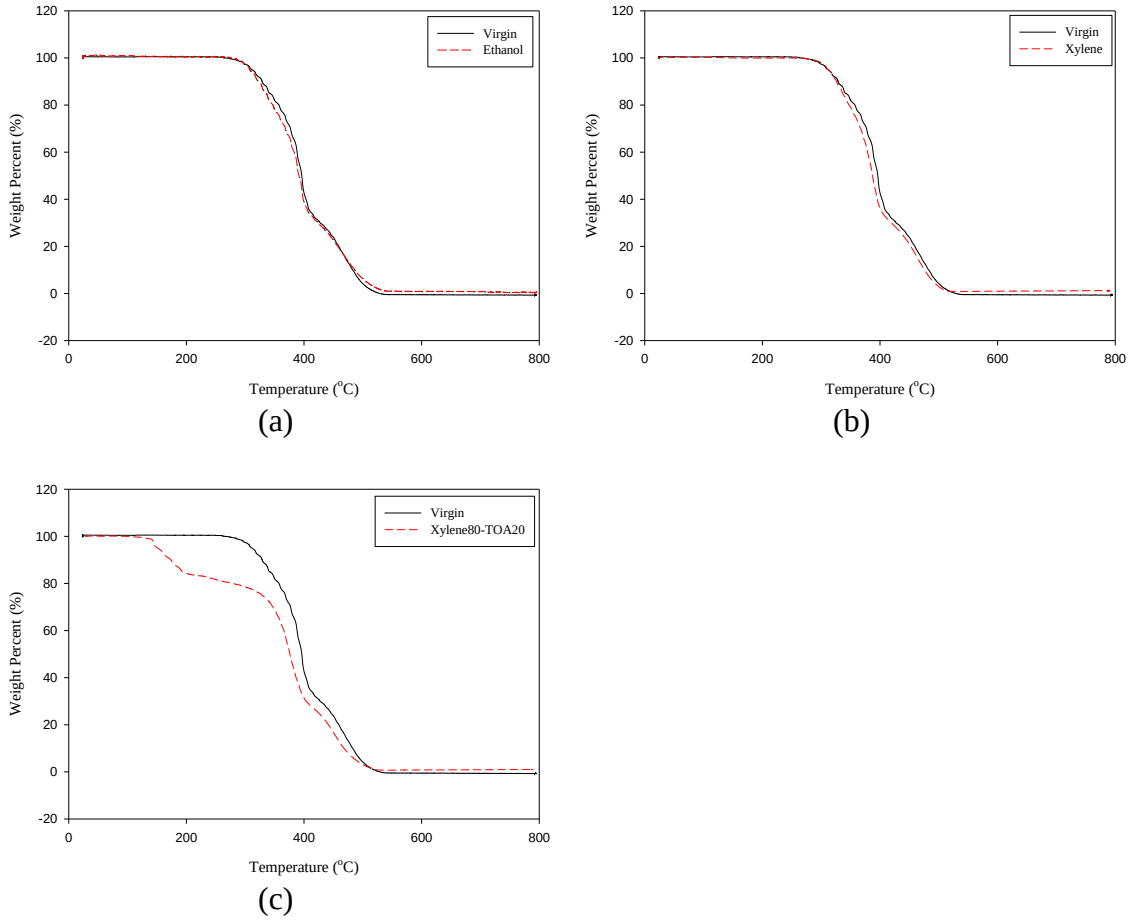

Figure C.1 Comparison of TGA results between virgin and (a) ethanol-soaked, (b) xylene-soaked and (c) xylene80/TOA20-soaked ECTFE membranes.

APPENDIX D

DETAILED EXPERIMENTAL DATA FOR SELECTED MEASUREMENTS

Tables D.1 – D.4 provide the detailed experimental data for seclected measurements.

Table D.1 Contact Angle Results of Ethanol-Water Mixtures on Dense/Porous ECTFE and PVDF Membranes

Ethanol Conc. (wt. %)	Dense ECTFE		Porous ECTFE		Dense PVDF		Porous PVDF	
	θ (degree)	cos θ	θ (degree)	cos θ	θ (degree)	cos θ	θ (degree)	cos θ
0.00	95.67	-0.10	114.33	-0.41	87.33	0.05	119.17	-0.49
5.00	89.50	0.01	108.50	-0.32	84.50	0.10	114.67	-0.42
10.00	86.67	0.06	104.67	-0.25	78.50	0.20	111.73	-0.37
15.00	80.17	0.17	101.67	-0.20	70.00	0.34	101.23	-0.19
20.00	75.67	0.25	97.33	-0.13	65.17	0.42	93.13	-0.05
25.00	72.33	0.30	95.07	-0.09	59.83	0.50	84.10	0.10
30.00	65.67	0.41	84.10	0.10	52.33	0.61	37.17	0.80

Table D.2 Contact Angle Results of 2-propanol-Water Mixtures on Dense/Porous ECTFE and PVDF Membranes

2-propanol Conc. (wt. %)	Dense ECTFE		Porous ECTFE		Dense PVDF		Porous PVDF	
	θ (degree)	cos θ	θ (degree)	cos θ	θ (degree)	cos θ	θ (degree)	cos θ
0.00	95.67	-0.10	114.33	-0.41	87.33	0.05	119.17	-0.49
5.00	86.67	0.06	103.17	-0.23	73.50	0.28	106.17	-0.28
10.00	82.33	0.13	98.50	-0.15	69.83	0.34	97.67	-0.13
15.00	68.50	0.37	87.17	0.05	55.33	0.57	69.50	0.35

Table D.3 Contact Angle Results of 1-butanol-Water Mixtures on Dense/Porous ECTFE and PVDF Membranes

1-butanol Conc. (wt. %)	Dense ECTFE		Porous ECTFE		Dense PVDF		Porous PVDF	
	θ (degree)	cos θ	θ (degree)	cos θ	θ (degree)	cos θ	θ (degree)	cos θ
0.00	95.67	-0.10	114.33	-0.41	87.33	0.05	119.17	-0.49
0.25	92.00	-0.03	111.93	-0.37	84.83	0.09	117.47	-0.46
0.45	89.67	0.01	110.27	-0.35	81.50	0.15	116.17	-0.44
0.87	86.50	0.06	108.33	-0.31	77.67	0.21	112.90	-0.39
1.59	79.33	0.19	104.80	-0.26	73.33	0.29	108.53	-0.32
2.78	73.50	0.28	100.07	-0.17	67.00	0.39	101.73	-0.20
3.96	58.67	0.52	94.83	-0.08	61.00	0.48	86.83	0.06

Table D.4 Summary of r_{max} and γ_L^w Estimated from LEP and Surface Tension Correlation

Membrane	Solvent*	Slope*	r_{max} (μm)*	Intercept*	γ_L^w (dyne/cm)*	Slope*	r_{max} (μm)*
	Ethanol	1.39	1.44	42.08	30.23	1.71	1.17
ECTFE	2-propanol	1.38	1.45	41.38	30.09	1.68	1.19
	1-butanol	1.40	1.42	41.34	29.45	2.06	0.97
	Ethanol	0.93	2.15	31.37	33.75	1.71	1.17
PVDF	2-propanol	0.98	2.04	35.20	35.97	1.68	1.19
	1-butanol	0.94	2.13	30.66	32.67	2.06	0.97

Note: * and ** were estimated from Equations (3.1) and (3.2), respectively.

APPENDIX E

CALCULATION OF WALL SHEAR STRESS AND SHEAR RATE IN CROSS-FLOW MICROFILTRATION

Equations used to calculate the wall shear stress (τ_w) and wall shear rate (γ) through a cylindrical pore are expressed as [107, 108]:

$$\tau_w = \frac{R \ \Delta P}{2 L} \tag{E.1}$$

$$\gamma = \frac{R \ \Delta P}{2 \mu L} \tag{E.2}$$

Here, R is the radius of membrane pore assumed to be straight and cylindrical; ΔP is the applied pressure difference over the membrane; L is the membrane thickness; μ, the viscosity of the feed suspension, can be determined from Einstein equation [109].

$$\frac{\mu}{\mu_o} = 1 + \frac{5}{2}\phi \tag{E.3}$$

Here, μ_o is the viscosity of the liquid medium of the suspension and ϕ is the volume fraction of the solid in the suspension. The values of inside-the-membrane-pore τ_w and γ calculated for different test conditions in this cross-flow microfiltration study are summarized in Table E.1.

Table E.1 Values of τ_w and γ for Different Test Conditions in Cross-flow Microfiltration

Test conditions	τ_w (psi)	τ_w (Pa)	γ (s^{-1})
3.8 ppm – 1 psig	1×10^{-3}	6.9	6.3×10^{3}
3.8 ppm – 2 psig	2×10^{-3}	13.8	12.6×10^{3}
3.8 ppm – 4 psig	4×10^{-3}	27.6	25.2×10^{3}
1.9 ppm – 1 psig	1×10^{-3}	6.9	6.8×10^{3}
1.9 ppm – 2 psig	2×10^{-3}	13.8	13.6×10^{3}
1.9 ppm – 4 psig	4×10^{-3}	27.6	27.1×10^{3}

As was mentioned earlier, the governing fouling mechanism of the tests operated using 3.8 ppm at 1 psig (6.9 kPag) and 2 psig (13.8 kPag) is pore blocking. Here it shows that these runs had relatively low value of γ. In the tests operated using a more dilute suspension, the membrane itself plays a more important role on fouling. For the tests (3.8 ppm – 4 psig and 1.9 ppm – 4 psig) with higher shear rates (25.2×10^{3} and 27.1×10^{3}, respectively), less internal fouling is observed. It needs to be mentioned that the value of γ was determined by using the exact applied pressure difference across the membrane. At the beginning of MF test, there is no fouling. Thus, the values of applied pressure difference across the membrane 1, 2 and 4 psig are the exact values of ΔP in Equation (E.1). However, fouling was observed as time goes by. The internal pore blocking or the built-up cake would cause additional resistance over the entire membrane, therefore, results in an increase of ΔP (Alternatively, with applied ΔP remaining constant, the ΔP over the membrane only

will decrease). The results shown in Table E.1 were calculated with the assumption that ΔP is constant during MF. Generally, comparison of shear rates at different experimental times should be comparable to that at the beginning of MF. In this case, it can provide a broad guideline on the values of shear rate at different ΔP.

One may wonder about the maximum size of a particle that can pass through the membrane pores easily. When the nanoparticle diameter (48 nm) is not smaller than the membrane pore size (200 nm) by orders of magnitude, the effective solute diffusion coefficient is decreased by a drag factor G_{Dr} (r_p, r_m) [110]:

$$G_{Dr} = 1 - 2.1004\left(\frac{r_p}{r_m}\right) + 2.089\left(\frac{r_p}{r_m}\right)^3 - 0.948\left(\frac{r_p}{r_m}\right)^5 + \cdots \quad \text{(E.4)}$$

Here, r_p and r_m are the radius of smaller nanoparticles and membrane pores, respectively. Based on the above equation, the particles with smaller size are likely to pass through the membrane pores. Note: this equation (Faxen Equation) is valid only when (r_p/r_m) < 0.5.

REFERENCES

[1] S. Ebnesajjad, P.R. Khaladkar, Fluoropolymers Applications in Chemical Processing Industries - The Definitive User's Guide and Databook, in, William Andrew Publishing/Plastics Design Library.

[2] C.W. Extrand, The use of fluoropolymers to protect semiconductor materials, J. Fluor. Chem., 122 (2003) 121-124.

[3] E. Giannetti, Thermal stability and bond dissociation energy of fluorinated polymers: A critical evaluation, J. Fluor. Chem., 126 (2005) 623-630.

[4] J. Sun, Y. Zhang, X. Zhong, Radiation crosslinking of polytetrafluoroethylene, Polym., 35 (1994) 2881-2883.

[5] J.G. Drobny, Technology of Fluoropolymers, Second Edition, CRC Press Taylor & Francis Group, 2009.

[6] S. Roy, A. Thongsukmak, J. Tang, K.K. Sirkar, Concentration of aqueous hydrogen peroxide solution by pervaporation, J. Membr. Sci., 389 (2012) 17-24.

[7] J. Tang, K.K. Sirkar, S. Majumdar, Permeation and sorption of organic solvents and separation of their mixtures through an amorphous perfluoropolymer membrane in pervaporation, J. Membr. Sci., 447 (2013) 345-354.

[8] H.-J. Müller, A new solvent resistant membrane based on ECTFE, Desalination, 199 (2006) 191-192.

[9] S. Ramaswamy, A.R. Greenberg, W.B. Krantz, Fabrication of poly (ECTFE) membranes via thermally induced phase separation, J. Membr. Sci., 210 (2002) 175-180.

[10] I.J. Roh, S. Ramaswamy, W.B. Krantz, A.R. Greenberg, Poly(ethylene chlorotrifluoroethylene) membrane formation via thermally induced phase separation (TIPS), J. Membr. Sci., 362 (2010) 211-220.

[11] J.S. Mrozinski, R.P. Swenson, K.D. Weilandt, J.F. Hester, Microporous material from ethylene-chlorotrifluoroethylene copolymer and method for making same, in, Google Patents, 2011.

[12] D. Mullette, H.J. Muller, Poly(ethylene chlorotrifluoroethylene) membranes, in, Google Patents, 2009.

[13] K.S. Cheng, C.P. Doh, L.Y. Yen, R.B. Patel, T.D. Gates, Perfluorinated thermoplastic filter cartridge, in, Google Patents, 2008.

[14] K.K.C. Ho, G. Kalinka, M.Q. Tran, N.V. Polyakova, A. Bismarck, Fluorinated carbon fibres and their suitability as reinforcement for fluoropolymers, Composites Sci. Technol., 67 (2007) 2699-2706.

[15] T.R. Dargaville, M. Celina, R.L. Clough, Evaluation of vinylidene fluoride polymers for use in space environments: Comparison of radiation sensitivities, Radiat. Phys. Chem., 75 (2006) 432-442.

[16] J. Pan, C. Xiao, Q. Huang, H. Liu, J. Hu, ECTFE porous membranes with conveniently controlled microstructures for vacuum membrane distillation, J. Mater. Chem. A, 3 (2015) 23549-23559.

[17] J.F. Kim, J.H. Kim, Y.M. Lee, E. Drioli, Thermally induced phase separation and electrospinning methods for emerging membrane applications: A review, AIChE J., 62 (2016) 461-490.

[18] S. Simone, A. Figoli, S. Santoro, F. Galiano, S.M. Alfadul, O.A. Al-Harbi, E. Drioli, Preparation and characterization of ECTFE solvent resistant membranes and their application in pervaporation of toluene/water mixtures, Sep. Purif. Technol., 90 (2012) 147-161.

[19] S. Lee, K.S. Knaebel, Effects of mechanical and chemical properties on transport in fluoropolymers. I. Transient sorption, J. Appl. Polym. Sci., 64 (1997) 455-476.

[20] L. Singh, K. Devgan, K.S. Samra, Effect of swift heavy ion irradiation on ethylene–chlorotrifluoroethylene copolymer, Radiat. Phys. Chem., 81 (2012) 1741-1746.

[21] G. Guerra, C. De Rosa, M. Iuliano, V. Petraccone, P. Corradini, G. Ajroldi, Structural variations as a function of temperature and dynamic-mechanical relaxations for ethylene-tetrafluoroethylene and ethylene-chlorotrifluoroethylene alternating copolymers, Die Makromolekulare Chem., 194 (1993) 389-396.

[22] E. Leivo, T. Wilenius, T. Kinos, P. Vuoristo, T. Mäntylä, Properties of thermally sprayed fluoropolymer PVDF, ECTFE, PFA and FEP coatings, Prog. Org. Coat., 49 (2004) 69-73.

[23] C.Y.O. Lin, J.P. Curilla, Temperature-related changes in dielectric constant and dissipation factor of insulations increase attenuation in data cables used in building plenums, in: Local Computer Networks, 1991. Proceedings., 16th Conference, 1991, pp. 74-79.

[24] R. Alicea-Maldonado, L.A. Colón, Capillary electrochromatography using a fluoropolymer as the chromatographic support material, Electrophoresis, 20 (1999) 37-42.

[25] E. Drioli, S. Santoro, S. Simone, G. Barbieri, A. Brunetti, F. Macedonio, A. Figoli, ECTFE membrane preparation for recovery of humidified gas streams using membrane condenser, React. Functional Polymers, 79 (2014) 1-7.

[26] M.S. Hedenqvist, J.E. Ritums, M. Condé-Brana, G. Bergman, Structure and properties of poly(ethylene-co-chlorotrifluoroethylene) and polyvinylidene fluoride exposed to water, hydrochloric acid, hydrobromic acid and tetrachloroethylene, Polym. Eng. & Sci., 44 (2004) 113-122.

[27] V. Goel, M.A. Accomazzo, A.J. DiLeo, P. Meier, A. Pitt, M. Pluskal, R. Kaiser, in Membrane Handbook, W.S.W. Ho and K.K. Sirkar (eds.), Kluwer Academic Publishers, Boston, MA (2001), Chap. 34.

[28] A. Thongsukmak, K.K. Sirkar, Pervaporation membranes highly selective for solvents present in fermentation broths, J. Membr. Sci., 302 (2007) 45-58.

[29] A. Thongsukmak, K.K. Sirkar, Extractive pervaporation to separate ethanol from its dilute aqueous solutions characteristic of ethanol-producing fermentation processes, J. Membr. Sci., 329 (2009) 119-129.

[30] Z.-F. Yang, A.K. Guha, K.K. Sirkar, Simultaneous and synergistic extraction of cationic and anionic heavy metallic species by a mixed solvent extraction system and a novel contained liquid membrane device, Ind. Eng. Chem. Res., 35 (1996) 4214-4220.

[31] A. Kiani, R. Bhave, K. Sirkar, Solvent extraction with immobilized interfaces in a microporous hydrophobic membrane, J. Membr. Sci., 20 (1984) 125-145.

[32] L. Kubišová, E. Sabolová, Š. Schlosser, J. Marták, R. Kertész, Membrane based solvent extraction and stripping of a heterocyclic carboxylic acid in hollow fiber contactors, Desalination, 148 (2002) 205-211.

[33] M.A. Barakat, M.H.H. Mahmoud, Recovery of platinum from spent catalyst, Hydrometallurgy, 72 (2004) 179-184.

[34] R. Chilukuri, Z.-F. Yang, K.K. Sirkar, Batch extraction studies of cationic and anionic heavy metallic species by a mixed solvent extraction system, Sep. Sci. Technol., 33 (1998) 2559-2578.

[35] C.A. Kozlowski, W. Walkowiak, Removal of chromium(VI) from aqueous solutions by polymer inclusion membranes, Water Res., 36 (2002) 4870-4876.

[36] T. Sato, T. Nakamura, Thermal decomposition of chloro complexes of manganese (II), cobalt (II), copper (II) and zinc (II) with tri-n-octylamine and tricaprylmethylammonium chloride, Thermochimica Acta, 47 (1981) 189-199.

[37] T. Sato, T. Takahashi, Thermal decomposition of the solvent extracted chloro complexes of uranium (VI) with trioctylamine and trioctylmethylammonium chloride, Thermochimica Acta, 92 (1985) 697-700.

[38] D. Desai, V. Shinde, Liquid anion exchange studies of quadrivalent thorium and cerium separation from associated metal ions, Analytical Letters, 13 (1980) 57-65.

[39] J.M. Wardell, C.J. King, Solvent equilibriums for extraction of carboxylic acids from water, J. Chem. Eng. Data, 23 (1978) 144-148.

[40] S. Ohno, Determination of iodine and bromine in biological materials by neutron-activation analysis, Analyst, 96 (1971) 423-426.

[41] S. Ohno, T. Ichikawa, Determination of thorium in bovine bone by neutron-activation analysis, Analyst, 97 (1972) 605-608.

[42] S.N. Patkar, A. Burungale, R. Patil, Separation and liquid-liquid extraction of thorium (IV) as sulphate complex with synergistic mixture of N-n-octylaniline and trioctylamine as an extractant, Rasayan J. Chem., 2 (2009) 825-832.

[43] K.W. Böddeker, Liquid Separations with Membranes: An Introduction to Barrier Interference, Springer, 2008.

[44] W. Ho, K. Sirkar, Membrane Handbook, Chapman & Hall, New York, NY, 1992.

[45] G. Foley, A review of factors affecting filter cake properties in dead-end microfiltration of microbial suspensions, J. Membr. Sci., 274 (2006) 38-46.

[46] R.W. Field, D. Wu, J.A. Howell, B.B. Gupta, Critical flux concept for microfiltration fouling, J. Membr. Sci., 100 (1995) 259-272.

[47] P. Bacchin, P. Aimar, R.W. Field, Critical and sustainable fluxes: Theory, experiments and applications, J. Membr. Sci., 281 (2006) 42-69.

[48] M.T. Aspelund, C.E. Glatz, Clarification of aqueous corn extracts by tangential flow microfiltration, J. Membr. Sci., 365 (2010) 123-129.

[49] P.G. Middlewood, J.K. Carson, Extraction of amaranth starch from an aqueous medium using microfiltration: Membrane characterisation, J. Membr. Sci., 405–406 (2012) 284-290.

[50] P.G. Middlewood, J.K. Carson, Extraction of amaranth starch from an aqueous medium using microfiltration: Membrane fouling and cleaning, J. Membr. Sci., 411–412 (2012) 22-29.

[51] T. Maruyama, S. Katoh, M. Nakajima, H. Nabetani, T.P. Abbott, A. Shono, K. Satoh, FT-IR analysis of BSA fouled on ultrafiltration and microfiltration membranes, J. Membr. Sci., 192 (2001) 201-207.

[52] Q. Gan, M. Xue, D. Rooney, A study of fluid properties and microfiltration characteristics of room temperature ionic liquids [C10-min][NTf2] and N8881[NTf2] and their polar solvent mixtures, Sep. Purif. Technol., 51 (2006) 185-192.

[53] M. Indlekofer, M. Funke, W. Claassen, M. Reuss, Continuous enantioselective transesterification in organic solvents. Use of suspended lipase preparations in a microfiltration membrane reactor, Biotechnol. Prog., 11 (1995) 436-442.

[54] K. Smolders, A.C.M. Franken, Terminology for membrane distillation, Desalination, 72 (1989) 249-262.

[55] L. Li, K.K. Sirkar, Influence of microporous membrane properties on the desalination performance in direct contact membrane distillation, J. Membr. Sci., 513 (2016) 280-293.

[56] L. Li, K.K. Sirkar, Studies in vacuum membrane distillation with flat membranes, J. Membr. Sci., 523 (2017) 225-234.

[57] S.D. Smith, Porosity Measurement of Microporous Membrane Material Test Method (MSTM), 3M Corporate Research Process Laboratory, Membranes & Separations Cluster, (2008).

[58] Anonymous, 3M Corporation, Product sheet, (2014).

[59] J. Mulder, Basic Principles of Membrane Technology, Springer Science & Business Media, 2012.

[60] G.B. Alexander, W.M. Heston, R.K. Iler, The solubility of amorphous silica in water, J. Phys. Chem., 58 (1954) 453-455.

[61] C. Herrero, P. Prádanos, J. Calvo, F. Tejerina, A. Hernández, Flux decline in protein microfiltration: influence of operative parameters, J. Colloid Interface Sci., 187 (1997) 344-351.

[62] W. Bowen, J. Calvo, A. Hernandez, Steps of membrane blocking in flux decline during protein microfiltration, J. Membr. Sci., 101 (1995) 153-165.

[63] E.M. Tracey, R.H. Davis, Protein fouling of track-etched polycarbonate microfiltration membranes, J. Colloid Interface Sci., 167 (1994) 104-116.

[64] A. Lim, R. Bai, Membrane fouling and cleaning in microfiltration of activated sludge wastewater, J. Membr. Sci., 216 (2003) 279-290.

[65] M.R. Wiesner, S. Veerapaneni, D. Brejchová, Improvements in Membrane Microfiltration Using Coagulation Pretreatment, in: R. Klute, H. Hahn (Eds.) Chemical Water and Wastewater Treatment II: Proceedings of the 5th Gothenburg Symposium 1992, September 28–30, 1992, Nice, France, Springer Berlin Heidelberg, Berlin, Heidelberg, 1992, pp. 281-296.

[66] A. Chapiro, Z. Mankowski, N. Schmitt, Unusual swelling behavior of films of polyvinyl- and polyvinylidene/fluorides in various solvents, J. Polym. Sci.: Polym. Chem. Ed., 20 (1982) 1791-1796.

[67] N. Uhrbrand, NACE - International Corrosion Conference Series: Corrosion protection with fluoroplastics, Paper No. 09317, 2009.

[68] G. Bristow, W. Watson, Cohesive energy densities of polymers. Part 1.—Cohesive energy densities of rubbers by swelling measurements, Trans. Faraday Soc., 54 (1958) 1731-1741.

[69] G. Bristow, W. Watson, Cohesive energy densities of polymers. Part 2.—Cohesive energy densities from viscosity measurements, Trans. Faraday Soc., 54 (1958) 1742-1747.

[70] C.M. Hansen, The universality of the solubility parameter, Industrial & Eng. Chem. Prod. Res. and Development, 8 (1969) 2-11.

[71] A.F. Barton, CRC Handbook of Solubility Parameters and other Cohesion Parameters, CRC Press, 1991.

[72] M.A. Kader, A.K. Bhowmick, Thermal ageing, degradation and swelling of acrylate rubber, fluororubber and their blends containing polyfunctional acrylates, Polym. Degrad. and Stab., 79 (2003) 283-295.

[73] C. Ursino, S. Simone, L. Donato, S. Santoro, M.P. De Santo, E. Drioli, E. Di Nicolo, A. Figoli, ECTFE membranes produced by non-toxic diluents for organic solvent filtration separation, RSC Advances, 6 (2016) 81001-81012.

[74] S. Ebnesajjad, Fluoroplastics, Volume 2: Melt Processible Fluoropolymers-The Definitive User's Guide and Data Book, William Andrew, 2015.

[75] C.L. Yaws, Yaws' Handbook of Thermodynamic and Physical Properties of Chemical Compounds, Knovel, 2003.

[76] C.L. Yaws, Yaws' Thermophysical Properties of Chemicals and Hydrocarbons, in, Knovel, 2010.

[77] R.C. Weast, M.J. Astle, Handbook of Chemistry and Physics, 59th ed., CRC Press, Inc., West Palm Beach, FL, U.S.A., 1975.

[78] R.S. Benson, Use of radiation in biomaterials science, Nuclear Instruments and Methods in Physics Research Section B: Beam Interactions with Materials and Atoms, 191 (2002) 752-757.

[79] G. Vazquez, E. Alvarez, J.M. Navaza, Surface tension of alcohol water + water from 20 to 50 .degree. C, J. Chem. Eng. Data, 40 (1995) 611-614.

[80] H.N. Dunning, E.R. Washburn, Diffusion coefficients and some related properties of the butyl alcohols in aqueous solutions, J. Phys. Chem., 56 (1952) 235-237.

[81] M.C. García-Payo, M.A. Izquierdo-Gil, C. Fernández-Pineda, Wetting study of hydrophobic membranes via liquid entry pressure measurements with aqueous alcohol solutions, J. Colloid Interface Sci., 230 (2000) 420-431.

[82] B.-S. Kim, P. Harriott, Critical entry pressure for liquids in hydrophobic membranes, J. Colloid Interface Sci., 115 (1987) 1-8.

[83] J. Yu, X. Hu, Y. Huang, A modification of the bubble-point method to determine the pore-mouth size distribution of porous materials, Sep. Purif. Technol., 70 (2010) 314-319.

[84] T.H. Lee, F.Y.C. Boey, K.A. Khor, On the determination of polymer crystallinity for a thermoplastic PPS composite by thermal analysis, Composites Sci. Technol., 53 (1995) 259-274.

[85] A.P. Mathew, K. Oksman, M. Sain, The effect of morphology and chemical characteristics of cellulose reinforcements on the crystallinity of polylactic acid, J. Appl. Polym. Sci., 101 (2006) 300-310.

[86] T. Suwa, T. Seguchi, M. Takehisa, S. Machi, Effect of molecular weight on the crystalline structure of polytetrafluoroethylene as-polymerized, J. Polym. Sci.: Polym. Phys. Ed., 13 (1975) 2183-2194.

[87] M.L. Occelli, S.S. Pollack, J.V. Sanders, Characterization of Siliceous Zeolites Crystallized in the Presence of Trioctylamine. Part I. Synthesis and Crystal Properties*, in: P.J. Grobet, W.J. Mortier, E.F. Vansant, G. Schulz-Ekloff (Eds.) Studies in Surface Science and Catalysis, Elsevier, 1988, pp. 45-55.

[88] H. Vázquez-Torres, C.A. Cruz-Ramos, Blends of cellulosic esters with poly(caprolactone): Characterization by DSC, DMA, and WAXS, J. Appl. Polym. Sci., 54 (1994) 1141-1159.

[89] C. Freitas, R.H. Müller, Correlation between long-term stability of solid lipid nanoparticles (SLN™) and crystallinity of the lipid phase, Eur. J. Pharm. Biopharm., 47 (1999) 125-132.

[90] A.R. Berens, I.M. Hodge, Effects of annealing and prior history on enthalpy relaxation in glassy polymers. 1. Experimental study on poly(vinyl chloride), Macromolecules, 15 (1982) 756-761.

[91] P. Toniolo, S. Carella, Halar® high clarity ECTFE film – an highly transparent film for new buildings structures, Procedia Eng., 155 (2016) 28-37.

[92] N. Del Fanti, M. Pianca, M. Fumagalli, G. Camino, Mechanism of thermal degradation of alternating ethylene-chlorotrifluoroethylene copolymers, J. Fluor. Chem., 58 (1992) 251.

[93] S.-Y. Lin, K.-S. Chen, L. Run-Chu, Organic esters of plasticizers affecting the water absorption, adhesive property, glass transition temperature and plasticizer permanence of Eudragit acrylic films, J. Controlled Release, 68 (2000) 343-350.

[94] T.S. Chow, Molecular interpretation of the glass transition temperature of polymer-diluent systems, Macromolecules, 13 (1980) 362-364.

[95] Y. Li, X. Li, C. Yang, Y. Li, Ligand-controlling synthesis and ordered assembly of ZnS nanorods and nanodots, J. Phys. Chem. B, 108 (2004) 16002-16011.

[96] M.B. Ahmad, W.H. Hoidy, N.A.B. Ibrahim, E.A.J. AI-Mulla, Modification of montmorillonite by new surfactants, J. Eng. Applied Sci., 4 (2009) 184-188.

[97] D. Lin-Vien, N.B. Colthup, W.G. Fateley, J.G. Grasselli, The Handbook of Infrared and Raman Characteristic Frequencies of Organic Molecules, Elsevier, 1991.

[98] C.J. Pouchert, The Aldrich Library of FT-IR Spectra, Aldrich Chemical Company, 1985.

[99] R. Heacock, L. Marion, The infrared spectra of secondary amines and their salts, Can. J. Chem., 34 (1956) 1782-1795.

[100] J. Mihály, S. Sterkel, H.M. Ortner, L. Kocsis, L. Hajba, É. Furdyga, J. Mink, FTIR and FT-Raman spectroscopic study on polymer based high pressure digestion vessels, Croat. Chem. Acta, 79 (2006) 497-501.

[101] G. Socrates, Infrared and Raman Characteristic Group Frequencies: Tables and Charts, John Wiley & Sons, 2004.

[102] K.J. Geretschläger, G.M. Wallner, J. Fischer, Structure and basic properties of photovoltaic module backsheet films, Sol. Energy Mater. Sol. Cells, 144 (2016) 451-456.

[103] J.W. Hong, J.B. Lando, J.L. Koenig, S.H. Chough, S. Krimm, Normal-mode analysis of infrared and Raman spectra of poly(vinyl fluoride), Vibrational Spectroscopy, 3 (1992) 55-66.

[104] P. Nallasamy, S. Mohan, Vibrational spectroscopic characterization of form II poly (vinylidene fluoride), Indian J. Pure Appl. Phys., 43 (2005) 821-827.

[105] I.M. Smallwood, Handbook of Organic Solvent Properties, Elsevier, 1996.

[106] D.R. Machado, D. Hasson, R. Semiat, Effect of solvent properties on permeate flow through nanofiltration membranes. Part I: investigation of parameters affecting solvent flux, J. Membr. Sci., 163 (1999) 93-102.

[107] M. Cheryan, Ultrafiltration Handbook, Technomic Publishing Co. Inc., 1986.

[108] Z. Tadmor, C.G. Gogos, Principles of Polymer Processing, John Wiley & Sons, 2013.

[109] R.B. Bird, W.E. Stewart, E.N. Lightfoot, Transport Phenomena, John Wiley & Sons, Inc., USA, 2002.

[110] K.K. Sirkar, Separation of Molecules, Macromolecules and Particles: Principles, Phenomena and Processes, Cambridge University Press, 2014.